
Editorial Office of *Earth's Cryosphere (Kriosfera Zemli)*
Institute of Geography, Russian Academy of Sciences
37 Vavilov str., office 22, Moscow, 117312, Russia
Editorial staff: *N.V. Arutyunyan*, *N.G. Belova, O.M. Lisitsyna, G.E. Oblogov*
Phone: 8(985) 957-10-01, e-mail: kriozem@gmail.com
Editor of the English translation: *D.E. Konyushkov*

Journal promoted by
Russian Academy of Sciences, Siberian Branch, Novosibirsk
Earth's Cryosphere Institute, Tyumen Scientific Centre SB RAS, Tyumen
Melnikov Permafrost Institute, SB RAS, Yakutsk

Editorial Manager *M.A. Trashkeeva*
Designed by *N.F. Suranova*
Typeset by *N.M. Raizvikh*

RUSSIAN ACADEMY OF SCIENCES
SIBERIAN BRANCH
EARTH'S CRYOSPHERE INSTITUTE, TYUMEN SCIENTIFIC CENTRE
MELNIKOV PERMAFROST INSTITUTE

EARTH'S CRYOSPHERE
SCIENTIFIC JOURNAL

Founded in January 1997	6 issues per year	Vol. XXVI, No. 4	July–August 2022

CONTENTS

EARTH'S CRYOSPHERE
SCIENTIFIC JOURNAL

Earth's Cryosphere, 2022, vol. XXVI, No. 4, pp. 3–15

GEOCRYOLOGICAL MONITORING AND FORECAST

DEVELOPMENT OF GEOCRYOLOGICAL MONITORING OF UNDISTURBED AND DISTURBED RUSSIAN PERMAFROST AREAS ON THE BASIS OF GEOTECHNICAL MONITORING SYSTEMS OF THE ENERGY INDUSTRY

V.P. Melnikov[1–4], V.I. Osipov[5], A.V. Brouchkov[6,*], A.G. Alekseev[7,8], S.V. Badina[6,9], N.M. Berdnikov[1], S.A. Velikin[10], D.S. Drozdov[1,11], V.A. Dubrovin[12], M.N. Zheleznyak[10], O.V. Zhdaneev[13], A.A. Zakharov[14], Ya.K. Leopold[15], M.E. Kuznetsov[16], G.V. Malkova[1], A.B. Osokin[17], N.A. Ostarkov[18], F.M. Rivkin[1], M.R. Sadurtdinov[1], D.O. Sergeev[5], R.Yu. Fedorov[1,2], K.N. Frolov[13], E.V. Ustinova[1,3], A.N. Shein[15]

[1] *Earth Cryosphere Institute, Tyumen Scientific Center, Siberian Branch of the Russian Academy of Sciences, ul. Malygina 86, Tyumen 625026 Russia*
[2] *Tyumen State University, ul. Volodarskogo 6, Tyumen, 625003 Russia*
[3] *Tyumen Industrial University, ul. Volodarskogo 38, Tyumen, 625000 Russia*
[4] *Cryosphere Interdisciplinary Research Methodology Department, Tyumen Scientific Center, Siberian Branch of the Russian Academy of Sciences, ul. Malygina 86, Tyumen, 625026 Russia*
[5] *Sergeev Geoecology Institute, Russian Academy of Sciences, Ulanskiy per. 13, build. 2, Moscow, 101000 Russia*
[6] *Lomonosov Moscow State University, Leninskie Gory 1, Moscow, 119991 Russia*
[7] *Research Center of Construction, Ryazanskiy prosp. 59, Moscow, 109428 Russia*
[8] *Moscow State University of Civil Engineering, Yaroslavskoe shosse 26, Moscow, 129337 Russia*
[9] *Plekhanov Russian University of Economics, Stremyannyi per. 36, Moscow, 117997 Russia*
[10] *Melnikov Permafrost Institute, Siberian Branch of the Russian Academy of Sciences, ul. Merzlotnaya 36, Yakutsk, 677010 Russia*
[11] *Ordzhonikidze Russian State University for Geological Prospecting, ul. Miklukho-Maklaya 23, Moscow, 117997 Russia*
[12] *Gidrospetsgeologiya, ul. Marshala Rybalko 4, Moscow, 123060 Russia*
[13] *Russian Energy Agency, prosp. Mira 105, build. 1, Moscow, 129085 Russia*
[14] *Transneft, Presnenskaya Naberezhnaya 4, build. 2, Moscow, 123112 Russia*
[15] *Arctic Research Center, ul. Respubliki 20, office 203, Salekhard, 629008 Russia*
[16] *FASI "Vostokgosplan", ul. Zaparina 67, Khabarovsk, 680000 Russia*
[17] *Nadymgazprom, ul. Pionerskaya 14, Nadym, 629730 Russia*
[18] *Ministry of the Russian Federation for the Development of the Far East and the Arctic, Bolshoy Mogiltsevskiy per. 7, build. 2, Moscow, 119002 Russia*

**Corresponding author; e-mail: brouchkov@geol.msu.ru*

Over the past 30 years, a significant rise in temperature of the upper horizons of permafrost has taken place in Russia: on average, by 2.5°C. This has caused permafrost degradation, which negatively affects both natural landscapes and engineering infrastructure. Economic entities try to protect their enterprises by investing both in engineering measures and in monitoring of changes in frozen ground under structures. One of the leading places in this area is occupied by the fuel and energy complex. A system of automated geotechnical monitoring of the frozen ground is beginning to be implemented at its enterprises, and in the near future (5–10 years) this will become mandatory for every facility in the permafrost zone. So far, in different regions and organizations, geotechnical monitoring of permafrost has been carried out according to different methods, often in a reduced volume, without taking into account natural trends, and in the absence ofappropriate analysis and forecast. Moreover, environmental changes occurring regardless of the economic activity of humans, are often ignored. This situation sharply reduces the efficiency of monitoring. The reason for the low efficiency of monitoring works is related to the shortcomings of the regulations for observation and data processing, on one hand, and to the insufficient volume of geocryological monitoring of natural conditions in undisturbed areas of the Russian Federation, on the other hand. As a result, the possibility of a medium-term (15–50 years), and long-term (over 50 years) forecasts of changes in permafrost is extremely limited. For the fuel and energy complex, the problem is aggravated by the lack of data exchange between its individual companies both within the regions and at the federal level. A scheme of the federal permafrost monitoring system is proposed. It implies the creation of a system of federal geocryological polygons, where two types of monitoring are combined: environmental monitoring of natural conditions and geotechnical monitoring of land and subsoil users (primarily, in the fuel and energy complex) – the so-called geocryological monitoring of undisturbed and disturbed areas.

Keywords: *global climate change, permafrost, fuel and energy complex, geocryological monitoring of undisturbed areas, geocryological monitoring of disturbed areas (geotechnical monitoring), geocryological station, thaw, damage, Arctic.*

Recommended citation: Melnikov V.P., Osipov V.I., Brouchkov A.V., Alekseev A.G., Badina S.V., Berdnikov N.M., Velikin S.A., Drozdov D.S., Dubrovin V.A., Zheleznyak M.N., Zhdaneev O.V., Zakharov A.A., Leopold Ya.K., Kuznetsov M.E., Malkova G.V., Osokin A.B., Ostarkov N.A., Rivkin F.M., Sadurtdinov M.R., Sergeev D.O., Fedorov R.Yu., Frolov K.N., Ustinova E.V., Shein A.N., 2022. Development of geocryological monitoring of undisturbed and disturbed Russian permafrost areas on the basis of geotechnical monitoring systems of the energy industry. *Earth's Cryosphere*, XXVI (4), 3–15.

INTRODUCTION

Permafrost regions of the Russian Federation are of particular importance for the country's economy because of the wide-scale economic activities, primarily of the enterprises of the fuel and energy complex (FEC), a key sector of the Russian economy. More than 90% of natural gas and 17% of oil are being produced in the Arctic Zone of the Russian Federation

Table 1. **Regions of the Russian Federation with permafrost**

Region	Total area, thousand km^2	Permafrost area in the okrug, thousand km^2	Permafrost area*, % of the total area	Gross regional product (2019), billion rubles	Oil extraction (2020), thousand tons	Gas extraction (2020), billion m^3
Northwestern Federal District		444* (254**)				
Arkhangelsk Oblast (without NAO)	113		27.6	559	–	–
Komi Republic	417		21.8	721	12 956	3.4
Murmansk Oblast	145		50.2	617	–	–
Nenets Autonomous Okrug (NAO)	177		94.2	331	14 117	1.2
Privolzhsky Federal District		2* (0.25**)				
Perm Krai	160		1.1	1495	16 037	0.5
Ural Federal District		877* (462**)				
Sverdlovsk Oblast	194		1.0	2530	–	–
Tyumen Oblast (without KhMAO and YaNAO)	160		0.2	1256	11 248	0.3
Khanty-Mansi Autonomous Okrug (KhMAO)	535		36.6	4563	210 755	32.1
Yamalo-Nenets Autonomous Okrug (YaNAO)***	769/684		99.2	3101	63 300	557
Siberian Federal District		2980* (1960**)				
Altai Republic	93		82.9	59	–	–
Altai Krai	168		2.2	631	–	–
Irkutsk Oblast	775		87.9	1546	17 317	3.0
Kemerovo Oblast	96		12.5	1110	–	–
Krasnoyarsk Krai	2367		84.6	2692	20 237	8.1
Republic of Tuva	169		99.8	79	–	–
Republic of Khakassia	62		57.8	256	–	–
Far Eastern Federal District		6227* (4936**)				
Amyr oblast	362		88.1	413	–	–
Republic of Buryatia	351		88.9	286	–	–
Jewish Autonomous Oblast	36		10.7	57	–	–
Zabaikalsky Krai	432		99.7	365	–	–
Kamchatka Krai	464		67.0	280	12	0.3
Magadan Oblast	462		99.1	213	–	–
Primorsky Krai	165		2.2	1067	–	–
Republic of Sakha (Yakutia)	3103		98.9	1110	16 172	8.0
Sakhalin Oblast	87		4.2	1173	18 348	33.5
Khabarovsk Krai	788		76.5	803	–	–
Chukotka Autonomous Okrug	738		96.8	95	–	0.1

* The entire permafrost zone area is taken into account.

** The area of permafrost from the surface is taken into account (the entire permafrost area minus the area of taliks in the zones of discontinuous and isolated permafrost).

*** Official data / data from OpenStreetMap shape-file.

(AZRF), a part of the permafrost area of Russia (Table 1). The production of liquefied natural gas (LNG) is projected to be increased to 100–120 million tons per year by 2035, covering up to 20% of the global LNG market [*Tikhonov, 2020*].

The economic development in permafrost regions of Russia is complicated by harsh natural processes. Starting from the late 1970s–early 1980s, the mean annual air temperature has been increasing in all regions indicating climate changes leading to transformations of landscapes, hydrosphere, and permafrost. On average, the rise in the mean annual air temperature was 0.35°C per decade for the period of 1960–1990 and increased to 1°C per decade for the period of 1990–2020 [*Malkova et al., 2022*]. Various climatic scenario forecasts suggest the further warming.

When considering the response of specific constructions to an increase in the permafrost temperature, we must also consider their deformation and destruction caused by the decrease in ground bearing capacity if the design margin of safety is reached or exceeded. Wherein, in the past 30 years, the ground temperature in the upper permafrost horizons has increased by 0.3–1.5°C [*Malkova et al., 2022*]. This is significant, although slightly lower than the recorded increase in air temperature. Permafrost temperatures within the developing natural gas fields of West Siberian lowlands have increased stronger: by 2.0–4.0°C and even more. In addition, the contribution of human impact is significant in this region. Over the same period, in the forest-tundra zone of West Siberia with discontinuous permafrost, permafrost table has deepened to 3–8 m from the surface within a 100-km-wide land strip; a supra-permafrost talik has formed.

Unfortunately, the modern geocryological knowledge of the northern territories largely does not correspond to the pace of economic development in the Arctic development [*Dubrovin et al., 2019; Zhdaneev, 2020*]. For many Arctic regions, the important factor is the loss of bearing capacity of foundation of buildings and constructions. Considerable part of existing data on permafrost state is now outdated and needs to be revised. The emerging risks of loss of the bearing capacity of foundations and the activation of dangerous cryogenic processes determine the need to establish the federal permafrost monitoring system in Russia.

Predictive information on the state of permafrost can only be provided by a combination of a reliable climate forecast with geocryological monitoring and forecasting. This can be achieved if there is an adequate system of geocryological monitoring, which should include two main mutually integrated blocks: monitoring of undisturbed areas (control of a set of natural conditions that determine the state of permafrost) and monitoring of disturbed areas – geotechnical monitoring (GTM) (control of a set of natural factors and human activity affecting the reliability of engineering infrastructure and associated geoecological safety).

At present, there are prototypes of the elements of both monitoring blocks in Russia, but they are mostly imperfect and, more important, are not integrated into a system with internal communications, information exchange, and access to representative organizational decisions.

Geocryological monitoring of undisturbed natural areas in the Russian Federation

Geocryological observations at undisturbed areas have a great practical meaning in addition to the scientific interest. They are the basis for an adequate interpretation of GTM data, as they make it possible to isolate the natural component in those environmental changes that are observed during the building and operation of technical constructions, as well as under the impact of other types of land use and management.

The system of geocryological observations at undisturbed areas in Russian permafrost zone is represented by a limited number of stations and sites for periodic visits and is managed by different ministries and departments. There are only two monitoring stations managed by the Ministry of Natural Resources of the Russian Federation: the Vorkuta polygon and the Marre-Sale station in Yamal. Some elements of the geocryological situation are monitored in the Baikal Natural Territory. Russian Academy of Sciences supports approximately 20 monitoring sites and 85 geocryological boreholes, including a modern station on the Samoylovsky Island in the Lena Delta. Russian universities also have a limited monitoring network. In West Siberia, PJSC Gazprom has a developed network of GTM at important infrastructure facilities and also monitors nearby undisturbed permafrost conditions in areas necessary from a technological point of view.

This is clearly insufficient. Thus, in Alaska (USA), there are already more boreholes for monitoring of undisturbed areas than in Russia, though the area of Alaskan permafrost is almost ten times smaller. In Canada, the number of monitoring boreholes is approximately the same as in Russia, though the area of Canadian northern territories and the degree of its development are considerably smaller than in Russia. On Spitsbergen, monitoring is carried out by the Norwegian Polar Institute. In the USA and Canada, the corresponding observations are carried out by the geological surveys of these countries together with state universities. In China, permafrost monitoring is performed by the Cold and Arid Regions Environmental and Engineering Research Institute belonging to the Chinese Academy of Sciences.

Available data are sufficient for revealing general global trends of permafrost thermal state and active

layer parameters (seasonally thawed layer, seasonally frozen layer) on a scale of 1:5,000,000 and smaller. Data analysis and generalization are carried out by national research organizations and are associated with international projects TSP (Thermal State of Permafrost), CALM (Circumpolar Active Layer Monitoring), GTN-P (Global Terrestrial Network for Permafrost). An updated summary of international activities is published on the annual basis [*Smith et al., 2021*].

However, these data are insufficient for an adequate description of the whole variety of features of the thermal state of permafrost due to the extremely complex mosaic patterns of northern landscapes. The size of natural territorial complexes (NTC) may be a few kilometers, often hundreds of meters, and their geocryological conditions strongly differ.

Thus, the tasks of the regional and local levels are currently not provided with background geocryological information.

The theoretical basis of the geosystem approach is the idea that geosystems form a spatial hierarchy, where taxa of each level can be typified by a set of internal properties and external features visible both directly in the field and on remote sensing data [*Melnikov, 1983; Drozdov, 2004; Popova, 2012*]. It should be noted that necessary geosystem characteristics include not only their natural properties but also typical reactions to certain types of human impact.

It is possible to describe the natural state of taxa on the basis of field sampling and remote sensing data, while the future phenomenological geotechnical forecast of the consequences of human impact is possible on the basis of data on typical reactions of geosystems. The last stage is the geocryological forecast that takes into account changes in the natural conditions. The monitoring of natural conditions includes (1) meteorological monitoring, which has been efficiently performed by the Russian Hydrometeorological Survey for more than 100 years, and (2) geocryological monitoring, the beginnings of which are barely glimmering in the Russian Academy of Sciences, universities and Rosnedra organizations, as mentioned above.

The monitoring of natural conditions at undisturbed areas by business entities is carried out very limitedly, which can be demonstrated by the example of Urengoy oil and gas-condensate field. Here, 52 landscape units (urochishches) can de distinguished according to landscape conditions. This information provides infrastructure development planning. Two types of urochishches often form a kind of

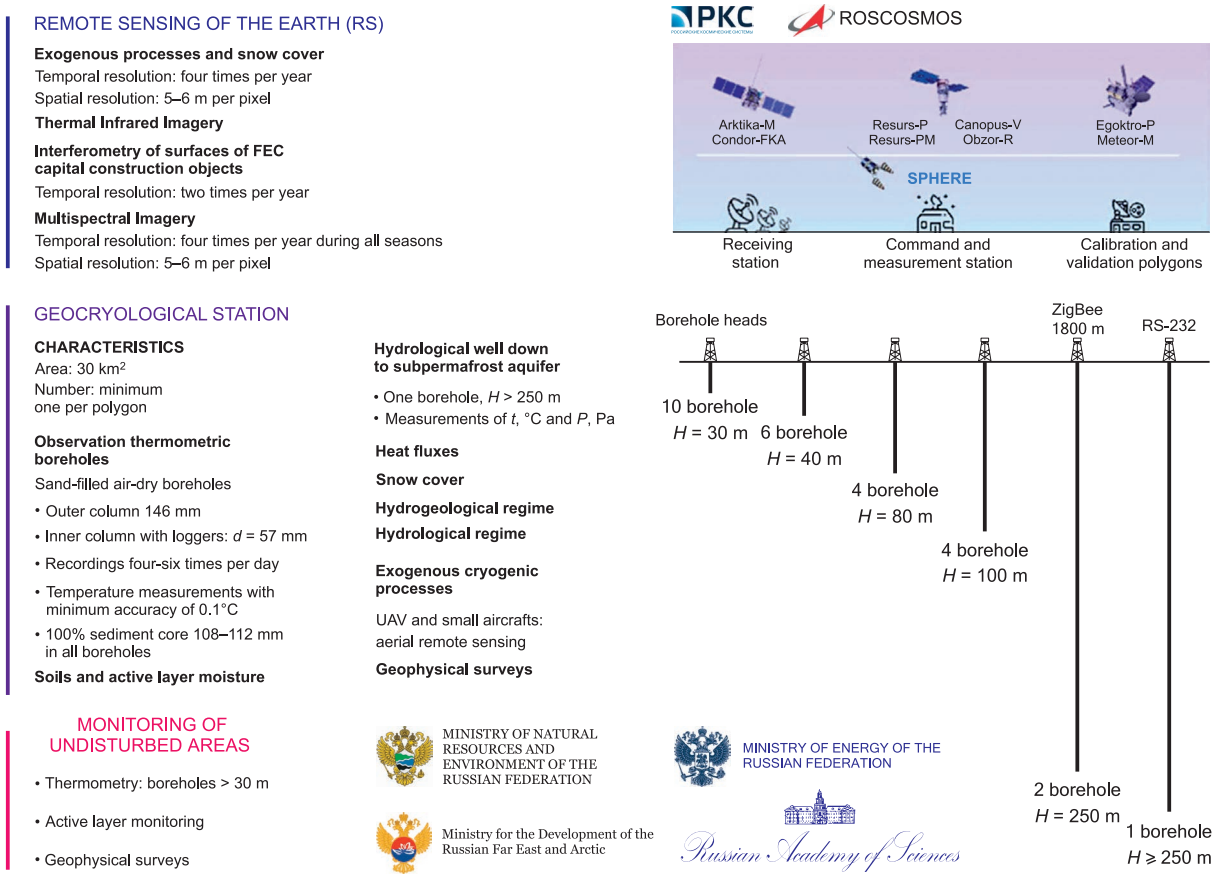

Fig. 1. Perspective elements of the permafrost monitoring system in the FEC.

stable natural territorial complexes (NTCs). The total number of such complexes (359) exceeds the number of urochishches by almost an order of magnitude. Each of the types of urochishches or NTCs can be found on different marine and alluvial terraces and in different natural subprovinces and localities of the region. Overall, the number of independent landscape units in the study area is increased to 2500. Ideally, data on ground temperatures must exist for each of them. In reality, only 14 monitoring boreholes with a depth of 10 m (reaching the depth of zero annual amplitudes) continued to operate in the field in August–September 2021.

Obviously, we should not consider drilling 2500 observation geocryological boreholes; we need a scientifically substantiated minimum of observation points and a substantiated distribution of this minimum over specially selected polygons, stations, and sites within the permafrost zone. In addition to these mentioned 10-m boreholes, this number must also include 30-m-deep boreholes for reliable fixation of the permafrost response to the 11-year solar cycle and 100-m-deep boreholes for accounting the influence of centennial fluctuations. The site selection is determined by the need to cover the variety of natural conditions, on one hand, and by the order of development of territories and regions, on the other hand (Fig. 1).

The program planned by the government to create 140 new observation geocryological boreholes at weather stations of Rosgidromet (Russian Hydrometeorological Service) [*TASS, 2022*] will not solve the problem, since the permafrost conditions at the weather stations do not represent the regional geocryological conditions. Moreover, the decision to place geocryological boreholes at weather stations should be considered deeply erroneous: it will not only lead to incorrect information but will also close the way for monitoring of undisturbed areas for other departments, since Rosgidromet is responsible for this area. The need for an urgent revision of the Rosgidromet Program is noted in the corresponding Report of the Russian Academy of Sciences [*Conclusion of RAS, 2021*].

As a result, the efficiency of geocryological monitoring of undisturbed areas, in which the USSR was once at the forefront, and now Russia lags behind other interested countries, is significantly reduced due to insufficient attention and funding of geocryological monitoring work by scientific institutions and relevant government departments in the Arctic. Geotechnical monitoring of industrial objects, which is widely implemented by fuel and energy companies, as well as by mining companies and other land users, is largely depreciated without reliable observations of undisturbed ground temperature, taliks, cryogenic processes, groundwater regime, the state of vegetation, the active layer depth, and hydrometeorological parameters.

Geotechnical monitoring in the Russian Federation (monitoring of disturbed areas)

Geotechnical monitoring of natural and technical systems (NTSs) or geotechnical systems is usually understood as a set of measures to control, predict, and manage their state to ensure operational reliability and environmental safety [*SP 22.13330.2016, 2016*]. Two main subsystems of NTSs can be distinguished: (1) NTSs mainly related to the natural component and (2) NTSs mainly related to the ***artificial (anthropogenic, technogenic)*** component. These subsystems interact with one another and intersect both in the feature space and in the geometric space [*Bondarik, 1981, 1993*]. They influence one another. As a result, the functioning of a technical object depends on natural conditions and their dynamics, and, conversely, the condition for preserving the environment is the design functioning of the artificial object. Geotechnical monitoring should track the course and results of this interaction in order to evaluate them and make current decisions on the optimal control of technical systems while ensuring environmental safety and nature conservation.

In the Arctic regions, geotechnical monitoring is carried out at enterprises of the oil and gas industry and coal companies, at thermal and hydropower plants, in large cities and settlements. It includes observations of ground temperature, groundwater level, and deformations at engineering facilities. Moreover, the geocryological component of geotechnical monitoring is very important. Unfortunately, the disadvantage of this monitoring is the almost complete absence of data on natural undisturbed conditions in the immediate vicinity of observation objects. The sparse network of monitoring of undisturbed areas available in Russia characterizes regional trends; it is not able to provide the necessary detail of current, and even more so predictive geocryological information for specific enterprises and municipalities.

In addition, the unsettled organizational and technical issues of the GTM data exchange between enterprises of different subordination and forms of ownership limits the dissemination of existing data that could be useful for current life activities, new construction, scientific research, as well as for other mining companies.

The use of relatively available data on the mean annual air temperature does not allow us to predict permafrost changes, because a large set of data on the current state and recent history of permafrost, active layer, and surface geometry is also required for the forecast [*Harris et al., 2017*]. In turn, to obtain this information, a set of monitoring observations should be implemented: Earth observation through remote sensing, geophysical surveys, geotechnical control systems (including observations and measurements in boreholes).

Regularly received remote sensing data will allow assessing surficial changes considering short- and long-term climatic fluctuations. As an example, the following remote sensing methods can be used for geotechnical monitoring of main oil and gas pipelines.

• Point radar interferometry – monitoring of the position of pipelines through satellite radar imagery and corner reflectors made of aluminum or carbon fiber. The existing equipment can provide measurement of deformations and displacements with an accuracy of 2–5 mm.

• High-precision photogrammetry – monitoring of the Earth's surface displacement through the unmanned aerial vehicles carrying the following main equipment: a stabilized video camera and a thermal imager, a camera, a geodetic receiver of the global navigation satellite system (GNSS receiver). The application of this method makes it possible to detect heaving, karst, landslide, and erosion processes, as well as to validate satellite data. The accuracy of the method is about 5 cm.

• Areal radar interferometry – monitoring of the Earth's surface geometry and global geodynamic processes by means of satellite radar scanning.

• Surface change monitoring using foreign orbital systems (COSMO-SkyMed, Ikonos, QuickBird, WordView, GeoEye-1) and Russian systems (two Arktika-M satellites, the first was launched into orbit on February 28, 2021); perspective remote sensing system Smotr, including radar satellites SMOTR-R, optical scanners SMOTR-V, and infrared scanners (a segment of the group of satellites SMOTR-I).

The developed branch of geophysical services in the oil and gas industry widely applies geophysical methods for obtaining data on the distribution and thickness of permafrost, ice content, and active layer depth relevant for Russia. Methods of electrical, electromagnetic, radar, and seismic surveys allow obtaining detailed data on the occurrence of permafrost, ice content and ground moisture, temperature gradient within permafrost. Permafrost geophysical data should be verified by direct observations (measurements) in boreholes.

Based on remote sensing and geophysical data, it is possible to conduct a fundamental modeling of the permafrost distribution in a particular region, subsequently regularly updating the model according to new remote sensing data, borehole sensors, and periodic (or monitoring) geophysical surveys.

Local research methods include, first of all, the following borehole data:

• thermometric measurements–constantly on a daily basis;

• hydrogeological observations–periodically;

• hydrological observations–periodically;

• leveling of ground benchmarks and deformation marks on the ground along the perimeter of industrial facilities of the FEC and directly on the facilities themselves;

• a snow survey, at least three times a year (in the snowy season).

For industrial and civil buildings and constructions, it is required to develop systems for monitoring and calculating the stress-strain state, considering the deviation of their geometry from the calculated one.

The geotechnical control system is considered as an integral part of the production operational control of buildings and constructions and the industrial safety system. The geotechnical control system implies the creation of specialized units – geotechnical monitoring services – the centers of responsibility for this area of work.

Geotechnical control solves the following tasks at all stages of the objects' existence, from the moment of their design and engineering surveys, including the stage of construction and operation.

1. Permanent instrumental monitoring of the dynamics of geocryological conditions in the foundations of engineering facilities and the spatial position of supporting constructions, equipment, and pipelines and their compliance with design and regulatory requirements.

2. Monitoring the dynamics of dangerous surficial cryogenic processes in the zone of potential impact on engineering constructions.

3. Integrated geotechnical forecast of the geocryological condition dynamics and the stability of bases and foundations, including using non-stationary numerical methods of thermal engineering and thermomechanical modeling.

4. Control of the stress-strain state of building structures, constructions, equipment, and pipelines using instrumental and calculation methods.

5. Control over the process of designing bases and foundations of objects, including the volume and quality of engineering surveys, selection of sites for construction, making fundamental decisions on the construction.

6. Development and implementation of technical measures to control the development of unacceptable deformations of buildings and constructions, stabilization of bases and foundations.

7. Improvement of the regulatory and methodological fundamentals in the field of design and construction on permafrost.

Geotechnical monitoring on objects belonging to PJSC GAZPROM

For the first time, systematic regime geotechnical observations were started at the Medvezh'e field (the first gas industry in the north of West Siberia) in the mid-1980s. At that time, widescale deformations of the bases and foundations of gas production facilities began to develop at the field due to difficult per-

mafrost-geological conditions, design flaws, and poor-quality construction. Ultimately, this resulted in numerous equipment failures. As part of the Nadym-Gazprom Production Association, a specialized subdivision was created to resolve the situation in the late 1980s – the Foundation Reliability Laboratory, whose functional duties included organizing and conducting routine observations on the dynamics of geocryological conditions at gas fields and on the stability of bases and foundations. The activity of the laboratory became a prototype of geotechnical monitoring.

With the commissioning of new fields and the development of an appropriate gas transmission network in the north of West Siberia, i.e. with the increase in the number of objects subjected to permafrost-related deformations, geotechnical monitoring technology began to be introduced everywhere – at the Urengoy, Yamburg, and Zapolyarnoe fields, at Transgaz facilities. To date, with the implementation of corporate standards of PJSC Gazprom, the geotechnical monitoring system has become an obligatory element in the design, construction, and operation of gas industry facilities [*STO Gazprom 2-3.1-072-2006, 2006*].

In addition to corporate standards, geotechnical monitoring is also determined by the requirements of federal legislation (federal laws *On Industrial Safety* No. 116-FL and *Technical Regulations on the Safety of Buildings and Constructions* No. 384-FL, sets of rules governing the construction and operation of engineering facilities in permafrost areas).

In the subsidiaries of PJSC Gazprom, geotechnical monitoring is carried out at all stages of the existence of facilities, from the moment of the start of design and engineering surveys, at the stages of construction and exploitation.

In accordance with the regulatory requirements and established practice, the designer is obliged to provide reasonable data on the permissible temperature regime of permafrost at bases of engineering constructions at the time of transfer of the load to the foundations and for the exploitation period within the design and working documentation for the construction of gas production facilities. As part of the design and working documentation, a geotechnical monitoring system is envisaged and includes a systematically distributed thermal and piezometric observation boreholes, deep geodetic benchmarks and deformation marks in an amount that allows obtaining geotechnical information sufficient to diagnose the current state of objects and predict the dynamics of geotechnical conditions.

In recent years, to reduce labor costs for geotechnical monitoring, systems for registering geotechnical parameters (permafrost temperature, spatial position of constructions) have been actively introduced using instruments with an automated system for polling sensors (loggers) and transmitting measurement results to central collection points via a radio channel or wired systems connections. Sensors have been introduced that register stresses in building structures, as well as inclinometers for registering rolls. Specialized software is being created to automate the processing of measurements and, as a result, to create an interactive local geoinformation system of integrated monitoring of undisturbed and disturbed areas [*Rivkin et al., 2010*].

Industrial practice shows that accidents, unacceptable deformations, equipment failures occurring due to the development of deformations caused by geocryological processes are practically excluded at facilities with an implemented system of geotechnical monitoring. The performance of regime observations allows identifying trends in the formation of non-design states of geotechnical systems before they reach unacceptable status, developing the management engineering solutions in a timely manner, and including them in plans for current and major repairs and reconstruction.

Geotechnical monitoring on objects belonging to PJSC TRANSNEFT

Since 2011, PJSC Transneft has developed and implemented a system of geotechnical monitoring in order to systematically monitor, measure, and control the parameters of trunk oil pipeline facilities located in the AZRF. Trunk oil pipelines with a total length of more than 7049 km, 45 site facilities, and 248 reservoirs are subject to monitoring.

Field surveys, airborne and ground-based laser scanning, and in-line diagnostics are used to monitor of the state of foundation bases, permafrost, geological processes, geometry, and stress-strain state of oil pipelines [*Makarycheva et al., 2019*]. The procedure and scope of work are determined in accordance with the design documentation, industry-specific regulatory and guidance documents of Transneft, and the approved monitoring program, given the requirements of state norms and rules applicable to the bases and foundations of buildings and constructions on permafrost [*SP 305.1325800.2017; SP 25.13330.2020; SP 497.1325800.2020*].

In accordance with the approved monitoring program, it is envisaged to monitor the position of oil pipelines using 7229 height detection devices twice a year, the positions of 20,047 oil pipeline supports twice a year, the positions of 653 shutoff valves and 118 chambers of cleaning and diagnostic tools twice a year, the positions of 75,796 towers of overhead power lines once a year, ground temperatures at 5348 thermometric boreholes monthly, operability of 103,907 ground thermal stabilizers in winter, 654 sites (102 km) with surficial geological processes, as well as monitoring the position of 248 reservoirs twice a year, positions of 3542 buildings and con-

structions of oil pumping stations (OPS) twice a year, positions of oil pipelines of OPS by 1657 devices for determining height twice a year, ground temperature at OPS by 1284 thermometric boreholes monthly, performance of 41,604 ground thermal stabilizers at OPS in winter, groundwater level for 32 hydrogeological wells four times per year. Investments into monitoring are increasing every year: "In 2021, Transneft allocated 615 million rubles to monitor production facilities in the permafrost zone, as follows from the presentation of the company... In 2022, Transneft plans to increase the total financing of this area up to 30%" [*PJSC Transneft, 2022*].

The results of the work performed are entered into the geographic information system created by Transneft Research Institute LLC, which has a built-in software and analytical modules that combine the data of design, executive documentation, surveys, and measurement results and allows for a comprehensive analysis of monitoring data, monitoring planning, and execution control. This work is carried out by the analytical center based on the Center for Monitoring and Geoinformation Systems of Pipeline Transportation Facilities belonging to Transneft Research Institute LLC. Further, modeling and forecasting changes in the parameters of the trunk oil pipeline objects in its environment are performed based on the calculation methods developed by PJSC Transneft for estimating the wall temperature, changes in the position of the trunk oil pipeline, its stress-strain state, and changes in the bending radii of pipe sections. Based on the simulation results, compensatory measures are formed and implemented to ensure the safe and reliable operation of oil trunk pipeline facilities under design conditions.

Additionally, continuous automated monitoring systems and so-called smart inserts have been introduced to control external influences in real time at the intersections of main oil pipelines with tectonic faults and landslide-prone areas. To control the level of seismic impact on the objects of trunk oil pipelines, a real-time operating seismic impact control system was introduced. In general, to automate the control of the position of pipelines, supporting constructions, and equipment at Transneft facilities, automated geodetic networks are currently being developed based on the domestic equipment of global navigation satellite systems.

Geotechnical monitoring on hydrotechnical objects

Geotechnical monitoring on hydrotechnical objects is carried out according to the Federal Law dated July 21, 1997 No. 117-FL *On the Safety of Hydrotechnical Constructions*. Elements of geotechnical monitoring are implemented during both construction and operation of the constructions. However, there is no obligation to single out geotechnical monitoring to a separate section of the project. The project of a hydrotechnical construction (HTC) assumes the monitoring of its safety, which is developed by the owner and/or operating organization while preparing the standards for the HTC operation and maintenance, as well as a safety declaration, i.e., the main documents containing information on the compliance of the HTC safety criteria.

The safety declaration must reflect the scope of field observations and general control of the safety of HTC. It also includes a list of monitored parameters – criteria for safe operation, as well as the set of measuring equipment, control sites, monitoring scheme, functions of the service for organizing the safety of HTC, etc. According to many experts, the preparation of the safety declaration by the HTC owner reduces the efficiency of control over the safe operation of HTC for the supervisory authorities, the state of which has begun to cause concerns in recent years.

In addition, the situation with the control of the state of HTC (especially hydropower) is aggravated by the physical aging of constructions. This leads to the disrepair state of most unique pioneer HTCs on permafrost for over 50 years of their operation due to insufficient knowledge of the functioning of natural and technical systems in the permafrost zone.

According to available data [*Malik, 2005*], about 48% of emergency situations at HTCs were recorded in permafrost area. The reason for such changes is the underestimation of cryogenic processes that occur because of the temperature impact of reservoirs not only directly within the body of ground structures but also in the most critical zones (in shore/dam, base/dam, and other contact zones).

In the permafrost area, the monitoring of the state of HTC and the territories adjacent to hydroelectric facilities should be carried out considering the influence of cryogenic and post-cryogenic processes major controls of the entire NTC stability. Failure to take this into account leads to major accidents, financial and environmental problems. At all northern hydroelectric power plants. where accidents have occurred in recent decades (Kolymskaya, 1988; Kureyskaya, 1992; breakthrough of the jumper at Svetlinskaya HPP under construction, 2001; Sayano-Shushenskaya, 2009; Bureyskaya, 2019), there was no geocryological monitoring of foundations.

The HTC safety level controlled by Rostekhnadzor is estimated as follows: 20% of HTCs have a normal level of safety; 37% have a reduced level of safety; 31%, unsatisfactory level; 12%, dangerous level of safety not to be subjected to exploitation [*Annual Report..., 2019*].

It is required to create a modern unified standard for geotechnical monitoring at HTCs in the permafrost zone, which includes a standard for monitoring and control systems for zones of active interaction between the main structures of hydroelectric facili-

ties and their reservoirs with the natural complex, with direct consideration for geocryological monitoring data using a wide range of geophysical methods.

Permafrost monitoring system in cities

The permafrost experimental monitoring system in Salekhard is one of the promising examples for use in the main settlements of the Arctic, which serve as centers of traditional land use and production bases for the development of natural resources in the regions. In the Yamalo-Nenets Autonomous Okrug, for the safe operation of buildings and constructions on permafrost, the Scientific Center for Arctic Studies has been developing a method for automated temperature monitoring since 2018 [*Gromadsky et al., 2019; Kamnev et al., 2021*], which implies the construction of thermometric boreholes in a ventilated underground to a depth no less than the actual length of the piles under residential buildings (10 m or more). Temperature sensors are installed on the temperature logging chain to a depth of 5 m through each 50 cm and then through each 1 m. The results of temperature measurements are automatically collected on the server and duplicated on a specially developed web resource for analyzing, visualizing, and exporting these ground temperature data.

To test the methodology with automatic temperature recording systems SAM-Permafrost in 2018–2021, 8 buildings were equipped in Salekhard and 1 building in Novyi Urengoy; overall, 26 sets of SAM-Permafrost were installed, and more than 100 thermometric boreholes were drilled. Monitoring revealed a local thaw zone under one of the buildings (Fig. 2), probably formed by infiltrating leaks from utilities.

Further temperature monitoring in Salekhard will make it possible to obtain data that will be used to calculate a non-stationary temperature field with subsequent recalculation (considering the geocryological structure) into the predicted bearing capacity of the foundations of controlled structures for several years ahead.

Federal monitoring system in FEC

A state monitoring system is required to predict the state of permafrost and provide measures to prevent damage. The system combines observation networks and analytical centers of ministries, departments, regional authorities, and business enterprises represented by a federal operator.

The initial basis of the system could be an array of geocryological data systematically collected by state and private companies in the FEC – major players in the economy of the Russian Arctic; and large miners represented by PJSCs Rosneft, Gazprom, NOVATEK, and others, who carry out their own permafrost monitoring [*Kryukov, 2020*]. It is important to (1) develop a unified methodology and requirements for the network of undisturbed monitoring sites and GTM sites and (2) develop a list of controlled parameters, output information, and work procedures with professional justification for the creation and placement of monitoring stations and observation points.

The new approach assumes a stage-by-stage creation of a system of state geocryological polygons as the highest level of permafrost monitoring in Russia, combining stations that characterize undisturbed geocryological conditions and objects of geotechnical monitoring of ground use, industrial facilities, transport systems, municipalities, and settlements [*Drozdov, Dubrovin, 2016; Melnikov et al., 2021*].

We suggest the organization of 15 geocryological polygons and stations (Fig. 3) for systematic monitoring and forecasting of permafrost changes throughout the country in accordance with the current concentration of the infrastructure of FEC and planned projects. Permafrost stations will presumably be in

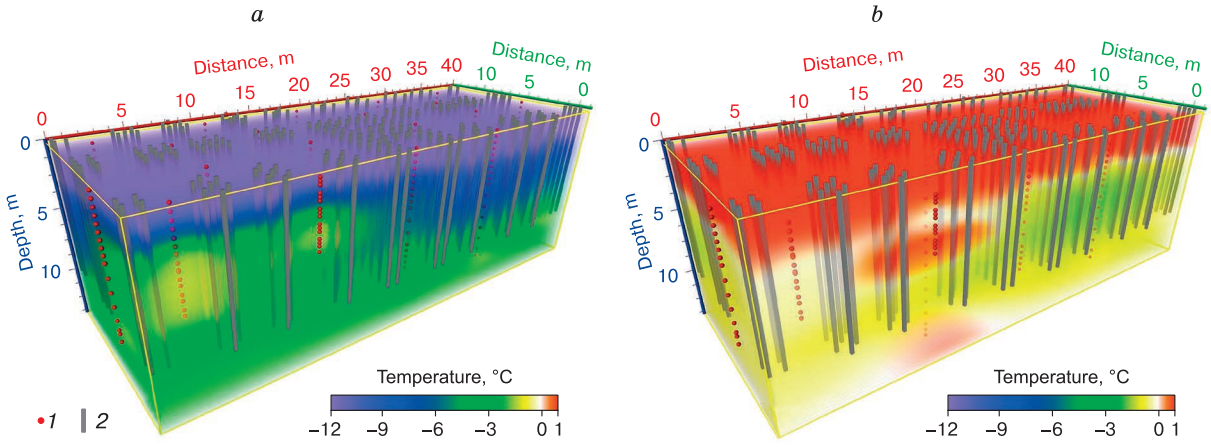

Fig. 2. 3D-interpolation of mean weekly ground temperatures recorded at the foundation base of residential building in Salekhard (ul. Zoi Kosmodemianskoy 68).

a – February 22–28, 2021; *b* – August 23–29, 2021. *1* – temperature logger, *2* – piles.

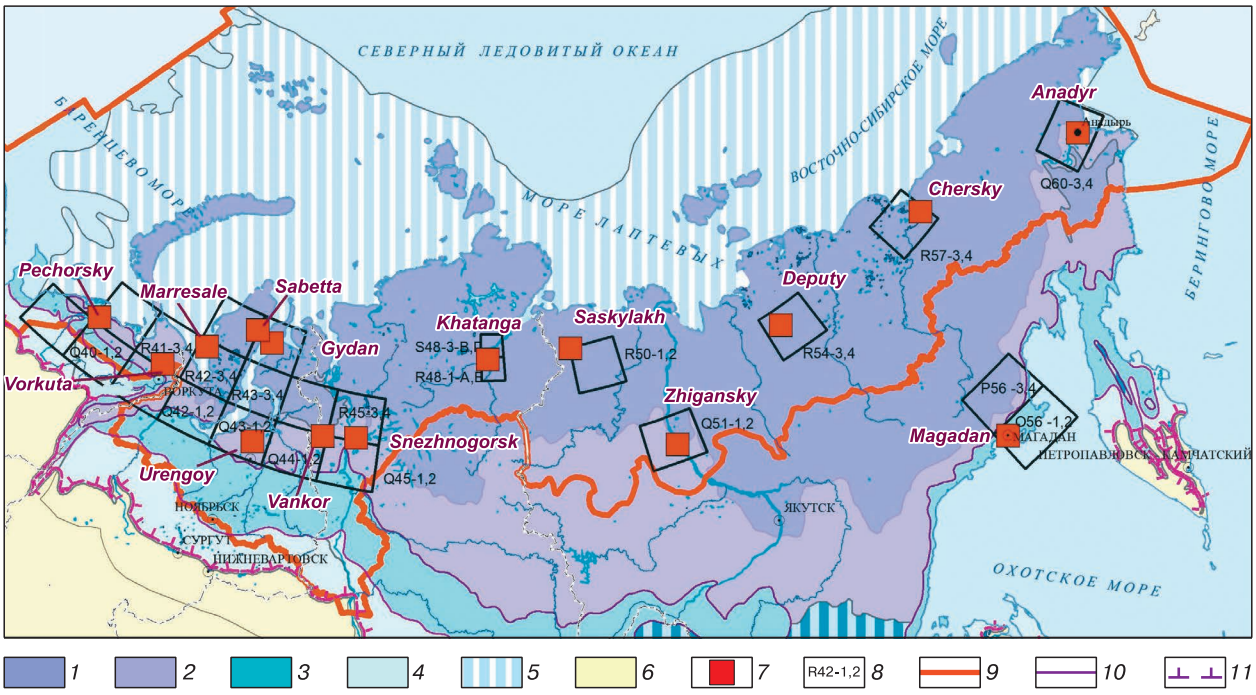

Fig. 3. Layout for the distribution of geocryological polygons for state permafrost monitoring on the Geocryological Map of Russian Federation.

Geocryological zones: (*1*) continuous permafrost (mean annual ground temperature below –5°C), (*2*) continuous permafrost (–1...–5°C), (*3*) discontinuous and sporadic permafrost, (*4*) isolated permafrost, (*5*) subsea permafrost, (*6*) no permafrost. Monitoring network: (*7*) geocryological polygons and their names, (*8*) topographic map sheets 1:500,000 scale selected for the substantiation of monitoring objects. Boundaries: (*9*) Arctic Zone of the Russian Federation, (*10*) geocryological zone, and (*11*) permafrost distribution.

Arkhangelsk (and/or Syktyvkar), Vorkuta, Salekhard, Norilsk, Yakutsk, and Magadan (Anadyr).

The proposed for implementation in FEC monitoring system should integrate regional observation networks of polygons, stations, permafrost stations and analytical centers; data from the geological and technical operation systems of fuel and energy companies; and design and technological enterprises for the reconstruction and restoration of buildings and constructions in the regions. The system will be able to provide forecasts of the state of permafrost for state and private economic entities in the regions, the government of the Russian Federation, federation subjects, and municipalities.

To obtain practical production results from the use of data collected at disparate fuel and energy facilities, it is necessary to combine the monitoring systems of individual fuel and energy enterprises into one software-analytical system [*Zhdaneev et al., 2021*] with the ability to predict changes in the weeks to several years within the boundaries of the constituent entities of the Russian Federation.

The FEC monitoring system should serve as the basis for the planned system for permafrost monitoring on a countrywide scale (Fig. 4). According to estimates, about 10–12 billion rubles are required for the deployment of a monitoring system nationwide, and about 5 billion rubles for the annual maintenance of its operation.

While assessing the costs for the creation and maintenance of the infrastructure and observation network of boreholes at stations and polygons, they were divided into two groups: (1) European and West Siberian and (2) East Siberian and Far East. This is because these macro-regions differ significantly in the structure and thickness of permafrost.

CONCLUSIONS

Since the 1970s, Russian permafrost has been experiencing continuous impact of the ascending branch of global climate fluctuations. FEC enterprises, one of the largest economic entities in the AZRF, are affected by changing permafrost, which requires considering not only its current state but also future characteristics. At present, however, it is impossible to perform a reliable forecast of changes in the permafrost state for a period of three to four years, which is necessary to ensure the uninterrupted operation of the existing infrastructure of the FEC and the development of new investment projects in the permafrost

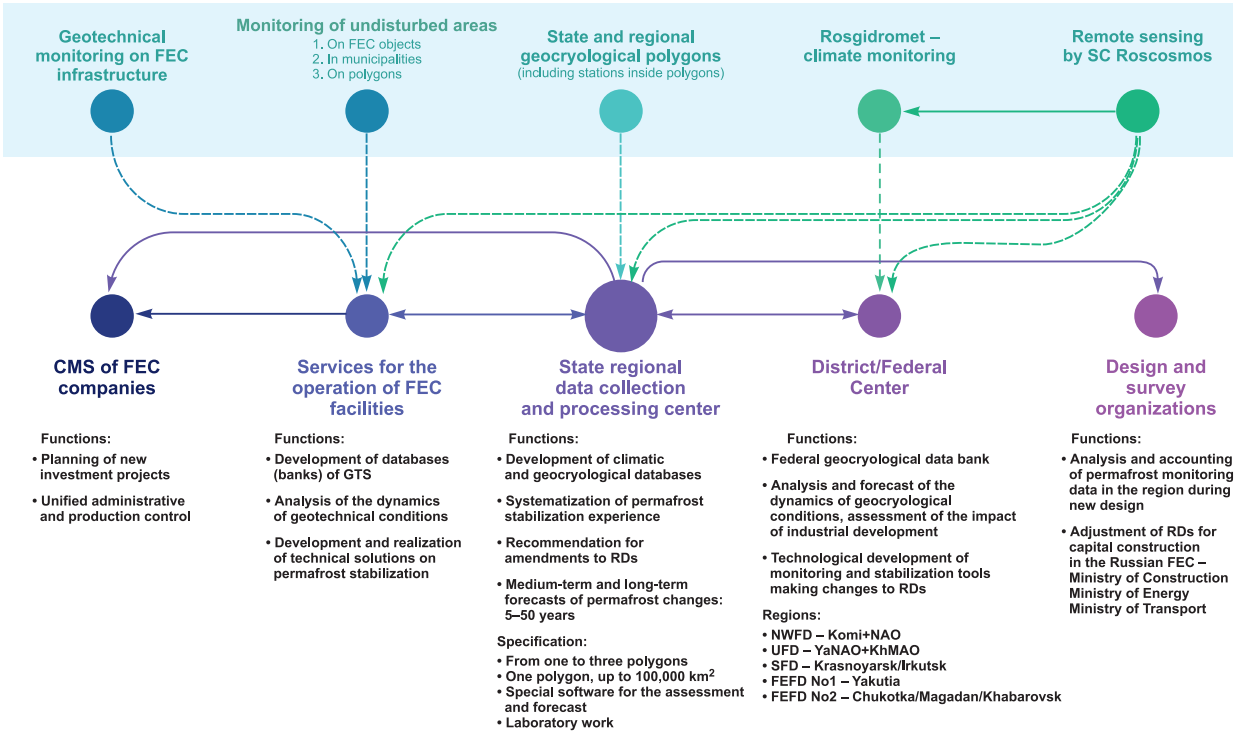

Fig. 4. Permafrost monitoring system on FEC objects as a part of general monitoring of the cryolithozone.

FEC – fuel- and energy complex, CMS – central management system, GTS – geological and technical supervision, RD – regulation documents, SC – state corporation, NWFD – Northwestern Federal District, UFD – Ural Federal District, SFD – Siberian Federal District, FEFD – Far Eastern Federal District, NAO – Nenets Autonomous Okrug, YaNAO – Yamalo-Nenets Autonomous Okrug, KhMAO – Khanty-Mansi Autonomous Okrug.

zone of Russia. This is because of the lack of integrated systems of permafrost monitoring data both on undisturbed natural areas and human-disturbed areas and construction objects (geotechnical monitoring).

Monitoring of undisturbed areas in the Russian permafrost zone is carried out by institutions of the Ministry of Natural Resources of the Russian Federation, the Russian Academy of Sciences, and the Ministry of Education and Science of the Russian Federation at a limited number of observation sites. The length of observation series reaches 50 years, but the overall coverage of observations of the diversity of natural conditions in the Russian permafrost zone is clearly insufficient.

Geotechnical monitoring, including temperature measurements, is carried out by the FEC companies and other regional production organizations and municipalities using various methods, often incompletely and without considering natural trends, adequate analysis of obtained data, and forecast of possible consequences, and also in the absence of an interdepartmental data exchange system.

The possibility of a reliable forecast of changes in the permafrost state for the medium (15–50 years) and long (over 50 years) terms is limited by the lack of data exchange on monitoring of undisturbed areas and geotechnical monitoring between the FEC companies, as well as between the regions and at the federal level. This situation takes place against the background of extreme insufficiency of permafrost monitoring data in all regions of economic activity.

An important part of adaptation to climate change in the future should be the system of state inter-departmental monitoring of permafrost, including both the analysis of background and geotechnical observations and the development of forecasts and technical solutions for engineering protection and environmental measures for the adoption of management decisions [*Dubrovin et al., 2019*]. The corresponding *Concept for the Study and Monitoring of Permafrost in Connection with the Development of the Arctic Zone of the Russian Federation* was developed and approved by the scientific councils of the country's leading universities and academic institutions [*Melnikov et al., 2018, 2021*]. The system should be created stepwise and meet the needs of economic management and rational environmental management, primarily solving the problems of preventing environmental accidents and making investment decisions for the development and reconstruction of fuel and energy facilities on permafrost, as well as the infrastructure of other business entities and municipalities.

Given the scale of the AZRF and new climate challenges, the reorganization of existing departmental permafrost monitoring systems requires the ***establishment of a new management structure and a system for financing these works***. Such a structure could be the "Federal Agency for Permafrost" (or "Committee..", as it was in the 1930s) under the Government of the Russian Federation, with the authority to ensure the creation of an interdepartmental monitoring system in the Arctic with the integration of networks of various departments and enterprises into it, with related legal rights. The most important component of this concept is the ***establishment of a federal (interdepartmental) analytical center and at least six regional branches in large cities of the Arctic***. This is necessary for the collection and analysis of data and development of forecasts and technical solutions to ensure the sustainability of industrial and civil infrastructure on a unified methodological and instrumental-analytical basis. Such centers can be created based on existing specialized institutions that have the appropriate personnel, scientific and industrial base. However, it is necessary to strengthen them with highly qualified geocryologists and appropriate material and technical support.

At the stage of preparation for the implementation of the monitoring program, it is necessary to develop regulatory and methodological documents (GOSTs, requirements, recommendations, instructions, etc.), without which it is impossible to imagine scientifically based unification of the construction of the observation network, processing of monitoring information, and development of state geocryological forecasts.

Given the interdisciplinarity and complexity of tasks for monitoring and predicting permafrost changes, searching for optimal engineering solutions for permafrost stabilization, it is advisable to create an interdepartmental working group under the Government of the Russian Federation with the involvement of representatives of relevant ministries, fuel and energy companies, specialized institutes of the Russian Academy of Sciences, institutions belonging to the Ministry of Higher Education and Science, and representatives of northern administrations for a broad discussion of the issue and establishment of a pilot regional project for a system of state interdepartmental monitoring of permafrost [*Dubrovin et al., 2019*].

The pilot project is proposed to be implemented in the form of a regional system for permafrost monitoring at FEC facilities based on the individual regions of the Russian Federation, where permafrost occupies a significant part of the area and where the problems of climate change, permafrost degradation, and sustainability of buildings and engineering constructions are the most relevant. Pilot regions can be the Yamalo-Nenets Autonomous Okrug, the Nenets Autonomous Okrug, the Krasnoyarsk Krai, the Republic of Sakha (Yakutia), and other regions.

If properly implemented, the system of state permafrost monitoring can significantly reduce, and in some cases eliminate the technical, economic, and environmental risks of the development of the Arctic territories of the Russian Federation. But it should not be forgotten that the accuracy of the assessment of the permafrost state and the need for long-term forecasts of changes in the environment and climate largely depend on fundamental research of the entire Earth's cryosphere.

References

Annual Report on the Activities of the Federal Service for Environmental, Technological, and Nuclear Supervision in 2019. – https://www.gosnadzor.ru/public/annual_reports/Годовой%20отчет%20о%20деятельности%20Ростехнадзора%20в%202019%20году.pdf (accessed: May 29, 2022) (in Russian).

Bondarik G.K., 1981. General Theory of Engineering (Physical) Geology. Moscow, Nedra, 256 p. (in Russian).

Bondarik G.K., 1993. Socio-environmental issues and engineering geology. *Geoekologiya,* No. 4, 27–31 (in Russian).

Conclusion of RAS: Draft of the Federal Law *On Amendments to Certain Legislative Acts of the Russian Federation Regarding the Establishment of a State System for Permafrost Monitoring* / Vice President of RAS V.N. Parmon (23 July 2021). Novosibirsk, Izd. SB RAS, 2 p. (in Russian).

Drozdov D.S., 2004. Information and Cartographic Modeling of Natural and Man-made Environments in Geocryology. Doctoral (Geol.) Diss., Tyumen, 409 p. (in Russian).

Drozdov D.S., Dubrovin V.A., 2016. Environmental problems of oil and gas exploration and development in the Russian Arctic. *Earth's Cryosphere* XX (4), 14–25.

Dubrovin V.A., Brushkov A.B., Drozdov D.S., Zheleznyak M.N., 2019. Knowledge, current state, prospects, and problems of development of the Arctic cryolithozone. *Mineral. Resursy Rossii. Ekonomika Upravlen.* **166** (3), 55–64 (in Russian).

Gromadsky A.N., Aref'ev S.V., Volkov N.G. et al., 2019. Remote monitoring of temperature conditions of permafrost soils under Salekhard buildings. *Nauchn. Vestn. YaNAO,* No. 3, 7–21. DOI: 10.26110/ARCTIC.2019.104.3.003 (in Russian).

Harris S., Brouchkov A., Cheng G., 2017. Geocryology: Characteristics and Use of Frozen Ground and Permafrost Landforms. United Kingdom, Taylor & Francis, 766 p. DOI: 10.4324/9781315166988.

Kamnev Y.K., Filimonov M.Y., Shein A.N., Vaganova N.A., 2021. Automated monitoring the temperature under buildings with pile foundations in Salekhard (preliminary results). *Geogr. Environ. Sustainability* **14** (4), 75–82. DOI: 10.24057/2071-9388-2021-021.

Kryukov V.A., 2020. On the interconnection and interaction of economic, industrial and scientific and technological policies. *Upravl. Naukoi: Teoriya i Praktika,* No. 2, 15–46. – https://doi.org/10.19181/smtp.2020.2.2.1 (in Russian).

Makarycheva E.M., Ibragimov E.R., Kuznetsov T.I., Shurshina K.Yu., 2019. Application of aerial laser scanning for geotechnical monitoring of trunk pipeline facilities. *Sci. Technol. Oil Petroleum Products Pipeline Transport,* No. 9, 21–31. DOI: 10.28999/2541-9595-2019-9-1-21-31.

Malik L.K., 2005. Risk Factors for Damage to Hydraulic Structures. Safety Concerns. Moscow, Nauka, 354 p. (in Russian).

Malkova G., Drozdov D., Vasiliev A. et al., 2022. Spatial and temporal variability of permafrost in the western part of the Russian Arctic. *Energies* **15** (7), 2311. DOI: 10.3390/en15072311.

Melnikov E.S. (Ed.), 1983. Landscapes of the Cryolithozone of the Western Siberian Gas-Bearing Province. Novosibirsk, Nauka, 165 p. (in Russian).

Melnikov V.P., Osipov V.I., Brushkov A.V. et al., 2021. Assessment of damage to residential and industrial buildings and structures during temperature changes and thawing of permafrost soils in the Arctic zone of the Russian Federation by the middle of the 21st century. *Geoekol. Inzhen. Geol., Gidrogeol., Geokriol.*, No. 1, 14–31. DOI: 10.31857/S0869780921010070 (in Russian).

Melnikov V.P., Trofimov V.T., Orlov V.P. et al., 2018. The development and adoption of the doctrine of studying "permafrost" is a necessary element of the development strategy of the AZRF. *Region. Energetika Energosberezhen*, No. 1, 40–41 (in Russian).

PJSC Transneft, 2022. Some messages of the First Vice-President of PJSC Transneft M.S. Grishanin during a teleconference with investors and analysts on 18.02.2022 (accessed: July 19, 2022). – https://www.transneft.ru/news/view/id/38511/ (in Russian).

Popova A.A., 2012. Geoinformation Cartographic Modeling of Engineering and Geocryological Conditions in the North of the Timan-Pechersk Oil and Gas Province along the Upper Horizon of the Permafrost. Cand. Sci. (Geol.) Diss., Tyumen, 139 p. – https://rosrid.ru/dissertation/detail/ekOdZnRWzxbi6TwyGJmrUBL8 (in Russian).

Rivkin F.M., Kuznetsova I.L., Ivanova N.V. et al., 2010. Multipurpose engineering geological cartographic for information support for engineering surveys, designing, and monitoring. In: Proc. 11th Congress of the IAEG, Auckland, New Zealand, 5–10 Sept. 2010. Auckland, CRC Press, p. 2415–2419.

Smith S.L., Romanovsky V.E., Isaksen K. et al., 2021. Permafrost. In: State of the Climate in 2020. *Bull. Amer. Meteor. Soc.* **102** (8), 293–297. DOI: 10.1175/BAMS-D-21-0086.1.

SP [Set of rules] 22.13330.2016, 2016. Soil Bases of Buildings and Structures. Moscow, Minstroy, 225 p. – https://docs.cntd.ru/document/456054206 (in Russian).

SP [Set of rules] 305.1325800.2017, 2017. Buildings and Structures. The Rules of Geotechnical Monitoring under Construction. Moscow, Standartinform. – https://www.minstroyrf.gov.ru/upload/iblock/a03/SP-497.pdf (in Russian).

SP [Set of rules] 25.13330.2020, 2020. Soil Bases and Foundations on Permafrost. Moscow, Minstroy. – http://sniprf.ru/sp25-13330-2020 (in Russian).

SP [Set of rules] 497.1325800.2020., 2020. Soil Bases and Foundations of Buildings and Structures on Permafrost. Moscow, Minstroy, 30 p. – http://sniprf.ru/sp25-13330-2020 (in Russian).

STO [Organization Standard] Gazprom 2-3.1-072-2006, 2006. Regulations for Geotechnical Monitoring of Gas Complex Facilities in the Permafrost Zone. Moscow, TyumenNIIgiprogas, 61 p. – https://samara-tr.gazprom.ru/d/textpage/8e/142/sto-gazprom-2-3.5-046-2006.pdf (in Russian).

TASS, 2022. The first station of the permafrost state monitoring network in Russia will be created on Hayes Island. – https://tass.ru/obschestvo/11802477 (accessed: May 29, 2022) (in Russian).

Tikhonov S., 2020. Will Russia be able to increase LNG production. *Rossiyskaya gazeta: Ekonomika,* Jan. 8, 2020. – https://rg.ru/2020/01/08/smozhet-li-rossiia-narastit-proizvodstvo-spg.html (in Russian).

Zhdaneev O., Frolov K., Petrakov Y., 2021. Predictive systems for the well drilling operations. In: Cyber-Physical Systems: Design and Application for Industry 4.0, New York, Springer, vol. 342, 347–368. DOI: 10.1007/978-3-030-66081-9_28.

Zhdaneev O.V. (Ed.), 2020. Issues of Technical Policy of the Fuel and Energy Sector of the Russian Federation. Moscow, Nauka, 304 p. – https://doi.org/10.7868/9785020408241 (in Russian).

Received April 11, 2022
Revised July 7, 2022
Accepted July 19, 2022

Translated by Yu.A. Dvornikov

EARTH'S CRYOSPHERE
SCIENTIFIC JOURNAL

Earth's Cryosphere, 2022, vol. XXVI, No. 4, pp. 16–31

REGIONAL AND HISTORICAL GEOCRYOLOGY

ORIGIN AND ISOTOPIC COMPOSITION OF PRECIPITATION AT EXTREMELY LOW TEMPERATURES IN YAKUTSK (EASTERN SIBERIA)

A.A. Galanin, M.R. Pavlova*, A.N. Vasil'eva, G.I. Shaposhnikov, N.V. Torgovkin**

Melnikov Permafrost Institute, Siberian Branch of the Russian Academy of Sciences, ul. Merzlotnaya 36, Yakutsk, 677010 Russia

**Corresponding author; e-mail: nigaer@yandex.ru*

***Corresponding author; e-mail: nick1805torg@gmail.com*

Isotopic (^{18}O, D) and chemical composition of atmospheric precipitation (1–2-cm snow layer on the surface of the snow cover and crystalline hoar) that fell in December 2020–January 2021 under anticyclonic weather, extremely low temperatures (–47 to –52°C) and dense ice fogs has been studied at six sites along a 25-km profile from Yakutsk. Samples from the surface of the snow cover are characterized by the lightest compositions (δ^{18} = –41.04 ± 5.11‰, δD = –326.43 ± 34.16‰, d_{exc} = 1.91 ± 7.72‰) and are noticeably depleted of deuterium. From the suburbs to the center of Yakutsk, a significant weighting of the isotopic compositions (by 10‰ for δ^{18}O and 80‰ for δD), a decrease in d_{exc} (from +10 to –6‰), and a fourfold increase in mineralization due to impurities of calcium carbonate have been found. The isotopic compositions of the samples of crystalline rime (δ^{18}O = –30.89 ± 5.62‰, δD = –285.88 ± 12.82‰, d_{exc} = –28.79 ± 32.53‰) notably differ from the isotopic compositions of other forms of atmospheric precipitation, water, and ice in the studied region. These samples display the greatest variations in δ^{18}O (from –24‰ in Yakutsk to –37‰ at a distance of 25 km from its center), δD (from –255.4 to –285.9‰), and d_{exc} (from –80 to +11.5‰). The isotopic and chemical compositions of the investigated precipitation indicate a significant proportion of technogenic water vapor entering the atmosphere during the combustion of hydrocarbon fuel. Based on the model of the Gaussian mixture and deuterium excess of the studied samples, it has been found that the maximum share of technogenic moisture in crystalline hoar reaches 26–32% near heat-generating stations; it decreases to 13–18% in the central part of the city and to 6.5–8.8% in the suburbs. In the surface layer of the snow cover, it reaches 5–6% in the central part of Yakutsk and decreases to 1% or less in the suburbs.

Keywords: *stable isotopes of water, atmospheric precipitation, snow, crystalline hoar, ice fog, low temperatures, technogenic sources of precipitation, fractionation, Yakutsk, Eastern Siberia.*

Recommended citation: Galanin A.A., Pavlova M.R., Vasil'eva A.N., Shaposhnikov G.I., Torgovkin N.V., 2022. Origin and isotopic composition of precipitation at extremely low temperatures in Yakutsk (Eastern Siberia). *Earth's Cryosphere*, XXVI (4), 16–31.

INTRODUCTION

In cold regions with a sharply continental climate, a decrease in temperature below –35...–40°C is often accompanied by specific atmospheric precipitation: arctic haze, ice (frosty) fogs, and crystalline hoar. These types of precipitation are formed during clear anticyclonic weather by the condensation of water vapor from an extremely dehydrated and supercooled atmosphere.

Ice fogs and crystalline hoar are constantly observed in Antarctica [*Ekajkin, 2016*], the continental regions of Alaska and Canada [*Bowling et al., 1968*], northern Europe [*Gallagher, 2020*], Siberia [*Shver, Izyumenko, 1982*], northern China [*Xing et al., 2020*], and other regions (Fig. 1). They have a strong negative impact on all types of ground and air transport, obstruct visibility, lead to icing of aircraft and power transmission lines.

It is generally accepted that the main causes of ice fog are the advection of cold air masses and associated vertical temperature inversions, which contribute to the deep cooling of the lower troposphere [*Bowling et al., 1968; Gallagher, 2020*]. However, the densest ice fog and severe frost occur more often within large settlements and are the result of burning of various types of fuel [*Bowling et al., 1968; Shver, Izyumenko, 1982; Xing et al., 2020*]. Emissions of dust, soot, and combustion aerosols further contribute to the formation of ice fogs, causing the condensation of supercooled atmospheric water even at low relative humidity values [*Gallagher, 2020; Xing et al., 2020*].

In Salt Lake City (USA), during the coldest periods of the year, the proportion of atmospheric water vapor derived from combustion of hydrocarbon fuels (combustion-derived water, CDW) reaches 10–13% [*Gorski et al., 2015; Fiorella et al., 2018*]. In the me-

tropolis of Xi'an (Northeastern China), the average share of CDW in the formation of winter precipitation is 6.2%, reaching 16.2% in some periods [*Xing et al., 2020*]. In absolute terms, about 10 million tons of CDW are emitted into the atmosphere of Xi'an annually, of which 52.5% is derived from combustion of natural gas; 45.8%, from coal; and 1.7%, from other types of hydrocarbons. The emitted CDW has the following isotopic characteristics [*Xing et al., 2020*]: natural gas – $\delta^{18}O = +13.2 \pm 0.7‰$, $\delta D = -160.8 \pm 2.8‰$, $d_{exc} = -266.5 \pm 3.8‰$; black coal – $\delta^{18}O = +4.2 \pm 1.3‰$, $\delta D = -102.2 \pm 16.3‰$, $d_{exc} = -135.5 \pm 26.4‰$. Combustion of various grades of gasoline and diesel fuel results in the formation of the most deuterium-depleted compositions ($-270‰ > d_{exc} > -330‰$). Close values ($-308‰ < d_{exc} < -125‰$) were obtained for CDW in the Salt Lake City area [*Gorski et al., 2015; Fiorella et al., 2018*].

The exotic isotopic composition of the CDW is determined both by the initial isotopic composition of hydrocarbon fuels and by the peculiarities of its oxidation during combustion. Water vapor is formed during the reaction of atmospheric oxygen enriched in ^{18}O atoms ($\delta^{18}O = +23.9‰$) relative to seawater [*Fiorella et al., 2018*] and fuel hydrogen significantly depleted in deuterium due to biochemical reactions during methane synthesis [*Sessions et al., 1999; Whiticar, 1999*]. Therefore, the water vapor formed during combustion is characterized by an unusually low deuterium excess [*Gorski et al., 2015; Fiorella et al., 2018; Xing et al., 2020*] compared to natural atmospheric moisture.

The unnatural, extremely deuterium-depleted isotopic composition of CDW differs sharply from the natural composition of the surface layer of the troposphere, in which the average value of d_{exc} near the dew point is about +10‰ [*Dansgaard, 1964*]. In the upper layers of the troposphere, it reaches +200‰, while in the most evaporatively fractionated surface waters it decreases to –60‰ [*Fiorella et al., 2018*]. The isotopic characteristics of CDW and atmospheric precipitation formed from it make it possible not only to identify the source of their origin but also to approximately estimate the volumes of combusted hydrocarbon fuels for specific areas [*Xing et al., 2020*].

In Yakutsk, a fall in temperature below –40°C is annually accompanied by stagnant phenomena in the atmosphere with the appearance of specific ice fog and crystalline hoar (Fig. 1). Fog density and hoar growth rate increase with decreasing temperature. So, in the central part of Yakutsk at –45°C, visibility does not exceed 1 km; at –50°C, it is no more than 100 m. The period of continuous ice fogs in Yakutsk, as a rule, lasts about 2 months from the beginning of December to the end of January, except for short periods of temperature rise to –40...–35°C. During winter fogs, small ice crystals of about 1 mm in size or less, in the form of needles, plates and six-ray snowflakes, almost continuously settle on the surface of the snow cover, roofs of houses, and branches of trees and shrubs. During this period, tree branches, electrical wires and other thin objects are encrusted with fine crystalline 4- to 5-cm-thick hoarfrost. At the end of winter period, when air temperature rises above –35°C, winter fogs are not formed, and hoarfrost on the trees and other objects gradually disappears as a result of sublimation and shedding.

Fig. 1. Ice fog and crystalline hoarfrost on tree branches regularly observed in Yakutsk and its environs from December to February at temperatures of –35°C and below.

To date, data on the isotopic composition (^{18}O and D) of CDW have been obtained and its significant role in the dynamics of the atmosphere over large megacities has been established [*Beesley, Moritz, 1999; Gorski et al., 2015; Fiorella et al., 2018; Xing et al., 2020*]. At the same time, data on the isotopic composition of atmospheric precipitation formed under conditions of extremely low temperatures are virtually absent.

Data on the isotopic composition of atmospheric precipitation during the coldest season in Yakutsk will be useful for the reconstruction of paleotemperatures based on the analysis of the isotopic composition of polygonal wedge ice.

The purpose of this article is to characterize the features of the formation of the isotopic compositions (^{18}O and D) of atmospheric precipitation falling in Yakutsk at extremely low temperatures. The factual material is the composition of snow cover and crystalline hoarfrost at six sites along a 25-km-long profile from the center of Yakutsk towards its outskirts studied in December 2020–January 2021 (Fig. 2).

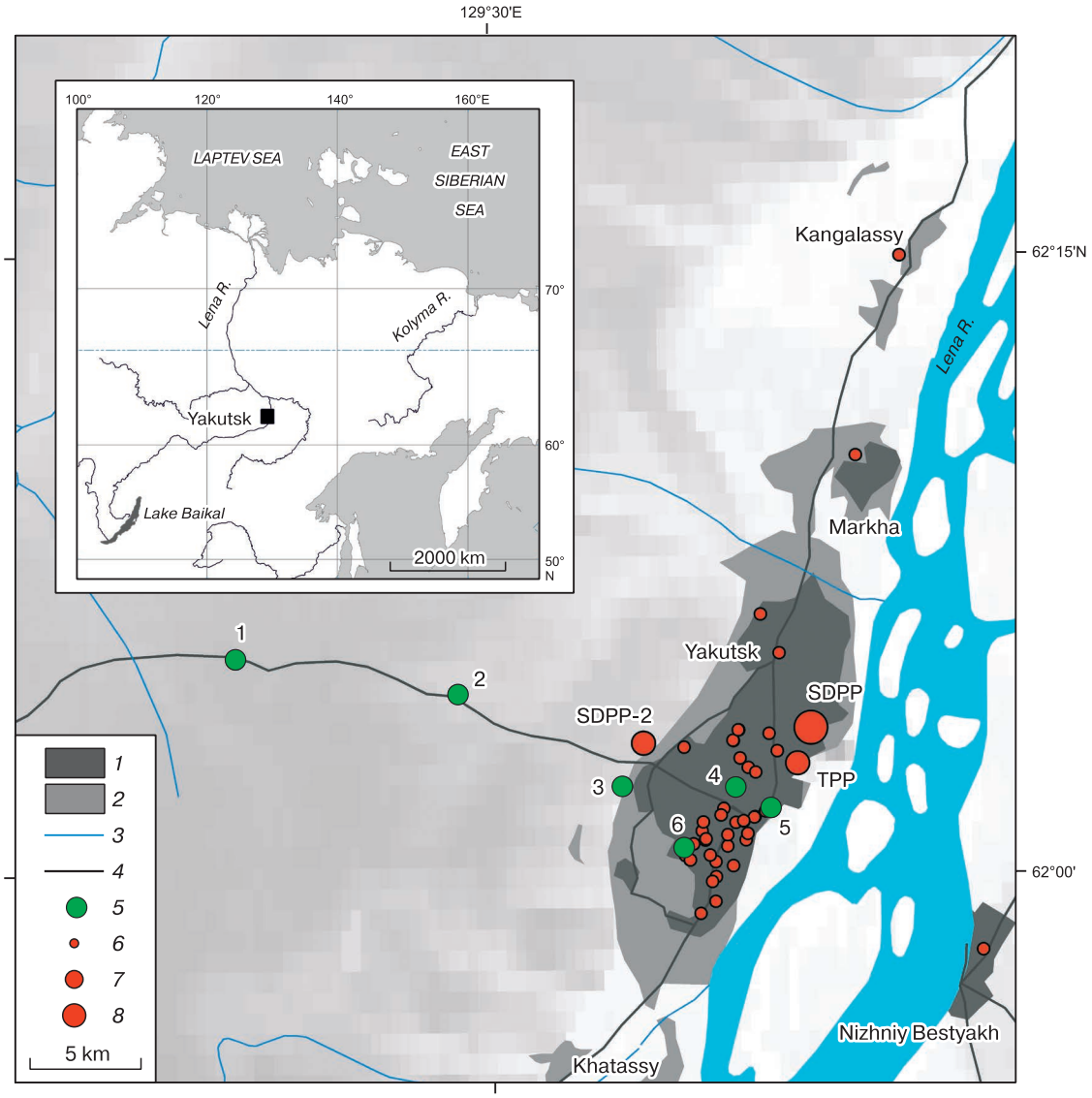

Fig. 2. Scheme of observation points (1–6) for snow cover and hoarfrost in the area of Yakutsk on December 14, 2020 and January 19, 2021.

1 – dense urban development with multistory buildings; *2* – one-story buildings; *3* – rivers; *4* – highways; *5* – observation points and their numbers; *6–8* – the largest sources of technogenic atmospheric emissions in Yakutsk (*6* – small heat generating stations (10–50 Gcal/h); *7* – powerful heat sources (469 and 497 Gcal/h); *8* – the largest heat source (661 Gcal/h)).

RESEARCH METHODS

The analysis of weather conditions for the period of sampling was carried out on the basis of data from the Yakutsk weather station [*Weather and Climate, 2004–2021*]. For the analysis, such indicators as the mean daily temperature (*T*), wind speed, atmospheric pressure, daily precipitation, visibility, and recordings of the thickness of crystalline frost on an ice machine were used. Figure 3 shows the time series of the dynamics of the main meteorological indicators from December 1, 2020 to February 28, 2021 with indication of sampling dates.

Atmospheric precipitation sampling was carried out at six observation points (o.p.) with natural vegetation along the transect stretching from the 25-th kilometer of the Vilyui tract to the center of Yakutsk (Fig. 2). The sampling was performed on December 14, 2020 (o.p. 6) and January 19, 2021 (o.p. 1–5) during peak air temperature drops to –48.0 and –50.9°C (Fig. 3). At each observation point, at least four precipitation samples were taken, including two hoarfrost samples from tree branches at a height of 1.0–2.0 m from the earth's surface, one precipitation sample from the snow cover surface (0–2 cm), one

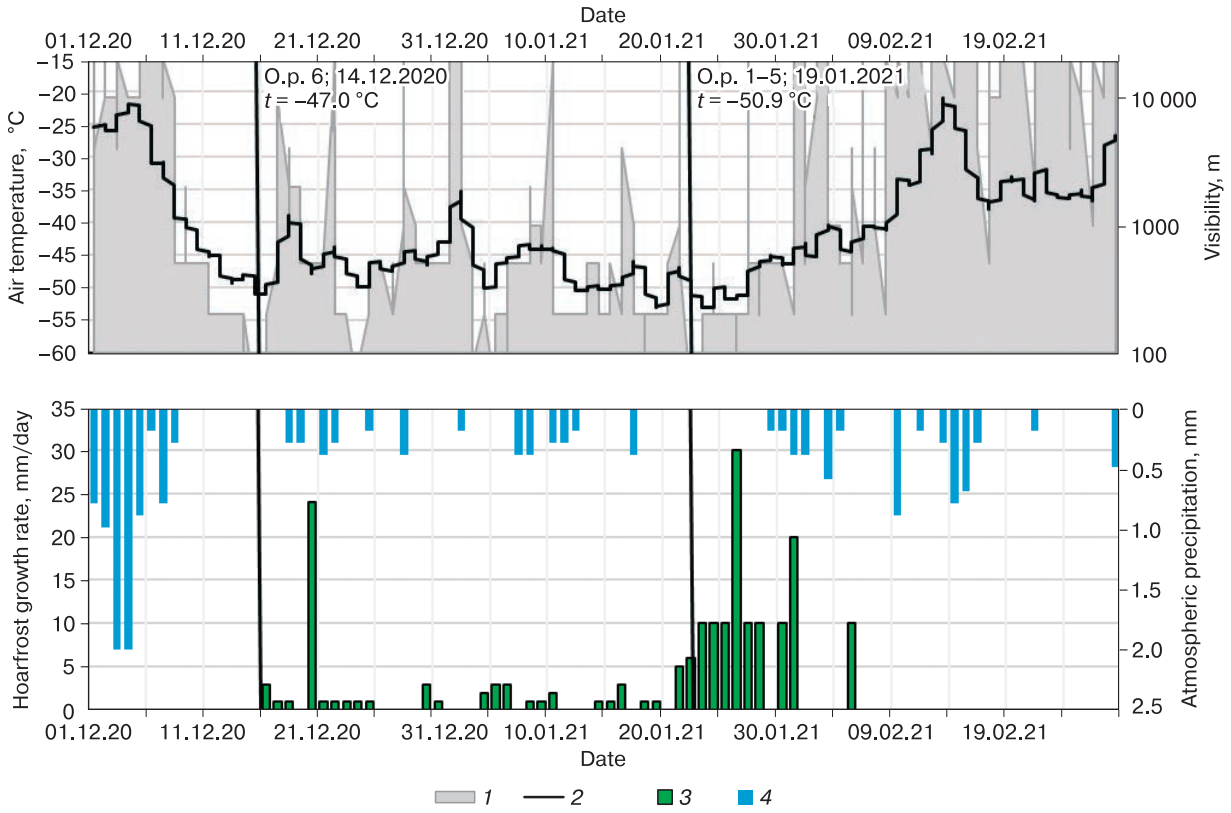

Fig. 3. Weather conditions in Yakutsk from December 1, 2020 to February 28, 2021 according to [*Weather and Climate, 2004–2021*].

1 – visibility; *2* – air temperature; *3* – growth rate of crystalline hoar; *4* – snow; o.p. – observation point.

averaged snow sample from the depth of 2–20 cm. The average thickness of the snow cover at the time of sampling was approximately the same at all sites (25–30 cm).

Observation point 1 (62°05′ N, 129°16′ E; 254 m a.s.l.) is located on the 25th kilometer of the Vilyui tract at a distance of 250 m from the highway, on the edge of a birch grove and a meadow. Weather conditions at the time of sampling: T = –52°C, calm, fog, maximum visibility 250–300 m.

Observation point 2 (62°04′ N, 129°28′ E; 219 m a.s.l.) is located on the 10th kilometer of the Vilyui tract at a distance of 200 m from the road, within a sparse birch grove. Weather conditions at the time of sampling: T = –52°C, calm, fog, maximum visibility 150–200 m.

Observation point 3 (62°02′ N, 129°36′ E; 158 m a.s.l.) is located on the suburbs of Yakutsk under the slope of Mount Chochur Muran at a distance of 200 m from the road, on the edge of a birch grove and meadow steppe. Weather conditions are similar to those at o.p. 1.

Observation point 4 (62°02′ N, 129°42′ E; 120 m a.s.l.) is located near the center of Yakutsk within a birch grove. Weather conditions at the time of sampling: T = –52°C, calm, fog, maximum visibility 100–150 m.

Observation point 5 (62°01′ N, 129°44′ E; 98 m a.s.l.) is located in the center of Yakutsk on the territory of a front garden with birch trees. Weather conditions at the time of sampling are similar to those at o.p. 4.

Observation point 6 (62°01′ N, 129°40′ E; 98 m a.s.l.) is located 20 m from the building of the Melnikov Permafrost Institute, Siberian Branch, Russian Academy of Sciences (MPI SB RAS), 100 m from the boiler house of the MPI SB RAS. Sampling was carried out within a birch grove. Weather conditions at the time of sampling: T = –48°C, calm, fog, maximum visibility 150–200 m.

The collected samples were packed in 10-mL airtight plastic bags and delivered to the laboratory of the MPI SB RAS. Next, the samples were melted at room temperature, poured into plastic cuvettes, and stored in a refrigerator at +5°C. Samples were analyzed within 1–2 weeks after sampling.

For the chemical analysis of snow and frost, samples were taken into plastic bags, melted at room temperature, and packed into 0.5-L plastic bottles prepared according to [*GOST 31861-2012, 2013*].

Taking into account the possibility of the influence of technogenic sources of water vapor on the formation of the isotopic compositions of the samples, the authors carried out mapping of the main heat generating stations of Yakutsk (Fig. 2). Among them, the largest are the Yakutsk Thermal Power Plant (SPP) (497 Gcal/h), State District Power Plant (SDPP) (661 Gcal/h), and SDPP-2 (469 Gcal/h). In addition, there are 45 more boiler houses with a capacity of 10 to 50 Gcal/h. All heat generating stations in Yakutsk operate on gaseous or liquid fuels and reach full capacity during the period of the lowest winter temperatures.

Analysis of the composition of stable isotopes (^{18}O and D) was carried out in the Russian–German Isotope Laboratory of the MPI SB RAS (Yakutsk) by laser absorption IR spectrometry on an automated complex PICARRO L2140-i with the technology of resonator ring spectroscopy CRDS (Cavity Ring Down Spectroscopy). The adopted internal water standards (MilliQ A-45, HDW-1, MXW, HGL-1, SEZ-2) and the AWIPotsdam protocol of the Stable Isotope Laboratory of the Alfred Wegener Institute (Potsdam, Germany) were applied. The reproducibility of δ^{18}O and δD measurements was ±0.04 and ±0.1‰, respectively (standard deviation 1σ, n = 6, measurement time 100 s).

Calibration was performed at least three times per standard run of a cassette of 33 liquid samples. At the end of the analysis, the 1σ values for δ^{18}O and δD were corrected for the combined standard deviation based on the method [*van Geldern, Barth, 2012*], which makes it possible to achieve a reproducibility of more than 0.01‰. A total of 26 samples were analyzed (Table 1).

Analysis of the ionic composition and other chemical properties of crystalline hoarfrost and snow samples was carried out by routine methods

Table 1. **Isotopic compositions of samples of fine crystalline hoarfrost and snow cover in the vicinity of Yakutsk in December 2020 – January 2021**

Observ. Point-Sample	δ^{18}O,‰	1σ,‰	δD,‰	1σ,‰	d_{exc}	Sample nature
				Site 1		
1-1	–36.60	0.02	–285.89	0.04	6.90	Hoarfrost on birch branches at a height of 1–2 m
1-2	–35.85	0.02	–286.55	0.04	0.21	Hoarfrost on birch branches at a height of 1–2 m
1-3	–45.04	0.01	–349.92	0.08	10.36	Snow cover surface (0–2 cm)
1-4	–30.31	0.02	–224.22	0.03	18.26	Average snow stock (2–20 cm)
				Site 2		
2-1	–37.42	0.02	–289.46	0.01	9.93	Hoarfrost on birch branches at a height of 1–2 m
2-2	–37.99	0.02	–292.34	0.06	11.57	Hoarfrost on birch branches at a height of 1–2 m
2-3	–46.45	0.02	–361.72	0.10	9.86	Snow cover surface (0–2 cm)
2-4	–31.05	0.02	–230.51	0.04	17.88	Average snow stock (2–20 cm)
				Site 3		
3-1	–35.35	0.01	–290.04	0.01	–7.27	Hoarfrost on willow branches at a height of 1–2 m
3-2	–33.72	0.02	–284.13	0.05	–14.36	Hoarfrost on willow branches at a height of 1–2 m
3-3	–45.01	0.01	–354.02	0.01	6.06	Snow cover surface (0–2 cm)
3-4	–29.36	0.01	–222.16	0.04	12.75	Average snow stock (2–20 cm)
				Site 4		
4-1	–30.77	0.01	–273.97	0.07	–27.84	Hoarfrost on birch branches at a height of 1–2 m
4-2	–30.18	0.01	–271.73	0.02	–30.27	Hoarfrost on birch branches at a height of 1–2 m
4-3	–38.37	0.01	–313.55	0.01	–6.55	Snow cover surface (0–2 cm)
4-4	–28.03	0.01	–213.66	0.02	10.61	Average snow stock (2–20 cm)
				Site 5		
5-1	–31.71	0.01	–279.85	0.03	–26.20	Hoarfrost on birch branches at a height of 1–2 m
5-2	–29.30	0.01	–271.83	0.02	–37.44	Hoarfrost on birch branches at a height of 1–2 m
5-3	–37.37	0.01	–304.05	0.05	–5.06	Snow cover surface (0–2 cm)
5-4	–28.65	0.01	–219.13	0.05	10.06	Average snow stock (2–20 cm)
				Site 6		
6-1	–22.95	0.01	–261.52	0.11	–77.93	Hoarfrost on a metal fence at a height of 1.5 m
6-2	–24.22	0.04	–260.74	0.10	–66.94	Hoarfrost on birch branches at a height of 1–2 m
6-3	–22.13	0.01	–258.78	0.10	–81.70	Hoarfrost on birch branches at a height of 1–2 m
6-4	–24.21	0.01	–255.41	0.05	–61.73	Hoarfrost on the roof of a car at a height of 1.5 m
6-5	–34.02	0.01	–275.36	0.10	–3.21	Snow cover surface (0–2 cm)
6-6	–29.30	0.01	–221.26	0.02	13.14	Average snow stock (2–20 cm)

Table 2.

Chemical composition of crystalline hoar and snow cover in Yakutsk in January 2021

Observ. Point-Sample	pH	Eh	Concentrations of main cations and anions, mg/L										Hardness, meq/L	Mineralization, g/L	Chemical type (according to A.V. Shchukarev)	Concentrations of microcomponents, mg/L				
			Ca^{2+}	Mg^{2+}	Na^{+}	K^{+}	NH_4^{+}	HCO_3^{-}	SO_4^{2-}	Cl^{-}	NO_2^{-}	NO_3^{-}				Sr^{2+}	Li^{+}	Ba^{2+}	HPO_4^{-}	F^{-}
1-2	7.28	556	4.08	2.11	0.4	0.10	1.90	24.95	2.30	0.69	0.03	4.00	0.380	0.0417	HCO_3 76/Ca 38 Mg 32	0.659	0.000	0.000	0.235	0.249
1-4	7.70	543	0.76	0.46	0.1	0.0	0.1	4.49	0.40	0.17	0.01	0.70	0.075	0.0073	HCO_3 74/Ca 43 Mg 43	0.000	0.016	0.000	0.049	0.040
2-2	7.17	545	4.53	0.46	0.2	0.05	0.5	13.97	1.8	0.52	0.01	1.00	0.264	0.0233	HCO_3 76/Ca 73	0.000	0.094	0.000	0.025	0.120
2-4	7.38	544	1.53	0.64	0.1	0.1	0.2	6.99	0.4	0.21	0.01	0.70	0.128	0.0109	HCO_3 74/Ca 50 Mg 35	0.000	0.025	0.000	0.026	0.017
3-2	6.64	517	18.12	3.67	0.4	2.00	5.00	79.85	8.00	3.46	0.10	8.00	1.206	0.1294	HCO_3 75/Ca 55	0.731	0.000	0.061	0.022	0.022
3-4	7.33	485	5.13	1.01	0.4	0.2	0.9	19.96	0.70	0.35	0.01	1.30	0.339	0.0306	HCO_3 88/Ca 60	0.283	0.000	0.000	0.015	0.297
4-2	7.20	443	18.12	1.83	0.5	1.5	5.7	74.86	9.0	1.73	0.15	5.00	1.055	0.1202	HCO_3 79/Ca 59	1.399	0.000	0.059	0.271	0.049
4-4	7.63	433	12.08	0.92	0.4	0.65	2.80	45.91	2.50	1.21	0.20	2.10	0.678	0.0699	HCO_3 85/Ca 65	0.450	0.000	0.000	0.042	0.655
5-2	7.81	393	27.18	0.92	1.3	4.6	7.5	105.3	13.40	2.25	0.20	8.00	1.432	0.1725	HCO_3 78/Ca 63	0.567	0.000	0.072	0.042	1.200
5-4	7.73	403	12.84	1.01	2.2	1.80	3.40	48.91	3.30	2.94	0.20	2.50	0.723	0.0804	HCO_3 80/Ca 57	0.532	0.000	0.033	0.435	0.435

in the certified laboratory of the Melnikov Permafrost Institute, Siberian Branch of the Russian Academy of Sciences. In total, ten samples were analyzed (Table 2).

Isotopic and chemical compositions of sediments at extremely low temperatures

The isotopic composition (δD and $\delta^{18}O$) of the entire set of samples (26 samples) is characterized by great variability both within one observation point depending on the type of sample (Table 1) and along the studied profile. On Fig. 4*a*, the entire sample is clearly divided into two linearly elongated sets of points. The first one is formed by samples of averaged snow cover (from a depth of 2–20 cm) and is described by the equation $\delta D = 8.38 \cdot \delta^{18}O + 24.98$ ($R^2 = 0.99$, $n = 12$), the coefficients of which are close to the equation $\delta D = 8.17 \cdot \delta^{18}O + 21.9$ ($R^2 = 0.99$, $n = 8$) obtained by T.S. Papina et al. [*2017*] for winter precipitation in 2014 in Yakutsk. On the whole, these equations point to the location of these compositions near the main meteoric water line (MMWL), which indicates their natural (atmospheric) origin under the conditions of kinetic (Rayleigh) fractionation. The second linear set is formed by samples of crystalline hoarfrost and surface snow (from a depth of 0–2 cm) and is extrapolated by the equation $\delta D = 2.22 \cdot \delta^{18}O - 206.9$ ($R^2 = 0.96$, $n = 14$), the coefficients of which indicate an unnatural source of atmospheric moisture, extremely depleted of deuterium. On Fig. 4*b*, all the studied compositions and the regressions approximating them are shown separately depending on the type of samples, which makes it possible to assess their role in the isotopic structure of the entire sample.

The samples of the average snow stock (2–20 cm) are characterized by the heaviest composition compared to the other samples ($\delta^{18}O$ = = −29.45 ± 1.1‰, δD = −221.8 ± 5.57‰, d_{exc} = = 13.78 ± 3.52‰). Their position near the local meteoric water line (LMWL) (Fig. 4*b*) and positive deuterium kurtosis (close to 10) indicate condensation under conditions of an equilibrium (Rayleigh) process [*Dansgaard, 1964*]. At the same time, the linear regression equation itself $\delta D = 4.98 \cdot \delta^{18}O - 75.3$ ($R^2 = 0.92$, $n = 6$) of these compositions differs significantly from the MMWL and LMWL equations for Yakutsk by a significantly lower slope, which is usually associated with the processes of evaporation fractionation [*Dansgaard, 1964; Papina et al., 2017; Galanin et al., 2019*].

According to the dependence [*Dansgaard, 1964*]

$$\delta^{18}O = 0.68\, t^{\circ} - 13.6, \quad -30^{\circ}C < t^{\circ} < 0^{\circ}C, \qquad (1)$$

the precipitation of this composition fell at temperatures from −21 to −25°C.

According to the dependence [*Papina et al., 2017*]

$$\delta^{18}O = 0.59\,t^{\circ} - 19.7\ (R^2 = 0.88), \qquad (2)$$

precipitation of the studied composition fell out at temperatures from –14 to –19°C.

In general, Eqs. (1) and (2) give convergent results and indicate that the studied precipitation fell at the very beginning of winter (in October–November 2020). Indeed, the main amount of snowfall in Yakutsk fell in October and November at temperatures of –12... –25°C (Fig. 3), while in December 2020 and January 2021, when the temperature dropped to –45...–50°C, the amount of precipitation was extremely low [*Weather and Climate, 2004–2021*]. Instead of snowfall during December–January, under conditions of anticyclonic calm weather, dense ice fogs and active growth of crystalline frost were observed (Fig. 3). The sum of observed atmospheric precipitation for the coldest month and a half did not exceed 7–10 mm.

At the ratio $\delta^{18}O/d_{exc}$, snow samples are approximated by the equation $d_{exc} = -3.02 \cdot \delta^{18}O - 75.3$ ($R^2 = 0.88$, $n = 6$) (Fig. 5). An increase in the deuterium excess in precipitation during the coldest days is associated with a faster decrease in the rate of fractionation of $H_2{}^{18}O$ molecules compared to $HD^{16}O$ [*Dansgaard, 1964*].

Negative correlations of d_{exc} with $\delta^{18}O$ and D are also characteristic of precipitation formed under conditions of equilibrium cooling (freezing) of a limited volume of water vapor in semi-closed and closed systems, for example, in caves with difficult air exchange [*Lacelle et al., 2009; Galanin, 2020*]. Unfortunately, the issues of the correlation of the deuterium kurtosis with the values of δD and $\delta^{18}O$ remain poorly covered in the scientific literature.

Samples from the snow cover surface (0–2 cm) are characterized by the lightest composition ($\delta^{18}O = -41.04 \pm 5.11$‰, $\delta D = -326.43 \pm 34.16$‰, $d_{exc} = 1.91 \pm 7.72$‰), which naturally becomes heavier along the sampling profile towards the center of Yakutsk (Figs. 4 and 6; Table 1). If we take into account similar weather conditions and air temperature (–45...–53°C) in Yakutsk and its environs in December 2020–January 2021, then the heaviest composition ($\delta^{18}O = -35...-38$‰, $d_{exc} = -6...-3$‰) was formed in the central part of the city (o.p. 4–6), while the lightest ($\delta^{18}O = -45...-46$‰, $d_{exc} = 6–10$‰) was formed in the outskirts of the city (o.p. 1–3). In terms of temperatures according to Eqs. (1) and (2), in Yakutsk (o.p. 4–6), precipitation of the upper (0–2 cm) snow layer condensed at the temperature range of –29...–34°C; beyond Yakutsk (o.p. 1–3), temperatures were lower (–45...–56°C). In fact, as observations at the Yakutsk weather l station (Fig. 3) and air temperature measurements at the time of sampling indicate, the weather conditions for all sampling points were approximately the same.

Samples taken from the surface of the snow cover 15–20 km from Yakutsk lie near the LMWL and are determined by positive values of $d_{exc} \approx +10$‰, which are characteristic of the equilibrium (Rayleigh) condensation of atmospheric vapor at low tem-

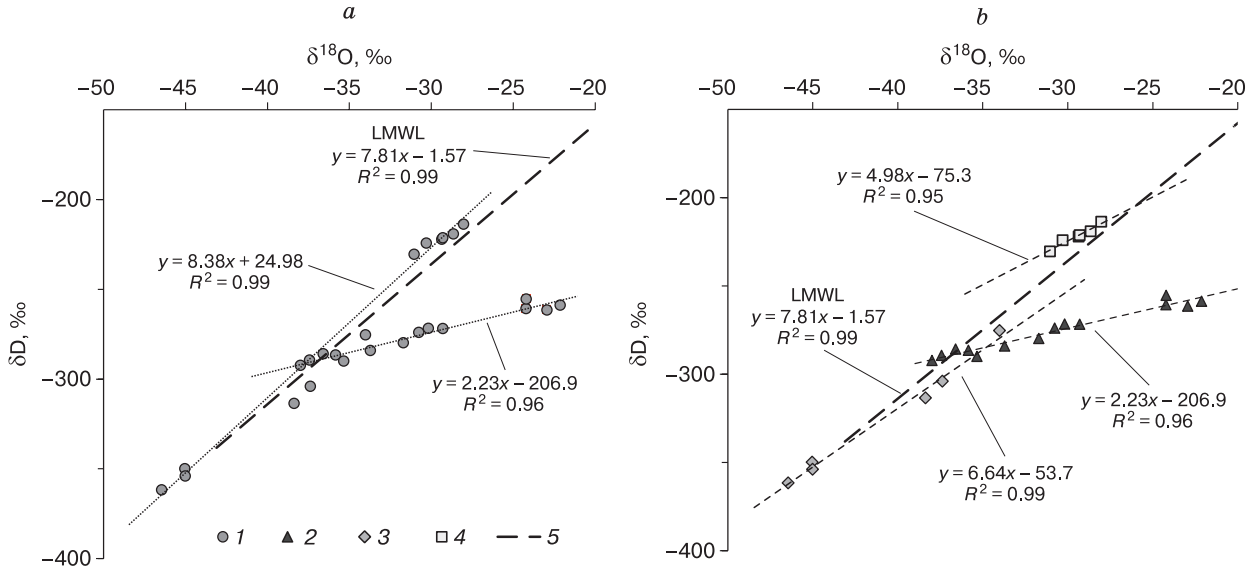

Fig. 4. The $\delta^{18}O/\delta D$ ratio in samples of snow cover and crystalline hoarfrost during the period of extreme subzero temperatures in the winter of 2020/21 in Yakutsk and its suburbs.

a – the entire sample; *b* – different groups of samples; *1* – crystalline hoarfrost; *2* – snow cover (including samples from the surface); *3* – snow cover surface (0–2 cm); *4* – annual precipitation in Yakutsk according to GNIP data [*Kurita et al., 2004*]; *5* – water vapor emitted into the atmosphere during the combustion of hydrocarbon fuels [*Xing et al., 2020*]. LMWL is a local line of meteoric waters.

peratures (Fig. 5). On the contrary, the samples taken in Yakutsk (o.p. 4–6) are characterized by negative d_{exc} values from –3 to –6‰, which is very uncharacteristic of fresh natural winter precipitation and indicates a different source of their origin.

The influence of an anthropogenic source on the composition of precipitation in Yakutsk in December 2020–January 2021 is emphasized by the nature of the variation in the isotopic composition along the studied profile (Fig. 4), which cannot be explained by the processes of equilibrium kinetic (Rayleigh) fractionation or by partial sublimation of snow from the surface. In the latter case, the similarity of weather conditions along the observation profile would lead to the same manifestation of sublimation and related fractionation effects at all sampling points.

The deuterium kurtosis of the surface snow samples also shows a significant negative correlation with the values of δD and $\delta^{18}O$ (Fig. 5). The regression looks like $d_{ex} = -1.36 \cdot \delta^{18}O - 53.7$ ($R^2 = 0.81$, $n = 6$).

Crystalline hoarfrost samples are characterized by the most exotic composition ($\delta^{18}O = -30.89 \pm 5.62$‰, $\delta D = -285.88 \pm 12.82$‰, $d_{exc} = -28.79 \pm 32.53$‰), which was not previously observed by the authors in natural atmospheric precipitation, as well as in all known types of terrestrial and ground ice in the region [*Galanin et al., 2019*]. Along the profile (Fig. 6), this composition experiences the strongest variation in $\delta^{18}O$, more than 1.5 times from –24‰ at o.p. 6 to –37‰ at o.p. 1. In the same interval, the δD values show less significant variations (by a factor of 1.12), decreasing from –255.4‰ (o.p. 6) to –285.9‰ (o.p. 1). The disproportionate decrease in $\delta^{18}O$ and δD values along the profile is clearly reflected in the d_{exc} value. Its lowest values from –66.9 to –81.8‰ (o.p. 6) and from –26.2 to –37.4‰ (o.p. 5) are typical for the territory of Yakutsk. As the distance from the city center increases, d_{exc} naturally increases and reaches positive values of 6.9–11.5‰ in hoarfrost samples taken at a distance of 15 and 25 km from the city center.

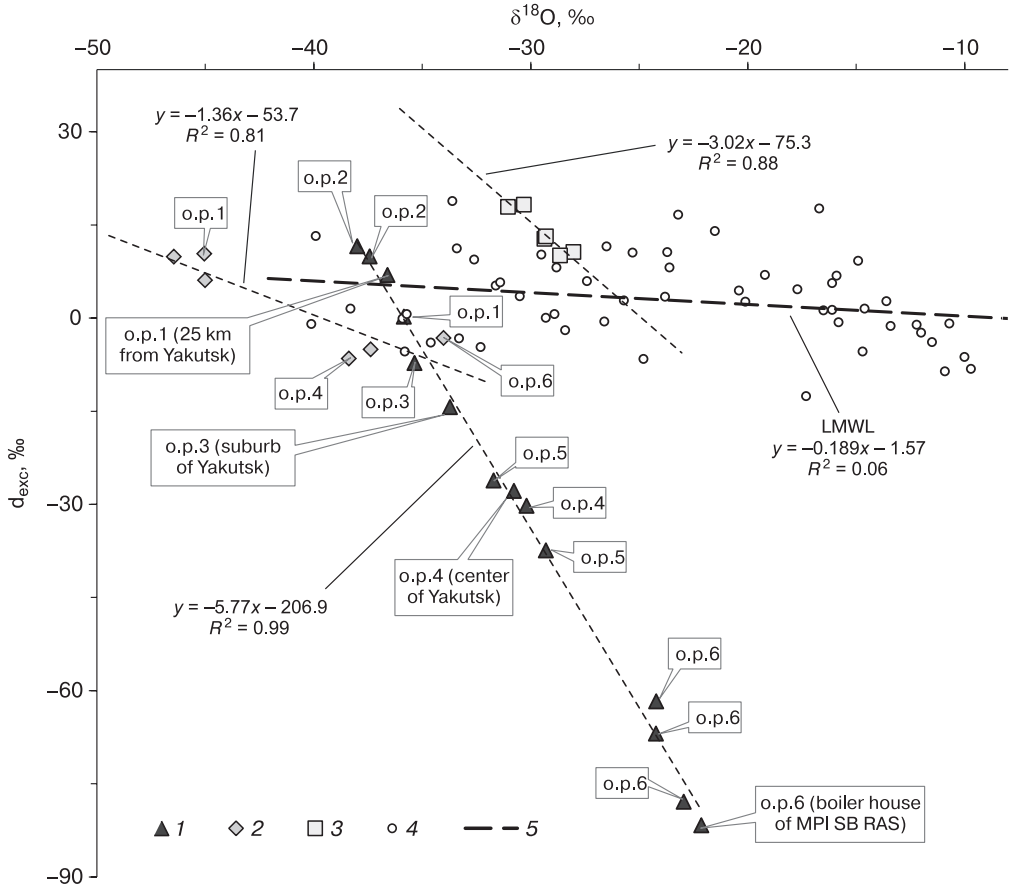

Fig. 5. The relationship between $\delta^{18}O$ and d_{exc} values in atmospheric precipitation during the period of extreme subzero temperatures in the winter of 2020/21 in Yakutsk and its suburbs.

1 – crystalline hoarfrost on trees at a height of 1.0–1.5 m above the snow cover; *2* – the surface of the snow cover (0–2 cm); *3* – averaged snow cover from a depth of 2–20 cm; *4* – atmospheric precipitation in Yakutsk according to GNIP data [*Kurita et al., 2004*]; *5* – local line of meteoric waters (all seasons) for the city of Yakutsk based on GNIP data. 1–6 – numbers of observation points (o.p.).

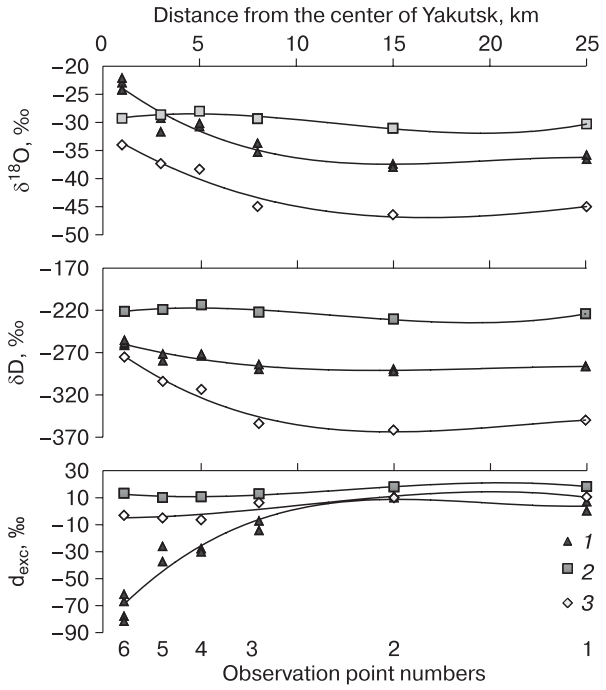

Fig. 6. Variation of the isotopic composition of the crystalline hoarfrost and snow cover along the profile of observation points.

1 – crystalline hoarfrost; *2* – the surface of the snow cover (0–2 cm); *3* – averaged snow cover (2–20 cm) at the end of January 2021.

The regression equation for the composition of crystalline hoar $\delta D = 2.23 \cdot \delta^{18}O - 206.9$ ($R^2 = 0.96$, $n = 14$) is characterized by an extremely low slope, indicating intensive evaporative fractionation of the moisture source. Among natural ices, the closest slope coefficient (2.7) was found for the composition of sinter ice in cold caves of Canada [*Lacelle et al., 2009*].

The exotic isotopic composition of crystalline hoar and the position of the observation points relative to the heat generating stations of Yakutsk (Fig. 2) allow us to conclude that the latter are the main source of moisture. Thus, the most contrasting isotope anomaly in crystalline hoar was established at o.p. 6 on the territory of the MPI SB RAS, 100 m from the nearest boiler house. The hoarfrost sample taken here on December 14, 2020 had the heaviest ($\delta^{18}O = -22.1‰$, $\delta D = -258.8‰$) and extremely fractionated composition with extreme values of $d_{exc} = -81.7‰$. Such a composition is not typical of the Earth's atmosphere and is probably formed during the combustion of hydrocarbon fuels at temperatures well above 100°C.

In terms of Eq. (1), the deposition of crystalline hoarfrost in different parts of the profile occurred at significantly different temperatures. Thus, the heaviest composition was formed in the center of Yakutsk and especially near the boiler house of the MPI SB RAS (o.p. 6) at a temperature of –15...–18°C. With distance from the city center, the condensation temperature naturally decreased, and the lightest composition was formed at a distance of 15–25 km from Yakutsk (o.p. 1) at a temperature of –35...–42°C.

Compared to snow cover samples, the composition of crystalline frost from tree branches is characterized by a high negative correlation between the deuterium excess and $\delta^{18}O$, described by the equation $d_{exc} = -5.77 \cdot \delta^{18}O - 206.9$ ($R^2 = 0.99$, $n = 14$) (Fig. 5).

Chemical composition of samples. According to the classification of S.L. Shvartsev [*1996*], in terms of total mineralization, all the samples of hoarfrost and snow are classified as ultra-fresh (0.0073–0.1725 g/L); in terms of total hardness, they are soft (0.075–1.432 meq/L). The samples taken in the suburban area (o.p. 1 and 2) are characterized by a bicarbonate magnesium-calcium composition, while urban samples (o.p. 3–5) are characterized by a bicarbonate calcium composition according to the classification of A.V. Shchukarev [*Shvartsev, 1996*].

Hoarfrost and snow cover samples are predominantly characterized by a neutral and slightly alkaline reaction ($6.64 < pH < 7.81$). The latter is typical for samples from the city center, which is due to pollution with ash from city boilers and vehicle emissions. The redox potential ($400 < Eh < 550$) in general indicates oxidizing conditions; its values are minimal within the city, and gradually increase in the suburbs both in hoarfrost and in the snow cover.

Within all observation points, the mineralization of crystalline hoarfrost is always two–four times higher than that of snow cover, which also indicates a strong genetic relationship of the former with an anthropogenic (technogenic) source. With distance from the city center, the concentrations of most cations and anions decrease in frost and snow cover by 4–20 times (Table 2, Fig. 7). This also indicates the technogenic origin of mineral pollutants, the content of which in Yakutsk exceeds the sanitary standards by 1.8 times on the average [*Makarov, Torgovkin, 2020*].

Among all cations, the maximum concentrations are characteristic of Ca^{2+} and reach 27.18 mg/L in the melt of crystalline hoarfrost from Yakutsk. Among the anions, HCO_3^- prevails, which indicates an increased emission of carbon dioxide within the city as a result of fuel combustion. The increase in the concentration of chloride ion in the city is also probably due to the anthropogenic factor, as sodium chloride is used to clear snow and ice from roads. The concentrations of all nitrogen compounds increase towards the center of Yakutsk by 3–4 times in snow cover and by 8–10 times in hoarfrost. Their sources are mainly the products of atmospheric nitrogen oxidation during the combustion of hydrocarbon fuel by heat-generating stations.

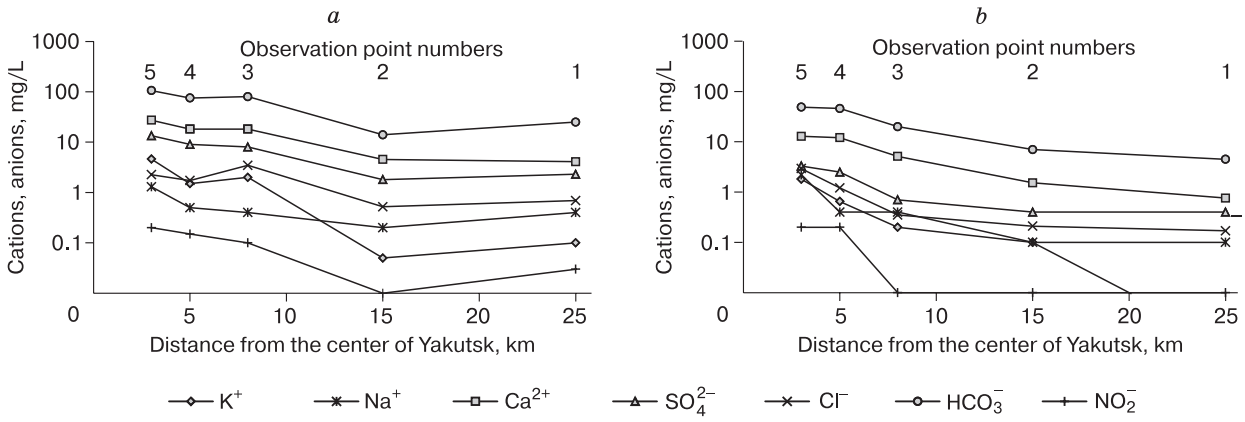

Fig. 7. Variation of the main cations and anions in (*a*) crystalline hoarfrost and (*b*) snow cover with distance from the center of Yakutsk along the sampling profile.

Among trace components in samples of hoarfrost and snow outside Yakutsk, there are small amounts of lithium (0.016–0.094 mg/L), fluorine (0.017–0.249 mg/L), and phosphorus (0.026–0.049 mg/L). In urban samples of snow cover, the contents of phosphorus (0.297–0.655 mg/L) and strontium (0.283–0.532 mg/L) increase significantly, while barium (0.059–0.072 mg/L) appears in hoarfrost samples, and the contents of strontium (0.567–1.399 mg/L) and phosphorus (1.200 mg/L) sharply increase.

In general, the chemical composition of crystalline hoarfrost and snow in Yakutsk shows significant similarity, which is due to the technogenic pollution of the city air by emissions from heat generating stations. Moreover, the maximum concentrations of pollutants are concentrated in crystalline frost, which is actively formed on trees and other objects in December and January. This is due to the fact that at the indicated time all heat generating stations in Yakutsk reach full capacity and emit maximum concentrations of pollutants – mainly water vapor and ash.

The calm weather prevailing during the period with the lowest temperatures does not contribute to the dispersion of emissions from heat generating stations, which form a continuous cloud of ice fog covering an area of about 100 km^2. The maximum fog density and the lowest visibility are typical for the central part of the city. The influence of anthropogenic sources of water vapor and chemical pollutants can be traced in the isotopic and chemical compositions of crystalline frost and snow cover to a distance of 10–15 km from the center of Yakutsk.

Thus, the isotopic and chemical compositions of atmospheric precipitation during the cold season is determined by the source of the CDW. The most exotic composition was found for precipitation in the center of the city and in the immediate vicinity of the thermal power station of the MPI SB RAS (o.p. 6). This composition is very similar to the composition of the CDW found earlier in other regions [*Gorski et al., 2015; Fiorella et al., 2018*] and is characterized by very low deuterium kurtosis values.

Influence of technogenic sources on the isotopic composition of atmospheric precipitation

Currently, Yakutsk is the largest and fastest growing city located in an extremely cold climate. In some years, extreme mean January temperatures down to –64.4°C (1891) and maximum summer temperatures of +38.4°C (2011) were recorded here [*Shver, Izyumenko, 1982*]. The mean annual precipitation varies from 147 mm (2001) to 330 mm (1971). The ratio of winter to summer precipitation is approximately 1:6 [*Gavrilova, 1962; Shver, Izyumenko, 1982*]. Snow cover usually appears in the first ten days of October and disappears at the end of April. The average thickness of the snow cover does not exceed 25–30 cm.

In recent decades, the growing pace of construction has led to an increase in the number and capacity of heat generating stations (Fig. 2), and the number of cars and other consumers of hydrocarbon fuel is growing.

Sources and volumes of CDW in Yakutsk. Despite climate warming, in recent decades in Yakutsk, an increase in the intensity and duration of winter ice fogs, as well as in the thickness of crystalline frost on trees, wires, and other objects has been observed. In addition, fogs begin to appear at air temperatures higher than –35°C, at which stable clear weather was previously observed. These phenomena are directly related to the increase in the volume of combusted hydrocarbons and the complete transition to natural gas. Thus, a sharp increase in the density and duration of ice fogs, as well as the rise in the temperature of their appearance, occurred in Yakutsk after the launch of an additional large SDPP-2 unit in 2017 (Fig. 2).

In total, there are three large thermal power plants operating in Yakutsk and generating about half

of the heat energy, and about 40 boiler houses with a capacity of 10–50 Gcal/h each. In addition, a certain amount of emissions is formed during the heating of private houses and the operation of vehicles. The total heat generation in Yakutsk during winter peak loads can be estimated at about 2000 Gcal/h.

Currently, all heat generating plants in Yakutsk have been switched to gas fuel, which consists mainly of methane and emits significantly more CDW than hard coal. The combustion of 1 kg of this gas releases about 13.3 Mcal of heat, as well as 2.21 kg of high-temperature water vapor [*Kuznetsov, 2010*]. With a capacity of 2000 Gcal/h, it is necessary to burn about 150 tons of natural gas every hour. At the same time, about $3.3 \cdot 10^5$ kg of CDW will be released into the atmosphere per hour, about $2.4 \cdot 10^8$ kg during the coldest month, and for the entire heating season this value can be $1.0 \cdot 10^9$ kg.

In Yakutsk, during the period of extremely low temperatures and calm weather, the CDW-released into the atmosphere quickly condenses, forming a scattering zone with a radius of about 10 km and an area of 314 km^2 ($3.14 \cdot 10^8$ m^2) in the center in Yakutsk. Assuming that during the two coldest months $2.4 \cdot 10^8$ kg of CDW is released into the atmosphere of Yakutsk, which is completely condensed within this zone, it is possible to approximately estimate the amount of technogenic precipitation ($2.4 \cdot 10^8$ kg/$3.14 \cdot 10^8$ m^2 = 1.53 kg/m^2 = 1.53 mm). Thus, during the two coldest months, 1.53 kg of technogenic precipitation falls on 1 m^2 of the 10-km zone around Yakutsk, which is equivalent to 1.53 mm. The share of CDW in the isotopic composition of precipitation varies significantly depending on the distance from the emission source. Therefore, 7–10 times more CDW (10–15 mm) should precipitate near the CDW sources, and its amount should decrease to 0.5–1.0 mm towards the suburbs of the city. This conclusion is well supported by visual observations of the thickness of crystalline hoar, which increases several times near heating plants and in the center of the city compared to the suburbs.

During the period of the lowest temperatures, the heat generating stations of Yakutsk reach their maximum capacity and emit the maximum amount of CDW. At the same time, a decrease in air temperature leads to an increase in the speed and narrowing of the condensation zone, which causes an increase in the share of CDW in precipitation near the sources of their release. The above estimates of CDW in Yakutsk are very approximate.

Estimation of the relative share of water vapor from the combustion of hydrocarbon fuels in Yakutsk based on the deuterium kurtosis and the Gaussian mixture model. The high proportion of CDW in the precipitation of the coldest period in Yakutsk is confirmed by calculations using the method based on a comparison of the deuterium excesses of in the samples and in the initial CDW [*Xing et al., 2020*]. This approach is based on the Gaussian mixture model, which makes it possible to calculate the proportion (X) of the anthropogenic source of water vapor in the sample based on the deuterium kurtosis using the formula

$$d_1 = d_2X + d_3(1 - X). \quad (3)$$

Here, the values d_1, d_2, d_3 are the deuterium excesses of the samples, the source of CDW, and the natural background. Assuming that the CDW had a minimum impact on the isotopic composition of precipitation at observation points 1 and 2 (15 and 25 km from Yakutsk), their averaged deuterium kurtosis was used as background values (d_3 = 10‰). Since almost all thermal power plants in Yakutsk use gaseous fuel, the deuterium excess of water vapor from natural gas combustion (d_2 = –266‰) was taken as the value of the deuterium surplus of the CDW [*Xing et al., 2020*]. Substituting the values of the deuterium excess of the studied samples (d_1) into equation (3) and solving it by the iteration method, we obtain the values of the share of CDW in the studied samples.

The performed estimates show that the highest values of the share of CDW (26–32%) are reached in the samples of crystalline hoarfrost taken at o.p. 6 on the territory of the MPI SB RAS, 100 m from the boiler house (–61.7‰ > d_{exc} > –80‰).

In the center of Yakutsk (o.p. 4 and 5), the composition of crystalline hoarfrost (–26.2‰ > d_{exc} > –37.4‰) testifies to the share of CDW of about 13–18%. In hoarfrost samples from the suburbs of Yakutsk (o.p. 3) with values of –7.3‰ > d_{exc} > –14.4‰, the proportion of CDW varies from 6.5 to 8.8%. In the surface layer of the snow cover, the share of CDW is 5–6% in the central part of Yakutsk and decreases towards the suburbs to 1% or less.

Discussion about the sources and mechanisms of formation of the isotopic composition of atmospheric precipitation in Yakutsk during the coldest season. The first systematic data on the isotopic composition of atmospheric precipitation in Yakutsk were obtained within the framework of the International Project for the Development of the Siberian Observation Network SNIP (Siberian Network of Isotopes in Precipitation) [*Kurita et al., 2004*]. Within the framework of this project, 43 samples were analyzed in Yakutsk, of which only a few characterize the isotopic composition of precipitation during the cold season.

Using the data from the SNIP database, the LMWL for North Asia was substantiated, which has the form $\delta D = 7.9 \cdot \delta^{18}O + 2.9$ and takes into account only mean monthly atmospheric precipitation with a volume of more than 10 mm [*Kurita et al., 2004*]. At the same time, the values given in the SNIP database

for 43 precipitation samples from Yakutsk are approximated by the equation $\delta D = 7.81 \cdot \delta^{18}O - 1.57$ ($R^2 = 0.99$) [*Galanin et al., 2019*].

According to [*Kurita et al., 2004*], the normalized mean annual isotopic composition for Yakutsk is characterized by $\delta^{18}O = -19.31‰$, and $\delta D = -153.9‰$; for precipitation from December to February, $\delta^{18}O = -33.0‰$, and $\delta D = -265.8‰$. The latter data poorly correlate with the results obtained by us, because precipitation in December 2020 and January 2021 had a significantly lighter composition ($\delta^{18}O = -41.04 \pm 5.11‰$, $\delta D = -326.43 \pm 34.16‰$, $d_{exc} = 1.91 \pm 7.72‰$). Such a significant discrepancy may be due to higher (by 4–5°C) mean winter temperatures recorded for the period from 1996 to 2000 [*Weather and Climate, 2004–2021*].

Fractionation of the isotopic composition of the snow cover as a result of its recrystallization ("metamorphization of the isotopic composition"). A study of the isotopic composition of the snow cover along the transect from Yakutsk to Magadan was performed within the framework of the international TVSSE (Trans-Verkhoyansk Snow Survey Expedition) in March 2001 [*Kurita et al., 2004*]. A total of 16 vertical isotope profiles were studied. In all sections of the snow cover, regardless of its thickness, four main stratigraphic layers were identified, differing in the morphology of snow crystals: freshly fallen snow, granular crystals (firn), crystals of deep frost in the form of goblets, and columnar crystals of deep frost [*Kurita et al., 2005*].

In all sections, a significant vertical variation of the isotopic composition was established (Fig. 8). It was especially pronounced in the snow cover of the Central Yakut Plain, as well as in the intermontane depressions of the Verkhoyansk and Kolyma Highlands, where $\Delta\delta D$ and Δd_{exc} in the snow reached 100 and 20‰, respectively [*Kurita et al., 2005*]. However, only three layers were isotopically expressed in most sections (Fig. 8).

A characteristic feature of all isotope profiles is the heaviest composition in the lower layers of the snow cover, which make up from 50 to 70% of its thickness. The same layers are characterized by the highest positive values of deuterium excess (10...25‰) [*Kurita et al., 2005*]. The lightest compositions are characteristic of the upper parts of all profiles and do not show a significant connection with the crystalline types of snow. At the same time, they have the lowest deuterium kurtosis (0...10‰). The isotopic composition of fresh snow in the surface layer (1–2 cm) is significantly heavier in most of the profiles and has a low d_{exc} value.

Similar vertical variations in the values of δD and d_{exc} are characteristic of the snow cover sections at o.p. 1–6 in Yakutsk and its environs in January 2021 (Fig. 8). For comparison, the sections also show samples of crystalline hoarfrost taken from tree branches at a height of 1.0–1.5 m above the snow cover surface. All sections are characterized by a heavier composition of the lower layer (–250... –220‰), which has the highest deuterium kurtosis (10...20‰) decreasing towards Yakutsk. The upper layer of snow cover with distance from Yakutsk (o.p. 1–3) is characterized by a significant decrease in δD to –350...–360‰ and a simultaneous increase in deuterium excess to +6...+10‰. In Yakutsk, the δD value in the upper snow cover varies from –275 to –313‰ and increases towards the city center. While the deuterium kurtosis significantly decreases and takes on negative values (–3...–6‰). The layer of crystalline frost at all sampling points is characterized by a significant weighting of its isotopic composition. The maximum increase in the value of δD by 50–60‰ is observed outside the impact zone of Yakutsk at o.p. 1 and 2, while d_{exc} practically does not change. Within the territory of Yakutsk (o.p. 4–6) in the layer of crystalline hoarfrost, the values of δD increase by 10–30‰, while the deuterium kurtosis sharply decreases to extremely low negative values (–27... –80‰). The lowest d_{exc} values are found in the samples taken in the center of Yakutsk (–27...–32‰) and near the building of the MPI SB RAS (–80‰). The authors attribute the latter to the influence of technogenic steam from the burned fuel. With the exception of the top layer of snow cover and crystalline frost at o.p. 4–6, the remaining isotopic profiles are very similar to the snow cover of other ultracontinental regions of Yakutia (Fig. 8) [*Kurita et al., 2005*].

Experimental studies show that as a result of a significant temperature gradient between the surface and the base of the snow cover, the processes of sublimation and desublimation develop in it, which leads to recrystallization and the formation of a deep hoarfrost layer. These processes are accompanied by significant isotope fractionation affecting mainly the base and the surface of the snow cover. while the isotopic composition of the middle part of the snow cover does not change significantly. The essence of this process is as follows [*Sommerfeld et al., 1991; Hachikubo et al., 2000*]. In winter, sublimation of light H_2O molecules and their upward migration through the pores in the snow cover from a warmer base to its much colder top and crystallization (desublimation) of these molecules in the near-surface layer take place. Conversely, in spring, the top of the snow cover heats up stronger than the base, which leads to the reverse process of the transfer of light molecules to the lower layers of the snow cover.

In other words, as a result of the so-called process of metamorphization of the isotopic composition of the snow cover, the composition of the latter becomes heavier within the subliming layer and, conversely, under the influence of desublimation, the composition of the layer becomes isotopically lighter [*Sommerfeld et al., 1991; Hachikubo et al., 2000; Ku-*

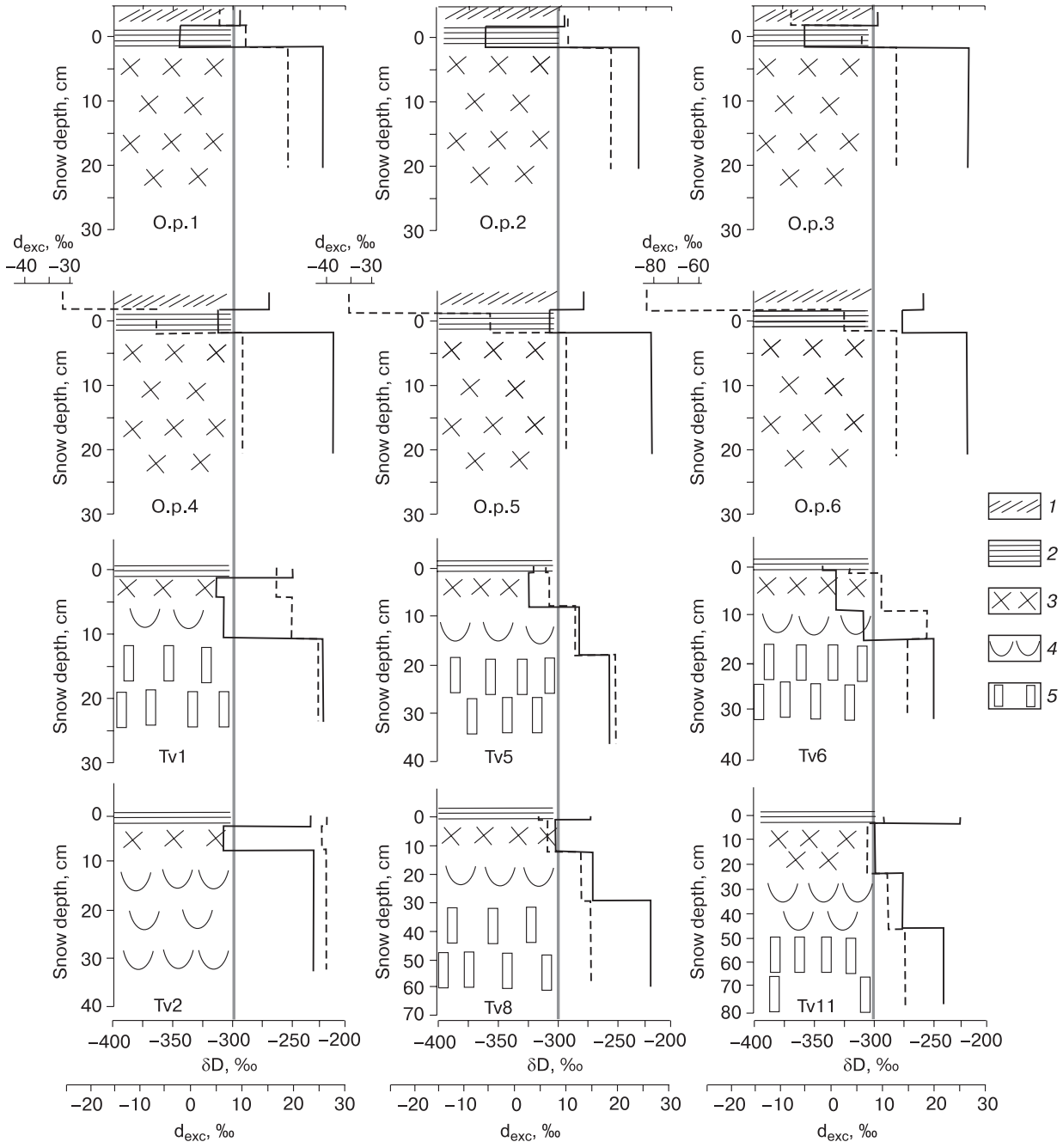

Fig. 8. Vertical distribution of δD (*solid line*) and d_{exc} (*dashed line*) in sections of the snow cover in Yakutia.

Observation points: o.p. 1–6 – Yakutsk and environs in December 2020–January 2021 (data from this article); Tv1–Tv11 – snow cover sections in March 2001 along the Trans-Verkhoyansk TVSSE profile according to [*Kurita et al., 2005*] (authors' designations). Precipitation type: *1* – hoarfrost on tree branches at a height of 1.0–1.5 m from the surface; *2* – loose fresh snow; *3* – fine-grained snow; *4* – large crystals of deep hoarfrost in the form of goblets; *5* – large columnar crystals of deep hoarfrost.

rita et al., 2005]. At the same time, despite the presence of signs of significant recrystallization in the studied sections of the spring snow cover along the TVSSE profile, it is not possible to explain both the heavy composition and the high kurtosis of the lower snow layers as a result of "metamorphization" [*Kurita et al., 2005*]. Indeed, kinetic fractionation and weighting of the isotopic composition of the lower layers of snow, their deuterium kurtosis should decrease. Conversely, if the light isotopic composition of the upper layers of the snow cover is associated with post-sedimentary enrichment in light isotopes as a result of

desublimation, then their deuterium kurtosis should increase.

Thus, vertical variations in the isotopic composition of the snow cover in spring along the TVSSE profile are due to differences in the initial composition of snow precipitation at the beginning, middle, and end of the winter period rather than to the snow cover metamorphism [*Kurita et al., 2005*]. The most isotopically heavy snow with a high deuterium kurtosis fell at the beginning of the winter period at relatively high air temperatures from undepleted moisture-bearing masses. The lightest snow is associated with the coldest period of winter, while its low deuterium excess is due to the large depletion of the air mass. Finally, a more isotopically heavier thin surface layer was formed in spring as a result of blizzard transport and new portions of snowfall that fell at higher temperatures at the end of the winter period [*Kurita et al., 2005*]. These conclusions are fully consistent with our results.

Isotopic composition of atmospheric precipitation in the winter period 2013–2014. A new series of observations over the isotopic composition of atmospheric precipitation in Yakutsk was carried out from October 2013 to September 2014 [*Malygina et al., 2015; Papina et al., 2017*]. A different sampling strategy was used than in previous studies [*Kurita et al., 2004, 2005*]. The sampling site was equipped on the roof of the building of the MPI SB RAN, located in the suburbs of Yakutsk (103 m a.s.l.). Snow was collected as it fell, melted, and immediately packed into sealed cuvettes with a volume of 10–20 mL. The analysis was performed at the Chemical Analytical Center of the Institute for Water and Environmental Problems of the Siberian Branch of the Russian Academy of Sciences (IWEP SB RAS), where the samples were sent in batches 2–3 times a year.

Selected cold season precipitation in 2013–2014 in Yakutsk (8 samples) are approximated by the equation $\delta D = 8.17 \cdot \delta^{18}O + 21.9$ ($R^2 = 0.99$, $n = 8$) and are characterized by weighted average values $\delta^{18}O = -31.65‰$ and $\delta D = -237.1‰$. Except for single outliers, the authors note a high value of $d_{exc} > +10‰$ for all samples [*Papina et al., 2017*]. Moreover, during the cold season, a continuous lightening of the isotopic composition and an increase in the deuterium surplus were observed, the highest value of which (+21.4‰) is typical for precipitation in February–March.

In addition to atmospheric precipitation, in January 2014, the vertical variation of the isotopic composition in the snow cover was studied at the Tuymada weather station, located 500 m from the building of the MPI SB RAS [*Malygina et al., 2015*]. Here, on a site of a natural pine–birch forest, a snow cover with a thickness of 21 cm was opened with a pit, in which three layers were visually distinguished. The lower layer (6 cm) was mainly composed of deep hoarfrost; the middle layer (12 cm) consisted of medium-grained white snow, and the upper layer (3 cm) consisted of freshly fallen slightly compacted blizzard snow.

Seven samples were taken every 3 cm, the analysis of which showed a large variation in the isotopic composition along the section. The composition of the lower layer was the heaviest ($\delta^{18}O = -17.1‰$, $\delta D = -160.6‰$), and the composition of the upper layer was the lightest ($\delta^{18}O = -45.0‰$, $\delta D = -350.6‰$). Even more unusual were the values of the deuterium kurtosis and its regular increase from −17.1‰ at the base of the lower layer to +25.3‰ in the middle layer and again decreasing to +10‰ in the upper layer.

The heavy composition of the lower snow layers and the low negative kurtosis are explained by the authors by the process of "metamorphization of the isotopic composition" [*Malygina et al., 2015*] as a result of the enrichment of the lower snow layers with isotopically heavier water vapor crystallization products (hoarfrost) coming from the underlying soil. This definition is completely different from the understanding of the process of "metamorphization of the isotopic composition" of the snow cover, considered in [*Sommerfeld et al., 1991; Hachikubo et al., 2000; Kurita et al., 2005*]. According to the results of these experiments, the isotopic composition of the lower layers of snow, which is heavier and depleted in deuterium, is associated only with isotope exchange within the snow cover profile, and not with the addition of moisture from outside.

The extremely high positive (+25.3‰) values of the deuterium kurtosis established by N.S. Malygina et al. [*2015*] in the middle snow layer of Yakutsk.

Thus, the data of N.S. Malygina et al. [*2015*] and T.S. Papina et al. [*2017*] strongly contradict the results of TVSSE [*Kurita et al., 2005*], according to which, in all 16 studied profiles of spring snow cover, the lower snow layer has the heaviest isotopic composition and the highest deuterium kurtosis. At the same time, the upper lightest layers are characterized by a low deuterium kurtosis reaching negative values in some samples.

The regression equation $\delta D = 7.01 \cdot \delta^{18}O - 19.7$ ($R^2 = 0.97$, $n = 8$), which characterizes the entire set of samples in the snow cover section, also calls into question [*Malygina et al., 2015*]. Its coefficients, according to the authors, indicate a significant "metamorphization" of the isotopic composition of the initial snow precipitation. In addition, this equation is almost identical to the regression equation $\delta D = 7.22 \cdot \delta^{18}O - 18.9$ ($R^2 = 0.95$, $n = 23$) obtained for Yakutsk atmospheric precipitation that fell during the warm period of 2014 [*Papina et al., 2017*]. The great similarity of these equations, which characterize fundamentally different atmospheric precipitation in different seasons of the year in the same area, raises questions about the reliability of the initial data.

According to the authors of this article, the problematic interpretation of the results obtained by N.S. Malygina et al. [*2015*] and T.S. Papina et al. [*2017*] for winter precipitation is due to the significant influence of CDW. Indeed, the sampling site – institute's roof – is located less than 100 m from the boiler house chimney. The boiler house, as shown by the data of this article, is a powerful source of CDW in winter. The same applies to the Tuymada station, where the snow cover section was studied. It is located at a distance of about 700 m from the boiler house.

CONCLUSIONS

The isotopic (^{18}O, D) and chemical compositions of atmospheric precipitation (crystalline hoar, snow cover surface, average snow stock) that fell in Yakutsk and its environs in December 2020–January 2021 was studied during the period of extremely low temperatures (from –47 to –52°C).

It was found that atmospheric precipitation of that period differed in its isotopic composition in on the type of precipitation (snow, hoarfrost) and on the distance from the center of Yakutsk. The main thickness (2–20 cm from the surface) of the snow cover on all plots is composed of precipitation at the beginning of winter, which fell at relatively high temperatures from –12 to –25°C in October–November 2020. In all observation points, this snow had the same isotopic composition ($\delta^{18}O$ = –29.45 ± 1.1‰, δD = = –221.8 ± 5.57‰, d_{exc} = 13.78 ± 3.52‰) attesting to its formation under the conditions of equilibrium kinetic fractionation and an insignificant fraction of CDW.

In the subsequent period, from mid-December 2020 to January 2021, precipitation in Yakutsk formed under conditions of anticyclonic calm weather and extremely low temperatures from –45 to –53°C. The total amount of precipitation in this period was about 6 mm and formed a thin surface layer of snow (0–2 cm) and hoarfrost of up to 10 cm in thickness on tree branches and other objects.

Samples from the surface of the snow cover (0–2 cm) had the lightest isotopic composition ($\delta^{18}O$ = –41.04 ± 5.11‰, δD = –326.43 ± 34.16‰, d_{exc} = 1.91 ± 7.72‰) and were noticeably impoverished in deuterium. Along the studied 25-km-long profile towards the center of Yakutsk, the composition became heavier by 10‰ in $\delta^{18}O$ and by 80‰ in δD with a decrease in d_{exc} from +10 to –6‰, and a fourfold increase in mineralization due to calcium carbonate impurities.

The most exotic isotopic composition ($\delta^{18}O$ = = –30.89 ± 5.62‰, δD = –285.88 ± 12.82‰, d_{exc} = –28.79 ± 32.53‰), which is not characteristic of any natural atmospheric precipitation, surface and ground waters, and ice in the region, was found for samples of crystalline hoarfrost, with the greatest changes in $\delta^{18}O$ from –24‰ in Yakutsk to –37‰ at a distance of 25 km from its center. In the same interval, δD changed from –255.4 to –285.9‰, and d_{exc} increased from –80 to +11.5‰.

In crystalline hoarfrost, the maximum proportion of CDW (26–32%) was obtained near the sources of the CDW (the building of the MPI SB RAS); in the central part of the city, it reached 13–18%; in the suburbs, it varied from 6.5 to 8.8%. In the surface layer of the snow cover, the share of CDW was 5–6% in the central part of Yakutsk and decreased towards the suburbs to 1% or less.

The exotic composition and the nature of the spatial variation of the isotopic composition indicate the decisive role of the anthropogenic source of water vapor in precipitation in Yakutsk at temperatures below –45°C. The influence of the isotopic composition of the anthropogenic source of water vapor is clearly manifested within a radius of up to 10 km from the center of Yakutsk. On the whole, this conclusion agrees well with the conclusions of predecessors about the presence of unknown sources of atmospheric moisture in Yakutsk in winter [*Kurita et al., 2005*].

The increase in recent years in the duration and frequency of ice fogs, as well as in the thickness of crystalline hoarfrost in Yakutsk, according to the authors, may be associated with the operation of a new state district power station and the transfer of most heat generating stations to gaseous fuel, which is characterized by a large specific emission of anthropogenic water vapor derived from fuel combustion.

Funding. *This work was supported by the Russian Science Foundation (grant No. 21-17-00054, https://rscf.ru/project/21-17-00054/).*

References

Beesley J.A., Moritz R.E., 1999. Toward an explanation of the annual cycle of cloudiness over the Arctic Ocean. *J. Climate*, No. 12, 395–415. DOI: 10.1175/1520-0442(1999)012<0395:TAEOTA>2.0.CO;2.

Bowling S.N., Ohtake T., Benson C.S., 1968. Winter pressure systems and ice fog in Fairbanks, Alaska. *J. Applied Meteorol.* **7** (6), 961–968. DOI: 10.1175/1520-0450(1968)007<0961:WPSAIF>2.0.CO;2.

Dansgaard W., 1964. Stable isotope in precipitation. *Tellus*, XVI (4), 436–468.

Ekajkin A.A., 2016. Stable Isotopes of Water in Glaciology and Paleogeography. Methodological Guidelines. St. Petersburg, SSC RF AANII, 68 p. – https://www.researchgate.net/publication/311419330_Stabilnye_izotopy_vody_v_

Fiorella R., Bares R., Lin J. et al., 2018. Detection and variability of combustion-derived vapor in an urban basin. *Atmos. Chem. Phys.* **18**, 8529–8547. DOI: 10.5194/acp-18-8529-2018.

Galanin A.A., 2020. Stable isotopes ^{18}O and D in cave ice of the Lena Pillars National Nature Reserve (Eastern Siberia). *Earth's Cryosphere* XXIV (1), 3–19.

Galanin A.A., Pavlova M.R., Papina T.S. et al., 2019. Stable isotopes ^{18}O and D in main sources of water runoff and permafrost of Central Yakutia (Eastern Siberia). *Ice and Snow* **59** (3), 333–354. DOI: 10.15356/2076-6734- 2019-3-414.

Gallagher M., 2020. Ice fog: the current state of knowledge and future challenges. *Meteorol. Monographs* **58**, 4.1–4.24. DOI: 10.1175/AMSMONOGRAPHS-D-17-0002.1.

Gavrilova M.K., 1962. The Climate of Central Yakutia. Yakutsk, 63 p. (in Russian).

Gorski G., Strong C., Good S. et al., 2015. Vapor hydrogen and oxygen isotopes reflect water of combustion in the urban atmosphere. *PNAS*, **112** (11), 3247–3252.

GOST 31861-2012, 2013. Water. General Requirements for Sampling. Moscow, Standardinform, 35 p. (in Russian).

Hachikubo A., Hashimoto S., Nakawo M., Nishimura K., 2000. Isotopic mass fractionation of snow due to depth hoar formation. *Polar Meteorol. Glaciol.*, No. 14, 1–7. – https://www.pnas.org/content/pnas/112/11/3247.full.pdf

Kurita N., Sugimoto A., Fujii Y. et al., 2005. Isotopic composition and origin of snow over Siberia. *J. Geophys. Res.* **110**, p. D13102. DOI: 10.1029/2004JD005053.

Kurita N., Yoshida N., Inoue G., Chayanova E.A., 2004. Modern isotope climatology of Russia: A first assessment. *J. Geophys. Res.* **109**, p. D03102. DOI:10.1029/2003JD003404.

Kuznetsov A.M., 2010. Specific fuel consumption for heat generation at CHPPs. *Novosti Teplosnabzheniya*, No. 4 (116), 22–23. – http://www.ntsn.ru/ (in Russian).

Lacelle D., Lauriol B., Clark I.D., 2009. Formation of seasonal ice bodies and associated cryogenic carbonates in Caverne de l'Ours, Que'bec, Canada: Kinetic isotope effects and pseudo-biogenic crystal structures. *J. Cave Karst Studies* **71** (1), 48–62.

Makarov V.N., Torgovkin N.V., 2020. Pollution of the atmosphere of the city of Yakutsk by suspended substances. *Prirodn. Res. Arkt. Subarkt.* **25** (1), 43–50. DOI: 10.31242/2618- 9712-2020-25-1-4.

Malygina N.S., Papina T.S., Eirikh A.N. et al., 2015. Isotopic composition of atmospheric precipitation and snow cover in Yakutsk. *Nauka Obrazovan.* **79** (3), 10–15 (in Russian).

Papina T.S., Malygina N.S., Eirikh A.N. et al., 2017. Isotopic composition and sources of atmospheric precipitation in Central Yakutia. *Earth's Cryosphere* XXI (2), 52–61.

Sessions A.L., Burgoyne T.W., Schimmelmann A., Hayes J.M., 1999. Fractionation of hydrogen isotopes in lipid biosynthesis. *Organic Geochem.* **30** (9), 1193–1200. DOI: 10.1016/S0146-6380(99)00094-7.

Shvartsev S.L., 1996. General Hydrogeology. Moscow, Nedra, 423 p. (in Russian).

Shver Ts.A., Izyumenko S.A. (Eds.), 1982. Climate of Yakutsk. Leningrad, Gidrometeoizdat, 246 p. (in Russian).

Sommerfeld R.A., Judy C., Friedman I., 1991. Isotopic changes during the formation of depth hoar in experimental snowpacks. In: *Stable Isotope Geochemistry: A Tribute to Samuel Epstein*, Spec. Publ. H.P. Taylor, J.R. O'Neil, I.R. Kaplan (Eds.). St. Louis, Geochem. Soc., No. 3, 159–168. – https://www.geochemsoc.org/files/1714/1269/7652/SP-3_205-210_Sommerfeld.pdf

van Geldern R., Barth J., 2012. Optimization of instrument setup and post-run corrections for oxygen and hydrogen stable isotope measurements of water by isotope ratio infrared spectroscopy (IRIS). *Limnol. Oceanogr. Methods* **10**, 1024–1036. DOI: 10.4319/lom.2012.10.1024.

Weather and Climate. Data Base Catalog, 2004–2021. – http://www. pogodaiklimat.ru (accessed: February 26, 2021).

Whiticar M.J., 1999. Carbon and hydrogen isotope systematics of bacterial formation and oxidation of methane. *Chemical Geol.* **161** (1–3), 291–314. DOI: 10.1016/S0009-2541(99)00092-3.

Xing M., Liu W., Li X. et al., 2020. Vapor isotopic evidence for the worsening of winter air quality by anthropogenic combustion-derived water. *PNAS*, **117** (52), 33005–33010. DOI: 10.1073/pnas.1922840117.

Received July 13, 2021
Revised June 10, 2022
Accepted July 17, 2022

Translated by A.V. Muravyov

EARTH'S CRYOSPHERE
SCIENTIFIC JOURNAL

Earth's Cryosphere, 2022, vol. XXVI, No. 4, pp. 32–40

PHYSICAL AND CHEMICAL PROCESSES IN FROZEN GROUND AND ICE

PHYSICAL MODELING OF FREEZING OF HEAVING SOIL. METHODS AND DEVICES

V.G. Cheverev[1,*], S.A. Polovkov[2], E.V. Safronov[1], A.S. Chernyatin[2]

[1] *Lomonosov Moscow State University, Department of Geocryology, Faculty of Geology, Leninskie Gory 1, Moscow, 119991 Russia*
[2] *Center for Monitoring and Geoinformation Systems of Pipeline Transport Facilities, Scientific Research Institute of Pipeline Transport (LLC Transneft Research Institute), Sevastopolsky prosp. 47a, Moscow, 117186 Russia*

**Corresponding author; e-mail: cheverev44@mail.ru*

We give the substantiation of the choice of methods and devices for laboratory modeling of the processes of freezing and heaving of soils in order to study their heaving properties and freezing parameters for verification of the developed mathematical methods of the process modeling. The methods under consideration make it possible to set and control in automated mode the dynamics of the temperature state, heat and water flows, heaving and shrinkage deformations, moisture content and bulk density, pore hydraulic pressure, and formation of segregation ice in freezing soils through the use of time-lapse video recording and the simulation of external mechanical and hydraulic loads.

Keywords: *physical modeling, methods, devices, freezing, soils, heaving, process parameters.*

Recommended citation: Cheverev V.G., Polovkov S.A., Safronov E.V., Chernyatin A.S., 2022. Physical modeling of freezing of heaving soil. Methods and devices. *Earth's Cryosphere*, XXVI (4), 32–40.

INTRODUCTION

Frost heaving of freezing soils is a dangerous geocryological process for buildings and engineering constructions in permafrost areas. Therefore, the prediction and control of this process are highly relevant.

Currently, despite many years of research into mechanisms and patterns of frost heaving and methods to reduce the negative impact of this process on the constructions, the heaving forecast problem is still far from a final solution. A number of mathematical formulas and equations of heat and mass transfer and deformations in freezing soils are proposed for semiempirical and numerical methods for predicting soil freezing and heaving of soils, which have not yet found experimental confirmation. The physical formulation of the problem for mathematical modeling of the freezing and heaving process needs significant development with due account for all the main factors of this complex process.

To verify the physical formulation of a numerical mathematical model of soil freezing and heaving, taking into account heat and mass transfer, ice formation, deformations of heaving and shrinkage, and pore pressure, the results of laboratory physical modeling are needed. To perform these laboratory experiments, appropriate methods and devices are needed.

In order to determine the methodologically important characteristics and parameters during the physical modeling of soil freezing, it is necessary to consider the mechanism of soil frost heaving.

The frost heaving deformations are caused by a set of heat and mass transfer, physicochemical and physico-mechanical processes depending on the properties of soils and external thermodynamic conditions.

The general frost heaving deformation consists of multidirectional deformations caused by segregation of ice, shrinkage and heaving, which can be expressed by the following equation [*Ershov, 2004*]:

$$H = h_f + h_{iw} - h_s, \quad (1)$$

where H is the resulting heaving deformation; h_f is the expansion deformation due to the water–ice phase transition in the soil; h_{iw} is the deformation of soil expansion due to freezing of water coming from the thawed zone to the frozen zone by cryogenic migration, including the flow of water through the thawed zone in transit from the underlying aquifer; h_s is the shrinkage deformation of the thawed zone due to outflow of water into the frozen zone in amounts exceeding the water content of the shrinkage limit.

Figure 1 presents the multi-layered dynamic structure of a freezing sample of finely dispersed soil. Frozen and thaw zones are distinguished in this structure. The frozen zone consists of the layers of the already frozen and freezing soils. In the thaw zone, a layer of transit moisture transfer and a layer with ini-

tial water content are distinguished. The freezing front (F_{fr}) marks the transition between the frozen and thawed zones.

A simplified scheme of freezing of the sample consisting of a frozen zone, an ice lens, a freezing zone, and a thawed zone is given in [*Gorelik, 2010, p. 51*]. The lens of ice grows on the border of the frozen and freezing zones. This is a specific case. A common case is when ice lenses appear and grow in the freezing zone simultaneously at different levels and with different intensities [*Cheverev, 2004*].

It follows from Fig. 1 that the method of physical modeling should include monitoring and measurement in time of deformation, mass-exchange and thermophysical parameters of processes, as well as boundary conditions for heat and mass exchange and external load. Let us consider this statement in more detail.

Deformation parameters. It follows from Eq. (1) that the heaving deformations in the frozen zone, shrinkage deformation in the thawed zone, and general frost heaving deformation of the soil along the height and width of the sample should be controlled in time. It is possible to calculate the time dependencies of moisture and soil density in height and width of the sample during freezing of a water-saturated soil sample, provided that these characteristics are determined as initial values before the experiment.

Thermophysical parameters. For physical modeling, it is necessary to control the temperature at the cold and warm ends of the sample, as well as to measure incoming and outcoming heat flows. In addition, it is necessary to monitor the movement of the freezing front in time.

Mass transfer parameters. During the physical modeling, it is necessary to determine the density of the water flow coming from the outside through the warm end of the sample and the distribution of pore pressure over the height of the melt zone over time. According to the temperature distribution in the frozen zone, it is possible to calculate the dynamics of pore pressure and its gradients. Taking into account the density of the moisture flow and the pore pressure gradient, the dependence of the soil moisture conductivity coefficient on temperature is calculated.

Cryogenic structure. To observe the formation of cryogenic structure in the soil on the lateral surface of the sample during its freezing, it is necessary to provide for the possibility of time-lapse video recording. Time-lapse videography is a special type of film and photography, in which a series of frames of the same object are photographed from the same shooting point at regular time intervals. It is intended for photographing slow processes.

Using special additional methods, it is necessary to determine temperature dependencies of the following soil characteristics: the coefficients of thermal

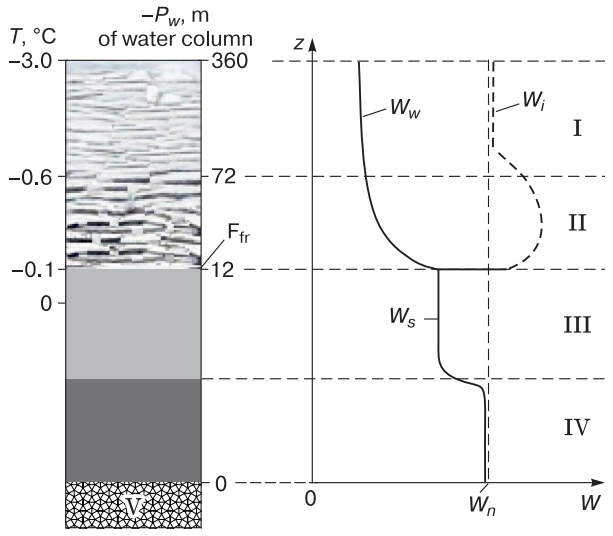

Fig. 1. A scheme of the characteristic zones and layers and parameters of freezing of silty clay soil.

I – frozen layer of the frozen zone; II – freezing layer of the frozen zone; III – layer of transit moisture transfer in the thawed zone; IV – layer of initial moisture in the thawed zone; V – capillary-water-saturated layer of sand. T – temperature (critical and characteristic values); P_w – pore hydraulic pressure; z – height; W_w, W_i, W_s, W_n – water contents corresponding to the unfrozen water, ice, shrinkage limit, and initial moisture, respectively; F_{fr} – freezing front.

conductivity and heat capacity in thawed and frozen zones, the unfrozen water content in the frozen zone, and the initial densities and water contents of the freezing soil.

On the side surface of the sample needle marks are installed using regular grid (10 × 10 mm) pattern to fix in time the layer-by-layer deformations of the freezing soil sample in height and width by videography.

This approach serves as the methodological basis for the selection of methods and devices to achieve the aim of the work – the physical modeling of soil freezing and heaving.

ANALYSIS OF EXISTING METHODS OF PHYSICAL MODELING

The heaving of freezing soils as a dangerous process for engineering constructions attracted the attention of Russian railway engineers at the end of the 19th century [*Shtuckenberg, 1894; Voislav, 1896*]. Since then, several hundred scientific papers have been published on the problem of frost heaving, which indicates both the significance of the process and its complexity.

The first simple experiment was carried out by S.G. Voislav in 1896. He experimentally established the heaving of the freezing soil placed in a bowl with water absorbed by the soil (Fig. 2).

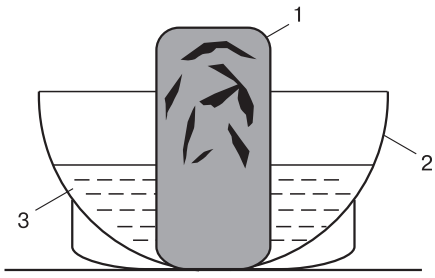

Fig. 2. Scheme of the experiment on freezing a soil sample in water [*Voislav, 1896*].

1 – soil; 2 – bowl; 3 – water.

Experimental investigation of the process of freezing and heaving of soils was carried out in more detail at the beginning of the 20th century (Fig. 3) [*Taber, 1930*]. A sample of clay for freezing was installed with a stamp in a sleeve with a porous bottom. The sample was frozen using a cryostat, the body of which had thermal insulation to ensure unilateral freezing of the sample. The sleeve with a porous bottom was installed in a container with water and sandy bed.

The experiments of S.G. Voislav and S. Taber were important for their time, but the potential of such devices is insufficient for modern physical modeling.

In studies of the mechanism of cryogenic migration and frost heaving performed up to 1990, the authors applied basically the same type of devices that provided for unilateral freezing of soil samples [*Bazhenova, Bakulin, 1957; Nersesova, 1961; Ananyan, 1970; Alekseev, 2020*].

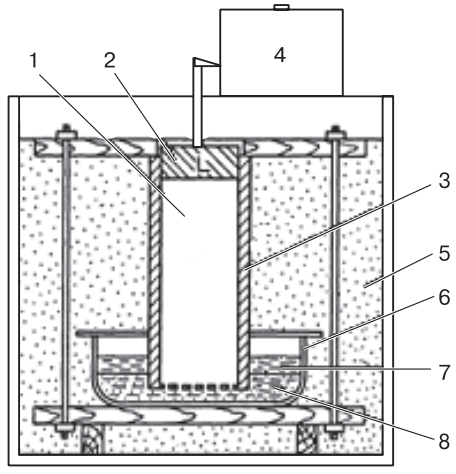

Fig. 3. A device for freezing a soil sample [*Taber, 1930*].

1 – clay sample, 2 – stamp, 3 – sleeve with a porous bottom, 4 – cryostat, 5 – thermal insulation, 6 – reservoir, 7 – water, 8 – sand with water.

V.Ya. Lapshin and L.B. Ganeles [*1979*] experimented with large (about 0.2, 1, and 3 m) samples and found that the maximum heaving of soils appears upon the freezing rate of about 1.5–2 cm per day. An example of the hardware implementation of the method of physical modeling of soil freezing is the device, the scheme of which is given in Fig. 4. The device was installed in the freezer and consisted of a cylindrical body with thermal insulation and a Plexiglas cylinder with soil samples. The cylinder with the sample was placed on a water-saturated fine-grained sand. A container with water was applied to the sand. Thus, the inflow of water from the outside was realized (an open mass transfer system).

The boundary temperature conditions were set by electric heaters using thermo-elements and heat exchangers. The pressure ring protected the cylinder from lifting due to the tangential forces of heaving of the soil. The general deformations of the frozen soil sample were measured by a clock-type deformation sensor. This device did not provide instruments for measuring pore hydraulic pressure, pore fluid flow density, and dynamics of temperature field.

A disadvantage of this device was also the absence of the possibility of observing the development of cryogenic structure, the advance of the freezing front, layer-by-layer deformations, and the intensity of the water flow into the sample.

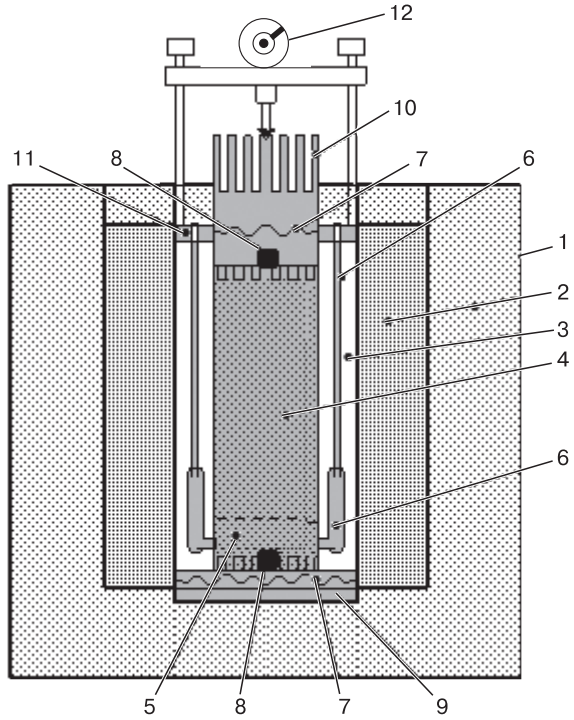

Fig. 4. Soil heaving meter [*Lapshin, Ganeles, 1979*].

1 – carcass, 2 – thermal insulation, 3 – Plexiglas cylinder, 4 – soil sample, 5 – fine sand, 6 – reservoir with water, 7 – electric heater, 8 – thermoelement, 9 – heat exchanger bottom, 10 – heat exchanger top, 11 – ring, 12 – strain sensor.

E.D. Ershov, V.G. Cheverev, and Yu.P. Lebedenko [*1988*] proposed a method and device for determining the hydraulic component of the pressure of frost heaving of soil by measuring the maximum pressure, at which cryogenic migration and heaving stop, with a dynamometer; this stop corresponds to stopping of the meniscus in the capillary tube (Fig. 5). The idea of this method was as follows. A sample of completely water-saturated soil was placed in a sleeve, at the bottom of which there was a layer of sand for water supply to the lower end of the sample. With the help of thermo-elements, constant temperatures were maintained at the ends of the sample.

A subzero temperature corresponding to the transition of the soil state from plastically frozen to hard-frozen is set at the upper end, and a positive temperature of about +0°C is maintained at the lower end of the sample. After temperature stabilization at the ends of the sample, the movement of the meniscus in the capillary tube is recorded in time, which allows calculating the amount of water entering the sample through unit area per unit time. During freezing, frozen and thawed zones separated by a freezing front appear in the sample. At the moment of the appearance of a frozen layer at the upper end of the sample, the screw is brought to the dynamometer. The value of the hydraulic component of the heaving pressure is determined by the dynamometer at the moment of stopping the flow of water into the sample through the lower end according to the meniscus stop; this ensures an important advantage in the possibilities of measurements.

It should be noted that with the stop of cryogenic migration under the action of the load, the freezing front does not stop and its progress causes a reverse outflow of the pore solution from the front. A similar device was subsequently implemented by V.G. Cheverev in the first normative document on laboratory determination of the degree of frost heaving of soils [*GOST 28622-1990, 1990*].

The closest technical solution for the purposes of physical modeling of soil freezing and heaving is a device, the schematic diagram of which is given in Fig. 6. Note the specific features of this device. In all cases, the external water source is located at the same level with the porous plate in the upper part of the chamber. An independent measurement of the full heaving is performed using a DC displacement sensor. Ten thermistors are mounted along the sample in contact with it.

Experiments with a freezer were carried out inside a room with a constant temperature close to the average temperature at the ends of the sample. The freezing of the sample was carried out from the bottom up, and the resistance to movement of the frozen part of the sample was reduced by using Teflon lubricant inside the chamber. A computer in combination with a multi-program unit made it possible to change the temperature at each end of the sample at a given rate.

The disadvantages of the device (Fig. 6) are: the lack of control over the layer-by-layer heaving of the freezing zone and shrinkage of the thawed zone of the

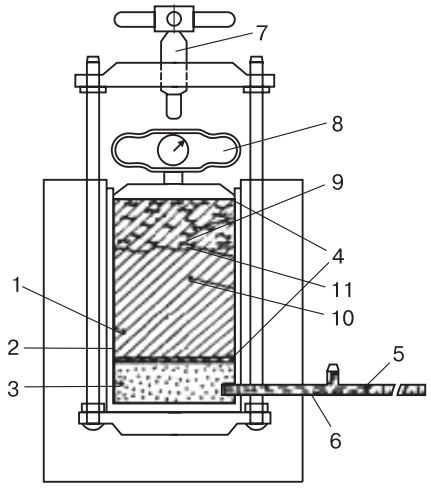

Fig. 5. Device for determining the pressure of frost heaving of soil [*Ershov et al., 1988*].

1 – soil sample, 2 – sample sleeve, 3 – capillary-saturated fine sand, 4 – thermoelements that do not interfere with the flow of water, 5 – meniscus; 6 – calibrated glass capillary, 7 – screw, 8 – dynamometer, 9 – frozen zone, 10 – thawed zone of the soil sample, 11 – freezing front.

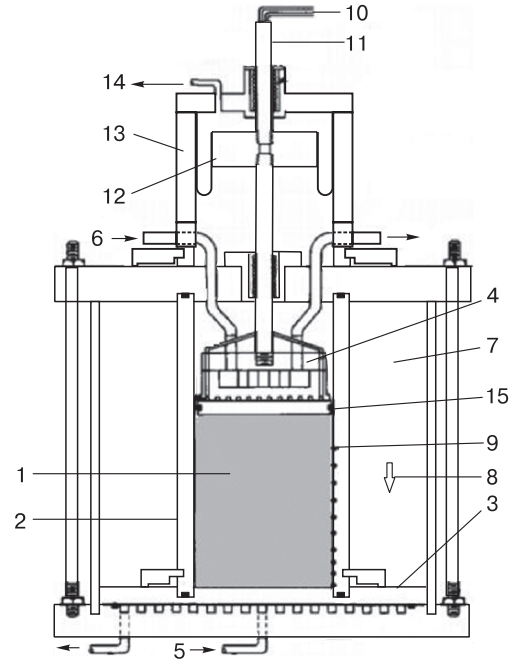

Fig. 6. Diagram of the freezer [*Penner, 1986*].

1 – soil sample, 2 – chamber (plastic pipe), 3 – cold stamp, 4 – warm stamp, 5 – cold antifreeze, 6 – warm antifreeze, 7 – thermal insulation, 8 – direction of heat flow in the sample, 9 – thermistors, 10 – a tube for supplying water to the sample, 11 – a tube for controlling the heaving deformation of the sample, 12 – piston,13 – cylinder, 14 – compressed air inlet, 15 – porous plate.

soil during its freezing, the lack of the means for measuring the pore pressure along the height of the thawed zone and the high-temperature frozen zone. Time-lapse video recording of ice segregation and measurement of the density of water flow into the sample from the outside are also not provided.

It was shown in [*Cheverev et al., 2013*] that the orientation of the sample, i.e., the change of the cryogenic migration vector to the gravity vector, does not significantly affect the final results, since the suction force of cryogenic migration is many times greater than the gravity force in soil samples of relatively small height. As a result, freezing of the soil from below under other equal conditions, as shown by comparative tests [*Cheverev et al., 2013*], does not affect the final result in determining the degree of frost heaving of the soil, but has a significant technological benefit, because only in this case a large-area cooling plate can be used in the device and several soil samples can be simultaneously placed on it for freezing at a given temperature.

Another positive effect is that when freezing from below, the frozen layer is immobile and heaving goes upward. This eliminates the problem of soil freezing from the inner surface of the sleeve and artificial containment of the heaving. It becomes possible to assess the influence of hard-to-control freezing forces in this process.

The boundary conditions for freezing a soil sample to determine the soil heaving capacity according to the standard procedure [*GOST 28622-2012, 2012*] assume cooling of one end to –4°C and heating of the other end to +1°C. The use of artificial heating does not allow us to freeze the sample completely, the freezing front slows down its movement and practically stops at the level of approximately 2/3 of the sample height. At the same time, favorable conditions arise for the intensive growth of a thick layer of ice at the freezing front (Fig. 7). As a result, the tested soil, in accordance with the provision of the standard [*GOST 28622-2012, 2012*], becomes excessively heaved, although initially it may not be.

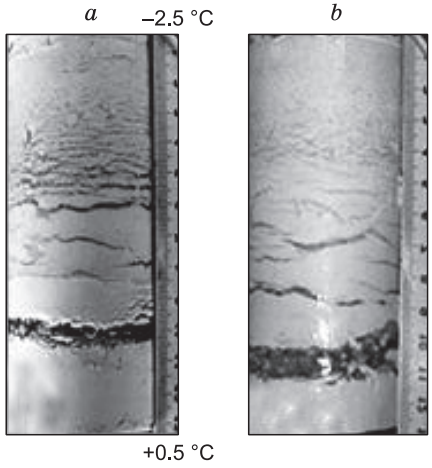

Fig. 7. Cryogenic structure of kaolinite silty clay frozen with boundary conditions of –2.5 and +0.5°C under loads:

a – 0.06 MPa; *b* – 0.04 MPa [*Cheverev et al., 2013*].

In the natural environment, the freezing of the seasonally thawed layer (STL) usually occurs in other thermal and physical conditions. In the autumn–winter period, the freezing of the STL comes from the soil surface and from the permafrost table. Between the two freezing fronts, a layer is formed, in which there is practically no temperature gradient, and the average temperature in this layer corresponds to the temperature of the beginning of soil freezing. This phenomenon was not taken into account in the standard procedure for measuring soil heaving [*GOST 28622-2012, 2012*].

To take into account this natural phenomenon under laboratory conditions, it is advisable to create a zone with zero temperature around the sleeve with the sample while eliminating local heating of the warm end of the sample. At the same time, the side wall of the sleeve must have sufficient thermal resistance to protect the temperature field of the freezing soil. For example, the wall thickness of a plexiglass sleeve of 15 mm, as experiments have shown, is sufficient.

It is also advisable to provide a method for determining the degree of heaving of a freezing soil sample with normal, increased, or decreased hydraulic pressure from the warm end of the sample. Without going into detail, such freezing options are dictated by the diversity of natural hydrogeological conditions; some of them are considered in [*Gorelik, 2010*].

Laboratory experiments are conducted and planned in order to accurately measure the movement of water through the thawed and freezing zones of the soil in dependence on the pore pressure gradient, temperature gradient, and chemical potential gradient in the frozen zone. Such carefully measured experimental data form the basis for determining, which mathematical model of the freezing process is correct and adequately reflects the physical essence of the heaving process.

METHODOLOGY OF THE PHYSICAL MODELING

The authors carried out laboratory physical modeling of one-sided freezing of soil samples with an influx of moisture from the outside under fixed boundary conditions for temperature. As tested model (reference) soil, a natural dusty, heaving clay of kaolinite composition was used. As a result of the research, the characteristics of the reference soil, the parameters of its freezing and heaving process were obtained under given boundary conditions for heat and mass transfer. These data were used in the future

to verify the physical formulation of the mathematical model of freezing and heaving of soils, taking into account heat and mass transfer and shrinkage of the melt zone.

Devices for physical modeling

The instrumental base to carry out the investigations consisted of the following devices: (1) a meter of frost heaving of soils; (2) a cryothermostat (CTS); (3) a special mold for compacting the tested soil; (4) a universal meter (thermograms of freezing–thawing of soil and the unfrozen water content); (5) devices for determining hydraulic conductivity of fine-earth soils in the thawed state by the method of stationary moisture exchange; and (6) a thermal conductivity meter for the frozen soil by the method of stationary thermal regime; other auxiliary equipment.

The studied characteristics of the model soil are as follows: the dependence of its bulk density and water content at capillary moisture saturation on the load in the thawed state; the unfrozen water content (W_w) in the temperature range of 0 to –5°C; thermograms of freezing–thawing; thermal conductivity and heat capacity of the soil in the thawed and frozen states; effective heat capacity (taking into account the heat of phase transitions); the dependence of the moisture transfer coefficients on the temperature in the frozen and thawed state.

Methods for determining these characteristics and the results of their application are described in articles and monographs [*Cheverev, 2003a,b, 2004; Cheverev et al., 2021*].

The boundary conditions measured and controlled in time, the parameters of the soil freezing process and its characteristics are as follows: the boundary conditions of the freezing and heaving process, the dynamics of the temperature field and pore pressure [*Cheverev et al., 2021, Fig. 8*], the movement of the freezing front, the flow of cryogenic migration, layer-by-layer deformation of frost heaving of the freezing zone and shrinkage of the thawed zone, and video fixation of the cryogenic structure formation.

To achieve the research goal, an automated device was developed, the main distinguishing feature of which, giving a significant positive effect, was that the soil samples were frozen from the bottom up, and the water supply went from the top to the bottom. At the same time, an external load was applied from above from the side of the thawed zone (Fig. 8). The justification for the validity of the application of the proposed technique (we are talking about freezing from below) to determine the characteristics of the frost heaving of soils is given in [*Cheverev et al., 2013*], as well as in the description of the design of testing equipment (see below).

The device consists of a high-temperature freezer, in the internal volume of which a positive temperature of 0–0.1°C is maintained. At the bottom of the chamber, there is a cooling thermal plate with a cavity, in which the antifreeze of the cryothermostat circulates. Two supports are installed on the thermal plate performing the role of the power frame of the device together with the thermo-plate. A pipe (the square-section 70 × 70 mm and the height 150 mm) made of transparent acrylic glass with a metal bottom and with a vertical channel is installed on the thermal plate. The channel is filled with an aqueous salt solution, the freezing temperature of which corresponds to the temperature at the freezing front of the soil. This temperature is equated to the temperature of the beginning of freezing of the tested soil according to the results of preliminary determination.

In the lower part of the channel, a metal plug tightly adjacent to the thermal plate is installed, thanks to which, as established by experiment, the supercooling of the solution at the initial stage of freezing is reduced. The position of the freezing front in the soil sample in time is determined visually using time-lapse video, as well as the distribution of temperatures along the height of the sample using a set of temperature sensors.

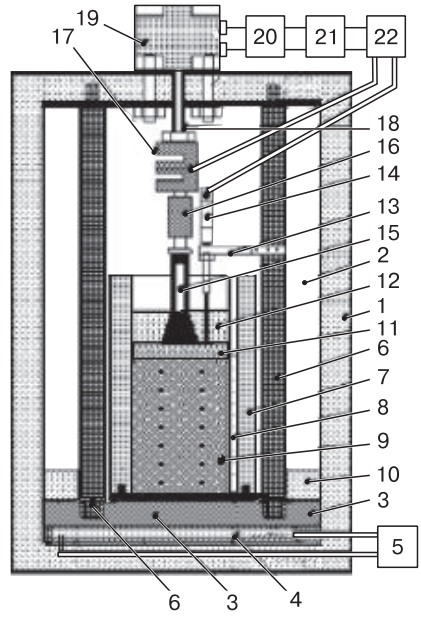

Fig. 8. A device for physical modeling of freezing and heaving of soil with control of boundary conditions and determination of the process parameters.

1 – high-temperature freezer, 2 – internal volume of the chamber to maintain a temperature of 0°C, 3 – thermal plate with a hollow, 4 – hollow, 5 – circulating liquid thermostat for freezing a soil sample, 6 – support racks, 7 – a sleeve for placing the tested soil sample, 8 – cylindrical channel filled with an aqueous solution, 9 – soil sample, 10 – thermal insulation ring, 11 – ceramic capillary-pore water-saturated plate, 12 – a layer of capillary saturated fine-grained sand, 13 – bracket, 14 – displacement sensor, 15 – support rack, 16 – coupling, 17 – force sensor, 18 – pneumatic cylinder rod, 19 – pneumatic cylinder, 20 – pneumatic actuator, 21 – air compressor, 22 – electronic control unit.

As a justification for the appropriateness of the load application from the thawed zone, we note the following. Since the force of action is equal to the force of counteraction, it is possible to apply a load and measure the heaving force from both the frozen and thawed zones, which in this case is equivalent. This condition is ensured by the fact that the ceramic porous plate must have sufficient strength against destruction when a load is applied and, at the same time, maintain a hydraulic conductivity of no less than the hydraulic conductivity of the soil of the thawed zone. The area of the plate should be as close as possible to the area of the soil sample, ensuring free sliding along the sleeve. The size of the base area of the support post should be smaller, which is necessary for the free movement of water into the freezing soil sample from the sand layer through the porous plate.

With this variant of physical modeling, the area on which the load acts is equal to the area of the frozen soil surface, taking into account the correction for the friction force of the soil in the thawed and freezing zones on the surface of the sleeve. The results obtained will be applicable in practice if the area of the heaving soil is equal to the area of the construction basement. However, if the area of the heaving soil is larger than the area of the basement, then the effect of normal heaving forces on the foundation increases proportionally to this difference.

Methods of physical modeling

The device described above allows testing under the following moisture conditions.

The first mode is a closed system without water supply from the outside. In this case, a waterproof film is placed between the sand layer and the soil.

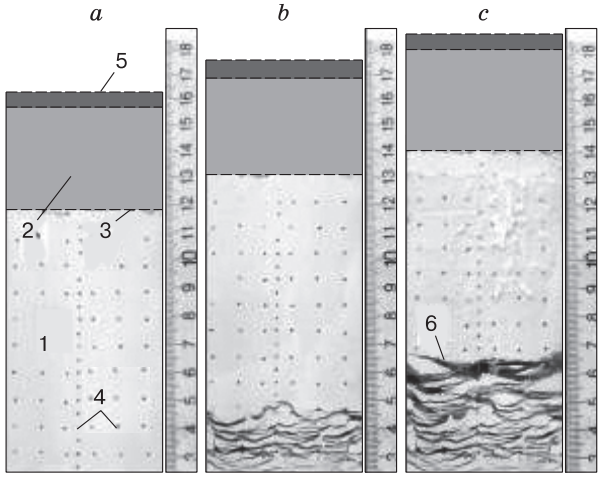

Fig. 9. Results of freezing of a sample of kaolinite clay (experiments without load).

a – before the experiment (0 h); *b*, *c* – during the experiment (*b* – 23 h; *c* – 63 h); 1 – soil sample; 2 – capillary-saturated fine-grained sand; 3 – the boundary between sand and clay; 4 – position sensors; 5 – metal plate with drainage holes; 6 – ice lenses.

The second mode is an open system, in which the flow of water from the outside takes place, but without pressure. In this case, the sand layer is moistened only up to the state of capillary saturation. Capillary water in the sand pores is a reserve for the flow of water from outside into the freezing ground. By varying the thickness of the sand layer, you can control the volume of the reserve water. At the same time, there is no hydrostatic pressure from the capillary-saturated fine-grained sand on the tested soil, since the water is in a capillary-suspended state. The water layer in the 3-cm-thick sand layer, taking into account its porosity, is 1 cm. This amount of water that has entered the freezing water-saturated soil during cryogenic migration and segregation of ice lenses will be sufficient for the soil to manifest a relative deformation of frost heaving of more than 0.1 f.u., if the initial height of the soil sample is 10 cm. In this case, the soil is assessed as excessively heaving. With an increase in the height of the tested soil sample, for example up to 15 cm, the thickness of the capillary-saturated sand layer should be proportionally increased to 4.5 cm.

The third mode is an open system, in which the flow of water from outside into the frozen soil sample occurs under pressure. In this case, a layer of water is maintained above the layer of water-saturated sand, the level of which relative to the surface of the soil sample determines the pressure.

The creation of various modes of water flow into the soil in this technical implementation allows us to study the dependences of the characteristics of heaving on various hydrogeological conditions of the soil freezing.

The design of the device also provides for the possibility of creating static pressure on the sample due to the existing pneumatic actuator. In the course of physical modeling, only the second mode has been used so far: an open system for water exchange at atmospheric pressure level.

Before the start of freezing, the temperature of the samples should be lowered to 0–0.1°C. For this purpose, the corresponding temperature is set in the cooling thermostat. The hollow plate is cooled to the specified temperature by pumping the thermostat antifreeze in a closed circle and thereby cools the tested soil samples. Thermal insulation of the freezer is efficient enough to exclude a significant influx of heat from outside. Precooling of the samples of the soil as a whole is completed after reaching a temperature of 0–0.1°C in the upper part of the chamber. This stage lasts for several hours.

The thermostat is switched to the freezing temperature of the soil (for example, –2.5°C), and the circulation of antifreeze is switched on. The plate acquiring a subzero temperature cools the lower layers of the soil sample that become frozen when their temperature reaches the freezing point and below. In this case, there is a freezing front separating the formed

frozen and the overlying not yet frozen (thawed) soil layer. Control over the advance of the freezing front in time and depth is carried out using a cylindrical channel (Fig. 8).

During the freezing of the heaving soil, the pore solution moves from the unfrozen zone to the freezing zone, where excess water freezes with the formation of ice lenses and soil heaving. During the freezing of a soil sample, its layer-by-layer heaving deformation is fixed with a help of a grid of position sensors by time-lapse video recording. Deformations are fixed in both vertical and horizontal directions. Zero deformations in the horizontal direction can occur when the soil reaches the shrinkage limit in the measured layer. At the same time, the pneumatic drive system works to maintain static pressure on the freezing soil sample, which is heaving, exerting back pressure on the force sensor and the rod of the pneumatic cylinder.

As an example, the results of freezing of the sample of kaolinite powdery clay obtained during the time-lapse survey tests at the time before the experiment (0 h) and after 23 and 63 h of freezing are shown in Fig. 9.

In this experiment, the soil sample in the form of a parallelepiped with transverse dimensions of 70 × 70 mm and the initial height of 120 mm was placed in a 15-mm-thick acrylic glass cage. The capillary-saturated sand was placed on top of the sample; in turn, on top of the sand, a metal stamp with holes was installed. Needle-type position sensors were used.

Figure 9 demonstrates that, due to the freezing from below, cryogenic structure of the wavy-layered horizontal type is formed in the soil After 63 h of freezing, the size of the ice lenses increased significantly to 3–5 mm, and the rate of freezing and heaving naturally decreased. The total heaving deformation (including heaving of the frozen and shrinkage of the thawed zones) of the clay sample upon its incomplete freezing reached 24 mm.

CONCLUSIONS

1. A brief analytical review of developments in the field of laboratory (physical) modeling of the heaving process during soil freezing, which, according to the authors is given. A comparison of the methods and devices simulating the heaving process in two significantly different ways is performed: freezing from above with water inflow from below and freezing from below with water inflow from above. It is shown that the second method has a number of advantages. Thus, it eliminates the influence of the freezing forces of the soil with the inner surface of the sleeve, allows one to increase the number of simultaneously tested samples, maintains the temperature conditions of laboratory modeling close to those under natural conditions of the seasonally freezing layer, and creates new opportunities for studying the freezing process taking into account changes in hydrogeological factors.

2. A structurally optimal set of methods is proposed for determining the characteristics and parameters of the heaving process. This set ensures measuring of a full set of physical characteristics of the freezing and heaving processes and the corresponding external conditions and yields promise for its further use for verification of existing and developed mathematical models of soil freezing and heaving.

Funding. *The study was carried out with the financial support of Transneft Research Institute LLC (contract No. 4220 P/20-511/2015 from November 19, 2015).*

References

Alekseev A.G., 2020. Laboratory studies of the pressure of cryogenic heaving of soils. *Vestnik NITs Stroitel'stvo,* No. 3, 5–12 (in Russian).

Ananyan A.A., 1970. Water in rocks, its migration during freezing. In: *Bound Water in Dispersed Systems,* Moscow, Izd. Mosk. Gos. Univ., Iss. 1, p. 146–154 (in Russian).

Bazhenova A.P., Bakulin F.G., 1957. Experimental studies of the mechanisms of moisture movement in freezing soils. In: *Materials on Laboratory Studies of Frozen Ground,* Moscow, Izd. Akad. Nauk SSSR, No. 3, p. 117–123 (in Russian).

Cheverev V.G., 2003a. Classification of water bonding forms in the frozen fine-grained soils. *Kriosfera Zemli* VII (3), 31–40 (in Russian).

Cheverev V.G., 2003b. Properties of bound water in cryogenic soils (analytic review). *Kriosfera Zemli* VII (2), 30–41 (in Russian).

Cheverev V.G., 2004. The Nature of Cryogenic Properties of Soils. Moscow, Nauchnyi mir, 234 p. (in Russian).

Cheverev V.G., Burnaev R.S., Gagarin V.E., Safronov E.V., 2013. Influence of external pressure on the degree of frost heaving of clay soils. *Kriosfera Zemli* XVII (4), 57–62 (in Russian).

Cheverev V.G., Safronov E.V., Korotkov A.A., Chernyatin A.S., 2021. Physical statement of the problem for a numerical model of soil freezing and heaving taking into account heat and mass transfer. *Nauki Tekhnolog. Truboprovodn. Transp. Nefti Nefteproduktov,* **11** (3), 244–256 (in Russian).

Ershov E.D. (Ed.), 2004. Methods of Geocryological Research: A Textbook. Moscow, Izd. Mosk. Gos. Univ., 512 p. (in Russian).

Ershov E.D., Cheverev V.G., Lebedenko Yu.P., 1988. *Method for Determining the Pressure of Frost Heaving of Soil: Patent No. 1596241*, Byull. 36, Publ. Sept. 30, 1990.

Gorelik Ya.B., 2010. On the calculation methods of the engineering construction displacements caused by heaving of freezing layer. *Kriosfera Zemli* XIV (1), 50–62 (in Russian).

GOST 28622-1990, 1990. Soils. The Method of Laboratory Determination of the Degree of Heaving. Moscow, Standartinform, 12 p. (in Russian).

GOST 28622-2012, 2012. Soils. The Method of Laboratory Determination of the Degree of Heaving. Moscow, Standartinform, 12 p. (in Russian).

Lapshin V.Ya., Ganeles L.B., 1979. Recommendations for Determining the Frost Heaving of Soils of the Bases of Buildings

and Structures. Sverdlovsk, Ural Politekhnich. Inst., 34 p. (in Russian).

Nersesova Z.A., 1961. Influence of exchange cations on water migration and soil heaving during freezing. In: *Research on the Physics and Mechanics of Frozen Soils*. Moscow, Izd. Akad. Nauk SSSR, Iss. 4, 251 p. (in Russian).

Penner E., 1986. Aspects of ice lens growth in soils. *Cold Reg. Sci. Technol.* **13**, 91–100.

Shtukenberg V.I., 1894. On the heaving control fight against the depths on the railways. *Zh. Ministerstva Putei Soobshcheniya* (Moscow), book 2, p. 24–30 (in Russian).

Taber S., 1930. The mechanics of frost heaving. *J. Geology* **38** (4), 303–313.

Voislav S.G., 1896. A brief description of the causes of heaving of the Nikolaev railway. *Tr. Byuro Issled. Pochvy* (Proceedings of the Bureau of Soil Research). St. Petersburg, 133 p. (in Russian).

Received July 5, 2021
Revised July 6, 2022
Accepted July 16, 2022

Translated by S.B. Sokolov

EARTH'S CRYOSPHERE
SCIENTIFIC JOURNAL

Earth's Cryosphere, 2022, vol. XXVI, No. 4, pp. 41–50

GEOLOGICAL CRYOGENIC PROCESSES AND FORMATIONS

MAPPING OF GIANT AUFEIS FIELDS IN THE NORTHEAST OF RUSSIA

O.M. Makarieva[1,2,*], V.R. Alexeev[1], A.N. Shikhov[3], N.V. Nesterova[2,4], A.A. Ostashov[4], A.A. Zemlyanskova[2,4], A.V. Semakina[5]

[1] *Melnikov Permafrost Institute, Siberian Branch of the Russian Academy of Sciences, ul. Merzlotnaya 36, Yakutsk, 677010 Russia*
[2] *St. Petersburg State University, Universitetskaya nab. 7-9, St. Petersburg, 199034 Russia*
[3] *Perm State University, ul. Bukireva 15, Perm, 614990 Russia*
[4] *Northeastern Permafrost Station, Melnikov Permafrost Institute, Siberian Branch of the Russian Academy of Sciences, ul. Portovaya 16, Magadan, 685070 Russia*
[5] *Perm Branch of Roslesinforg, ul. Marshrutnaya 14, Perm, 614990 Russia*

**Corresponding author; e-mail: omakarieva@yandex.ru*

Aufeis fields are widespread in the northeast of Russia and exert a substantial impact on many components of landscapes. The public availability of Landsat and Sentinel-2 satellite data has opened up new opportunities for aufeis mapping. Based on satellite images, we have compiled an up-to-date GIS dataset of aufeis fields and analyzed the long-term and seasonal variability of the largest aufeis in the northeast of Russia. The synthesis of historical (aerial photography obtained in the middle of the 20th century) and modern satellite data on aufeis has been used to prepare a new cartographic product, the Atlas of Giant Aufeis (Taryns) of the Northeast of Russia. In this paper, we consider the approaches to aufeis mapping applied in the Atlas, the main characteristics of aufeis fields based on historical and satellite data. According to Landsat images obtained in 2013–2020, we have delineated 9306 aufeis fields with a total area of 4854.5 km^2. Among them, there are 1146 giant aufeis fields of more than 1 km^2 in area. For these aufeis fields, we have analyzed long-term and seasonal dynamics of their area based on satellite images obtained for the period from the 1970s to the present. On this basis, a series of image-based maps have been created and included in the Atlas. For most of the giant aufeis fields, no substantial reduction in their area since the 1970s has been found. The largest aufeis in the northeast of Russia is located in the Syuryuktyakh River basin; its area immediately after the snowmelt season is, on average, 14.4 km^2 larger than the area of the Bol'shaya Moma aufeis, which was previously considered as the largest aufeis in Russia.

Keywords: *aufeis fields, mapping, atlas, Landsat and Sentinel-2 satellite data, aufeis cadaster, GIS database, northeast of Russia.*

Recommended citation: Makarieva O.M., Alexeev V.R., Shikhov A.N., Nesterova V.V., Ostashov A.A., Zemlyanskova A.A., Semakina A.V., 2022. Mapping of giant aufeis fields in the Northeast of Russia. *Earth's Cryosphere*, XXVI (4), 41–50.

INTRODUCTION

Aufeis is a form of terrestrial glaciation typical for mountainous areas in the permafrost zone. Aufeis fields are formed every year in the cold season as a result of layer-by-layer freezing of groundwater discharged to the surface. Aufeis forming near permanently active springs are called taryn (the term came from Yakut language). Aufeis-taryn may occupy considerable areas (up to 3–5% of the territory in some mountainous regions) and serve as a powerful regulator of groundwater flows and surface runoff [*Yoshikawa et al., 2007; Alexeev et al., 2011; Alexeev, 2016*]. The water reserves in aufeis of Russia amount to at least 50 km^3, which is almost equal to the annual runoff of the Indigirka River [*Sokolov, 1975*].

The most favorable conditions for the formation of aufeis-taryn, including giant ones, occupying the area of more than 1 km^2 [*Petrov, 1930*], are typical of the northeast of Russia (NER). The NER includes the basins of the Yana, Indigirka, Kolyma, Penzhina, rivers of the Okhotsk Sea basin running from the Suntar-Khayat Ridge, as well as the Anadyr River and other rivers of the Chukchi Peninsula.

The NER is characterized by predominantly mountainous relief, up to 3147 a.s.l., with the exception of the Yana-Indigirka and Kolyma lowlands. A larger part of the NER is located in the zone of subarctic continental climate with very cold winter (mean January air temperature is –36°C and below) and short warm summer [*National Atlas..., 2004*]. The entire territory, except for the coast of the Sea of Ok-

hotsk, is located in the zone of continuous permafrost [*Geocryology of the USSR, 1989*]. The thickness of permafrost in the upper reaches of the Yana and Indigirka rivers is up to 350–500 m and more on the top mountain slopes; the depths of seasonal thawing are 0.9–1.3 m [*Geocryology of the USSR, 1989*].

A relevance of the study of aufeis is determined by their fundamental importance and by practical reasons. The history of their research in Russia has more than 100 years.

The first scientific paper in Russian language on the nature of aufeis phenomena was published in 1903 on the basis of the year-round permafrost and hydrogeological observations in South Yakutia [*Podyakonov, 1903*]. Studies of aufeis dramatically intensified at the turn of the 1920s and 1930s which was related to the organization of the Yakut Expedition of the Academy of Sciences of the Soviet Union and the study of water resources and transportation routes in eastern regions of the country. Thus, V.G. Petrov developed methods on dealing with groundwater aufeis located near road structures [*Petrov, 1930, 1934*]. N.I. Tolstikhin classified groundwater feeding aufeis in relation to the permafrost, clarified the definition of aufeis, and distinguished between suprapermafrost, permafrost, and subpermafrost water aufeis [*Tolstikhin, 1931*]. The works of V.P. Sedov and P.F. Shvetsov, in particular, the work [*Shvetsov, Sedov, 1941*], were crucial for the study of the NER aufeis. For the first time in the history of aufeis research, they created situational maps of aufeis fields with indication of the ice thickness distribution and sources of the aufeis formation. It was found that the main part of aufeis fields is formed by deep groundwater sources that discharge freely to the surface.

In the 1940s, attention to the study of aufeistaryn in the NER increased due to the discovery and development of the richest mineral deposits (gold, tin, tungsten, uranium, etc.).

The works of [*Chekotillo, 1941; Zonov, 1944*] were most important. In the article [*Zonov, 1944*], the author considers aufeis in the entire Yana-Kolyma mountainous area and for the first time identifies and describes aufeis fields that do not melt away completely in summer. In the 1940s, the staff of the Dal'stroy expeditions made a great contribution to the study of permafrost and groundwater. The results of their long-term research were summarized by [*Simakov, 1949*]. The first map of aufeis in the Indigirka River basin was published [*Shvetsov, 1951*].

Regular observations of aufeis fields continued during a quarter of the century, generally, because of the effort of the staff of the Melnikov Permafrost Institute, SB RAS. For the first time, the maps of aufeis areas [*Sokolov, 1975*] and detailed aufeis zoning [*Tolstikhin, 1974, 1975*] were made for the NER. In the 1960s, special aufeis research sites were arranged on several rivers in the NER. The longest series of observations (from 1962 to 1992) was obtained at the Anmangynda aufeis research site organized by the Kolyma Administration for Hydrometeorological and Environmental Monitoring in 1962. Materials of the Anmangynda long-term observations are summarized in [*Alexeev et al., 2012*].

A hydrological role of aufeis and their contribution to the annual runoff distribution was determined. It was established that, in winter, aufeis accumulate up to 70% of subsurface runoff; in summer, the same amount of water enters the river network as a result of aufeis ablation. In most cases, the contribution of aufeis ablation to the annual river discharge is 3–7%, reaching 25–30% in some river basins with the highest aufeis percentage [*Sokolov, 1975; Reedyk et al., 1995*].

Since the early 1990s, the study of aufeis in the NER has ceased. However, at present, the practical importance of their study has increased due to the development of the Arctic regions. For example, aufeis negatively affects the stability of engineering constructions and complicates transport communication, which has been first shown in the works of the classics of geocryology [*Lvov, 1916; Sumgin, 1927; Petrov, 1930*]. Springs, which feed aufeis, may, in some cases, serve as the only source of water supply to settlements [*Simakov, 1949; Simakov, Shilnikovskaya, 1958; Alexeev, 1987*].

Aufeis zones of river valleys and aufeis themselves are well visible on aerial and satellite images. The use of the Earth remote sensing (ERS) data makes it possible to determine the boundaries of the aufeis landscapes and calculate the area of ice fields at a certain point in time during different stages of their development. This provides broad opportunities for the study of the distribution patterns and spatiotemporal variability of aufeis phenomena. The first large-scale studies in this direction were carried out in the NER in the middle of the 20th century. The Map of Aufeis in the NER on a scale of 1:2 M and the Cadaster of Aufeis, which is a supplement to the map, were compiled on the basis of the systematization of aerial photography in the 1940s and 1950s [*Simakov, Shilnikovskaya, 1958*]. They contained data on 7448 aufeis, the area of which ranged from 0.01 to 81.1 km^2 (the area was determined by aufeis glades). The materials were handwritten and kept in the archive of the Geological Administration in Magadan.

For the first time, satellite imaginary data on aufeis were applied in the 1970s [*Topchiev, 1979*]. Satellite images were also actively used during the construction of the Geocryological Map of the USSR, which was created in the early 1970s and completed in 1991 [*Geocryological Map..., 1996*]. This map demonstrates 5109 aufeis. The largest of them were given on a scale, the others were represented off-scale (by points). In 2013, these data were digitized, refined, and verified using the Landsat/ETM+ satellite im-

ages [*Prasolova et al., 2013*]. However, these digital data have not been published, which distinguishes aufeis from glaciers, for which there is an updated digital catalog [*GLIMS and NSIDC, 2017*].

In the recent decade, availability of Landsat and Sentinel-2 satellite data has significantly increased the ability to map aufeis. Thus, for the NER, data from Landsat-7, 8 satellites with a spatial resolution of 15 and 30 m have become available since 1999; the Landsat-1 (MSS sensor) data with a spatial resolution of 80 m have been obtained since 1973. This makes it possible not only to assess the current state of the aufeis, but also to analyze their long-term variability.

Like other snow-ice objects, aufeis are identified automatically on the basis of the normalized difference snow index NDSI [*Hall et al., 1995*] or more complex indices [*Morse, Wolfe, 2015*]. Some difficulties in the identification of aufeis on the images are related to their separation from the snow cover [*Pavelsky, Zarnetske, 2017; Makarieva et al., 2019*] and ice-covered water bodies [*Morse, Wolfe, 2015*]. However, these problems are successfully solved by the proper selection of images (the most informative images for the NER are those for the period from late May to mid-June), or through expert verification [*Makarieva et al., 2019*].

Public availability of satellite data and the opportunity to distinguish aufeis according to these data in a semiautomatic mode made it possible to create current cartographic databases of aufeis in river basins of the NER. Based on the synthesis of historical and modern materials on aufeis, the new cartographic product, the Atlas of Aufeis-Taryns in the Northeast of Russia, was prepared [*Alexeev et al., 2021*]. The present paper reports on the characteristics of the used data array and briefly discusses approaches to the mapping of aufeis on the basis of the cartographic and satellite data.

MATERIALS AND METHODS

Cartographic databases [*Makarieva et al., 2021a–d*] created by the authors of this work served as background information for aufeis mapping in the NER. The databases was formed with the use of two sources: the Map and Cadaster of aufeis in the northeast of the USSR [*Cadaster..., 1958; Simakov, Shilnikovskaya, 1958*] and the Landsat-8 satellite images. Specific features of these data and the methods of creating cartographic databases of aufeis were discussed in [*Makarieva et al., 2019*] using the Indigirka River basin as an example. It should be noted that only the actual area of ice, indicated on satellite images, was taken into consideration in this work. As a result, it turns out that the area of aufeis was 1.5–2.2 times smaller than in the Cadaster of 1958. The area of aufeis glades is significantly larger than the actual area of ice, but many of the aufeis glades remain partially or completely free of ice even at the beginning of the period of aufeis ablation.

Data on aufeis contained in the Cadaster (1958) are presented on the new map as point objects (with the area indicated in the Cadaster), while aufeis mapped on the basis of Landsat-8 images are presented as area objects (areas covered with ice at the time of the survey). By now, the database of aufeis has been created on the basis of Landsat images for the entire study territory, except for the Sea of Okhotsk coast.

The Landsat-8 images were downloaded from the USGS web service [*http://earthexplorer.usgs.gov*]. Images for the period of 2013–2020 were used for the aufeis mapping, but more than 50% of all data on aufeis were obtained from the images taken in 2016, when the stable period of low-cloudy weather was observed in early June. More than 130 scenes of Landsat-8 obtained in the first weeks after the loss of the snow cover were processed. The earliest date was May 15 and the latest was June 26. Data processing and interpretation of the aufeis distribution were carried out in the QGIS and ArcGIS packages.

To exclude erroneously selected objects and omissions of aufeis, the results of automated interpretation of aufeis were manually checked. This included determination of aufeis boundaries with the removal of snow-covered areas adjacent to aufeis, the removal of other ice objects, such as ice-covered lakes or riverbeds, and merging together parts of aufeis separated into pieces during ice melting. Such areas were considered as parts of a single aufeis if they were located within the same aufeis glade.

In total, 9306 aufeis with a total area of 4854.5 km^2 were identified within the study territory according to the images (Fig. 1). According to the Cadaster of 1958, there were 6704 on this territory, and their total area reached 9785 km^2. The correspondence of data on aufeis according to these two sources is presented in Table 1 for the five largest river basins of the study region.

Discrepancy between the total area of aufeis given in the Cadaster of 1958 and estimated from recent Landsat images is caused by the different accounting methods. In the Cadaster, the area of aufeis glades was estimated, while the Landsat images demonstrated the area covered with ice at the time of survey. The Landsat images were taken during the period of active melting of aufeis, so it was necessary to reconstruct their maximum area (before melting). This was done on the basis of data on the size category of aufeis and the number of days of the aufeis melting before the image was taken [*Sokolov, 1975*]. On average, the calculated maximum area of aufeis in the river basins was 15–30% larger than the area directly estimated from the images (Table 1).

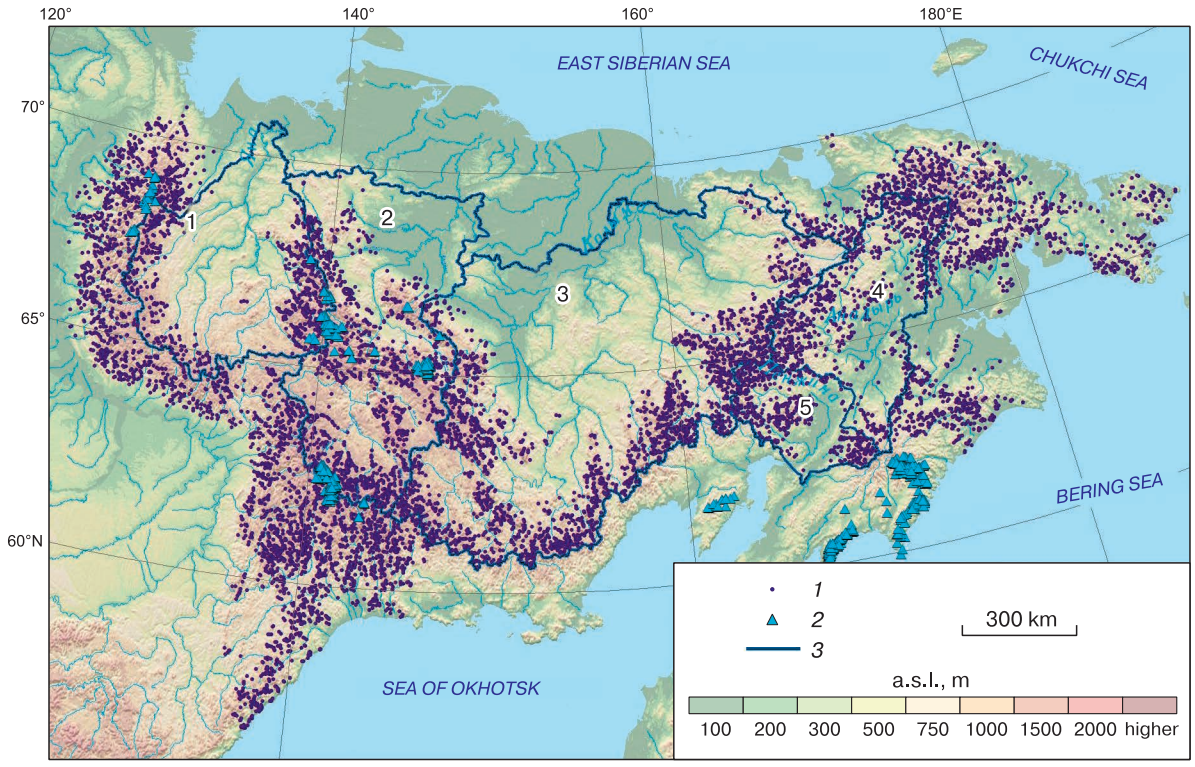

Fig. 1. Spatial distribution of aufeis in the northeast of Russia (excluding the northern coast of the Sea of Okhotsk) identified by the Landsat-8 satellite data.

(*1*) Aufeis (according to Landsat data), (*2*) glaciers (according to GLIMS data), (*3*) boundaries of river basins. Basins of large rivers: 1 – Yana, 2 – Indigirka, 3 – Kolyma, 4 – Anadyr, 5 – Penzhina.

Selective comparison of the reconstructed aufeis area with the area of aufeis glades gives ambiguous results. In most cases, the reconstructed area is close to the area of aufeis glades. However, there are numerous aufeis glades, for which the reconstructed area is several times smaller than the area of aufeis glade. In such cases, the aufeis in the images usually look like several ice massifs within one vast glade, and the total area of ice is many times smaller than the area specified in the Cadaster. Such aufeis presumably belong to the areas with extinction of aufeis processes according to the classification [*Zonov, 1944*]. However, to estimate real temporal changes in their area, additional studies of the images obtained in different years are required. The largest aufeis which demonstrate the signs of extinction are located in the Chukchi Peninsula.

Therefore, according to the modern data, the number of aufeis is greater than that indicated in the Cadaster of 1958, but their total area is significantly smaller. A similar result was obtained earlier for the Indigirka River basin [*Makarieva et al., 2019*]. How-

Table 1. **Comparison of Cadaster [*1958*] and Landsat image data on the number of aufeis areas within the five largest river basins in the NER**

River basin–outlet	Number and area (km^2) of aufeis according to the Cadaster of 1958		Number and area (km^2) of aufeis according to Landsat images		
	aufeis confirmed by Landsat images (by the presence of ice)	aufeis unconfirmed by Landsat images	aufeis confirmed by the Cadaster	aufeis absent in the Cadaster	maximum calculated aufeis area
Yana–Yubileiny	268 (616.4)	117 (122.2)	262 (309.8)	320 (102.4)	513.8
Indigirka–Vorontsovo	605 (1845.8)	243 (140.1)	582 (974.9)	572 (238.6)	1627.4
Kolyma–Chersky	1100 (1605.3)	662 (332.6)	1072 (714.2)	1138 (164.4)	1163.5
Anadyr–3 km upstream the Utesiki River	357 (661.2)	147 (101.7)	351 (280.6)	399 (71.4)	396.5
Penzhina–mouth	302 (410.9)	122 (125.5)	288 (106.5)	250 (48.7)	189.5

ever, this difference may well be related to the aforementioned differences in the approaches to the assessment of aufeis area rather than to a real decrease in the area of aufeis.

Creation of the maps of the spatial distribution of aufeis

An important indicator of the spatial distribution of aufeis and their significance for the hydrological regime of the territory is the aufeis percentage (aufeis area, % of the total area of the territory). It was calculated by two methods: in cells of a regular grid of 50 × 50 km and as an average for local catchments. In the first method, for each cell, the areas of all aufeis fields were summarized, and then the obtained values of the aufeis percentage were interpolated from a center of each cell. The tension spline method was used for interpolation.

The second method assumed the preliminary construction of a scheme of catchments. For this purpose, a thalweg network was created on the basis of the GMTED-2010 global digital elevation model (DEM) with a cell size of 230 m [*Danielson, Gesch, 2011*]. In further calculations, only those thalwegs, for which the catchment area exceeded 1000 DEM cells (approximately 50 km^2), were taken into consideration. All objects of the third and higher orders were selected from these thalwegs according to the Horton–Strahler scheme [*Strahler, 1952*], and then their catchment boundaries were plotted in automatic mode. Considering the low spatial resolution of the initial DEM, the manual editing of the selected catchment areas was necessary in many cases. Verification was performed by matching the selected catchment boundaries and the hydrographic network with the digital cartographic base of VSEGEI on a scale 1:2.5 M [*http://vsegei.com/ru/info/topo/*]. The percent of aufeis area of the total local catchment area was calculated at the next stage. The calculation was made both on the basis of historical data [*Cadaster..., 1958*] and recent satellite images.

ANALYSIS OF CARTOGRAPHIC MATERIALS PRESENTED IN THE ATLAS

The Atlas of Aufeis-Taryns in the Northeast of Russia presents the maps of the aufeis distribution compiled according to the Cadaster (1958) data and on the basis of Landsat images (for the latter, the minimum area is 1 ha). Aufeis in the basins of the main rivers of the NER (Indigirka, Yana, Kolyma, Anadyr), Chukotka rivers (Amguema, Lyulyuveem, Palyavaam), and the largest rivers of the Sea of Okhotsk basin (Penzhina, Ulbeya, Nyadbaki) have been mapped. The Atlas includes the maps of aufeis-taryn distribution in the basins of the largest rivers (Fig. 1) and their local catchments, the maps of the aufeis percentage in the large river basins (Fig. 2), the maps of

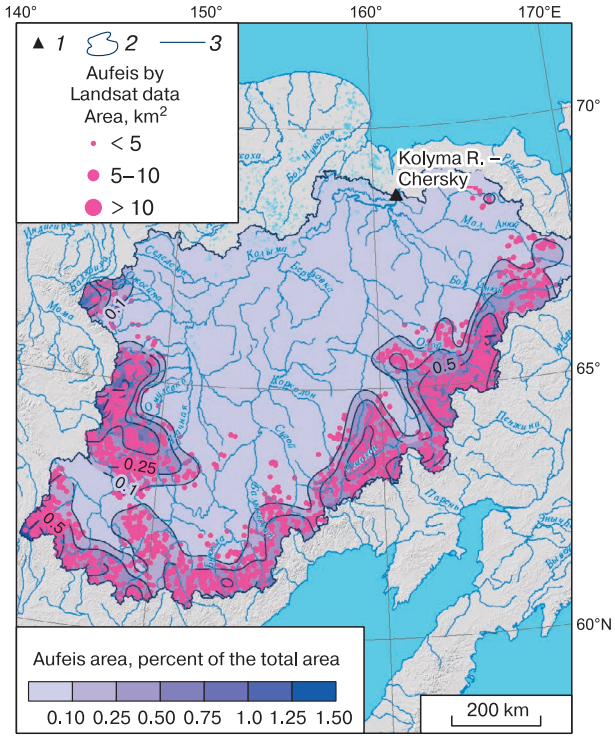

Fig. 2. Aufeis percentage in the Kolyma River basin according to Landsat-based data.

1 – Gauging stations, *2* – the Kolyma River basin, *3* – isolines of the aufeis percentage.

the aufeis percentage as a function of the river length for the main river basins, and a series of maps created on the basis of satellite imagery and characterizing the current state and dynamics of giant aufeis.

In addition, during expeditions of 2020–2021, we surveyed some aufeis glades in the basins of the Indigirka and Kolyma rivers from an unmanned aerial vehicle (UAV). The orthophoto maps of the Anmangynda aufeis and aufeis in the Kyubyume River basin [*Makarieva et al., 2021e*] and other objects were prepared on the basis of these data. They are also presented in the Atlas.

The map of aufeis resources (Fig. 3) gives the general characteristics of the water reserves that can be accumulated in the NER aufeis. Such a map was first published in the Atlas of Snow and Ice Resources of the World [*1997*] on the basis of data obtained by B.L. Sokolov. Aufeis resources (measured in millions of cubic meters per 1000 km^2) were calculated for the largest river basins of the NER.

The maximum aufeis percentage within the study area is typical of the Indigirka River basin and especially of some of its tributaries flowing down from the Chersky Ridge. The Syuryuktyakh River basin is characterized by the highest aufeis percentage (over 3%) in the NER.

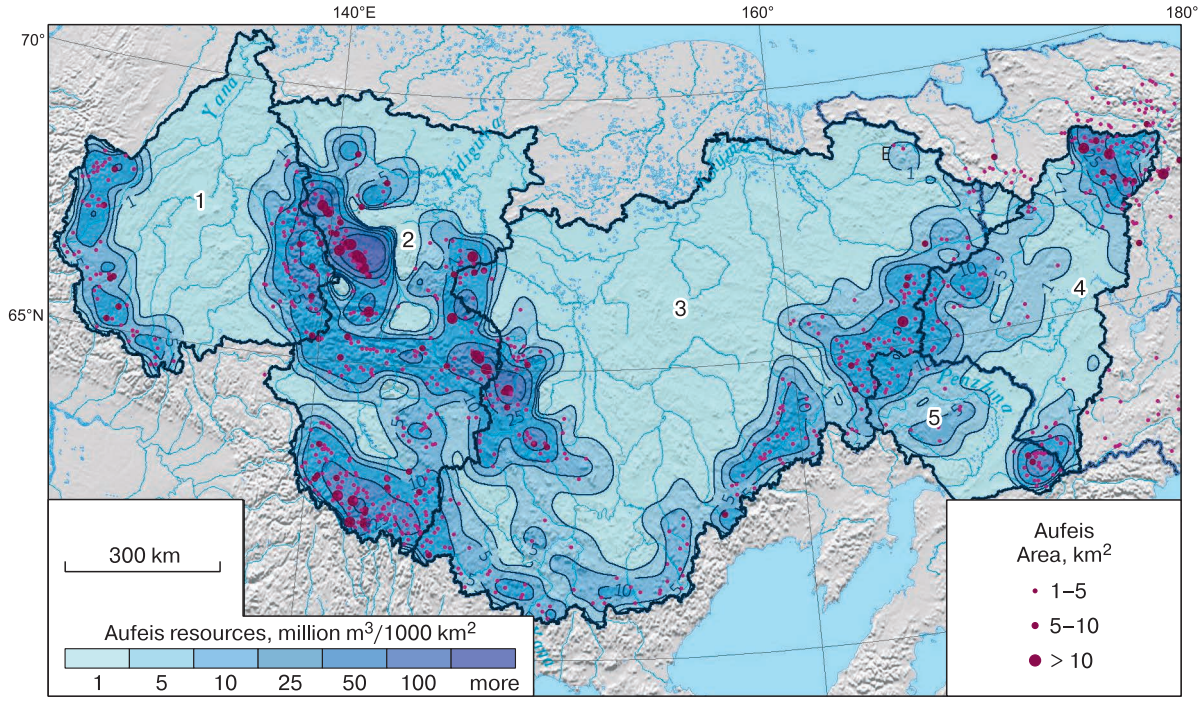

Fig. 3. Aufeis resources in the basins of the Yana (1), Indigirka (2), Kolyma (3), Anadyr (4), and Penzhina (5) rivers calculated on the basis of the Landsat-8 data.

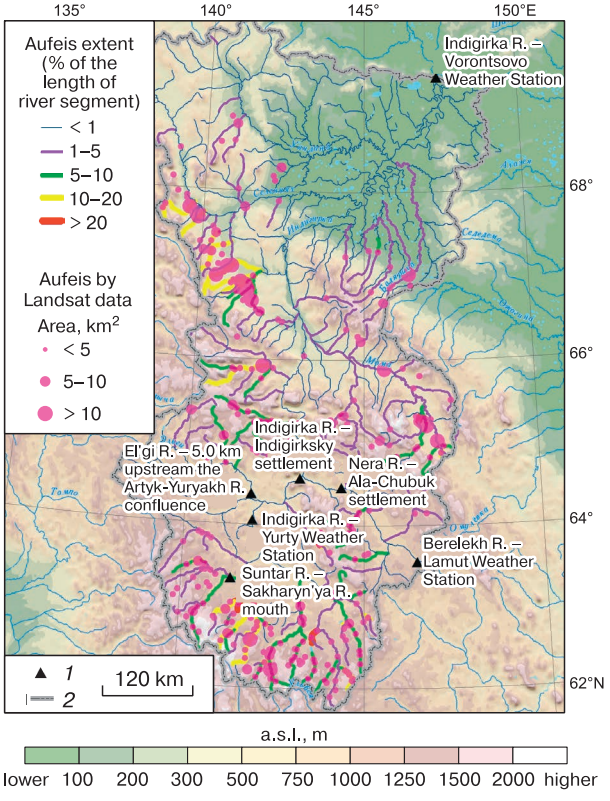

Fig. 4. Relative percentage of aufeis length along the river length in the Indigirka River basin.

1 – Gauging stations, *2* – catchment boundaries.

Taking into account aufeis fields obtained from satellite data and the VSEGEI cartographic base [*http://vsegei.com/ru/info/topo/*], the aufeis percentage along the length of the rivers was calculated (Fig. 4). This parameter characterizes the spatial distribution of aufeis along streams in general and has a high correlation with the aufeis percentage in the river basins.

Taking into consideration a low accuracy of the cartographic base, the aufeis percentage was assessed not for the streams themselves but for the 500-m-wide buffer zone around them. The width of the chosen buffer zone corresponds to the possible displacement of a stream according to the cartographic data relative to its true position.

According to V.G. Petrov's classification, giant aufeis are defined as aufeis having an area of more than 1 km^2 [*Sokolov, 1975*]. Overall, 1146 such aufeis have been detected in the NER. For 42 of them, the maximum calculated aufeis area exceeds 10 km^2. This estimate is significantly lower than that previously obtained on the basis of the area of aufeis glades. Therefore, in [*Ivanova, Pavlova, 2018*], 36 aufeis were identified in the Indigirka River basin and 14 aufeis in the Yana River basin with the area of more than 10 km^2. The most significant group of seven aufeis with the area of more than 10 km^2 is located in the Syuryuktyakh River basin, where the aufeis percentage exceeds 2%, according to satellite data.

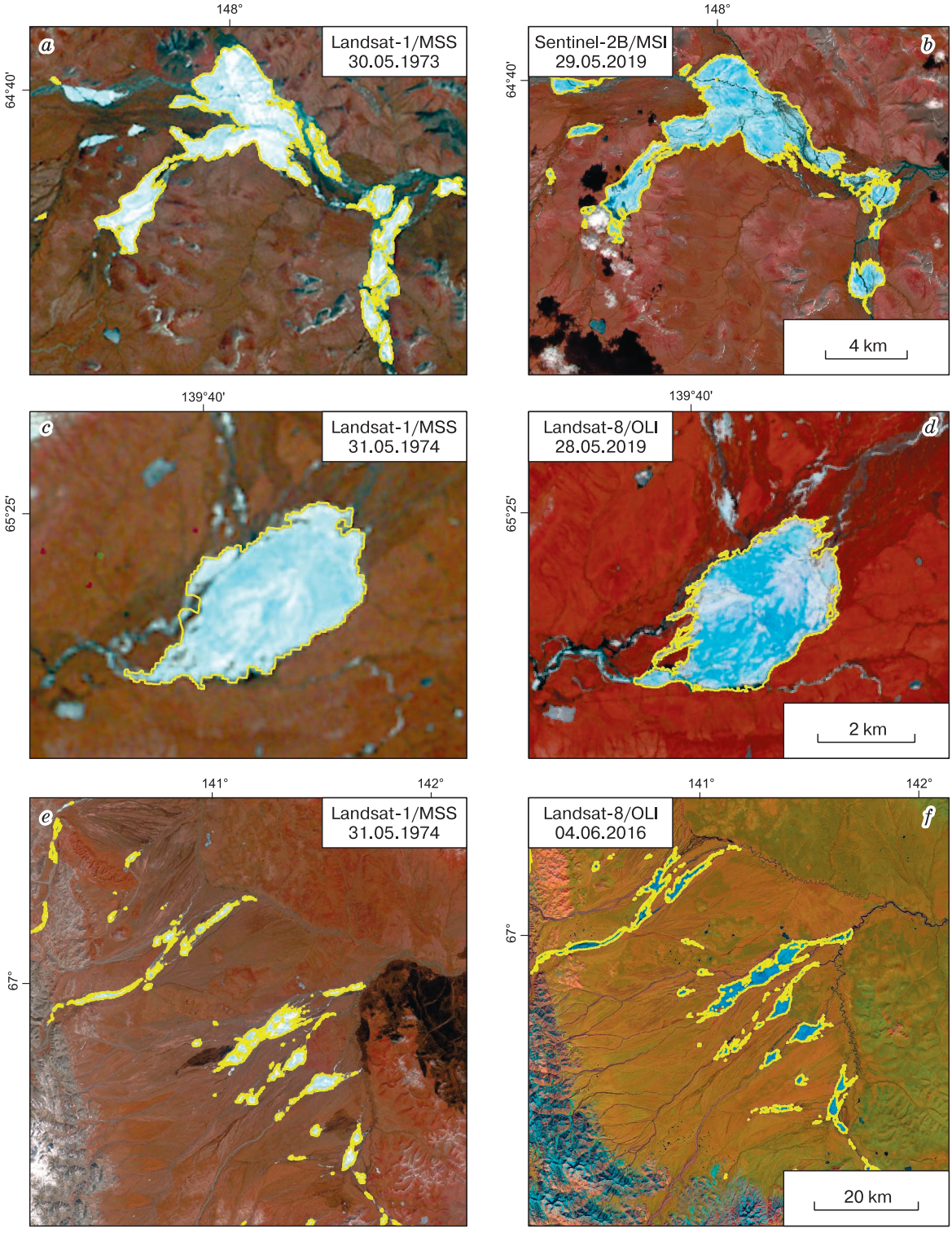

Fig. 5. Changes in the area of individual giant aufeis in the basins of the Kolyma (*a, b*), Yana (*c, d*) and Indigirka (*e, f*) rivers between 1973, 1974 and 2016, 2019 according to the Landsat and Sentinel-2 images.

Ice area (km^2): *a* – 35.7, *b* – 35.3, *c* – 9.2, *d* – 7.9, *e* – 163.3, *f* – 223.0.

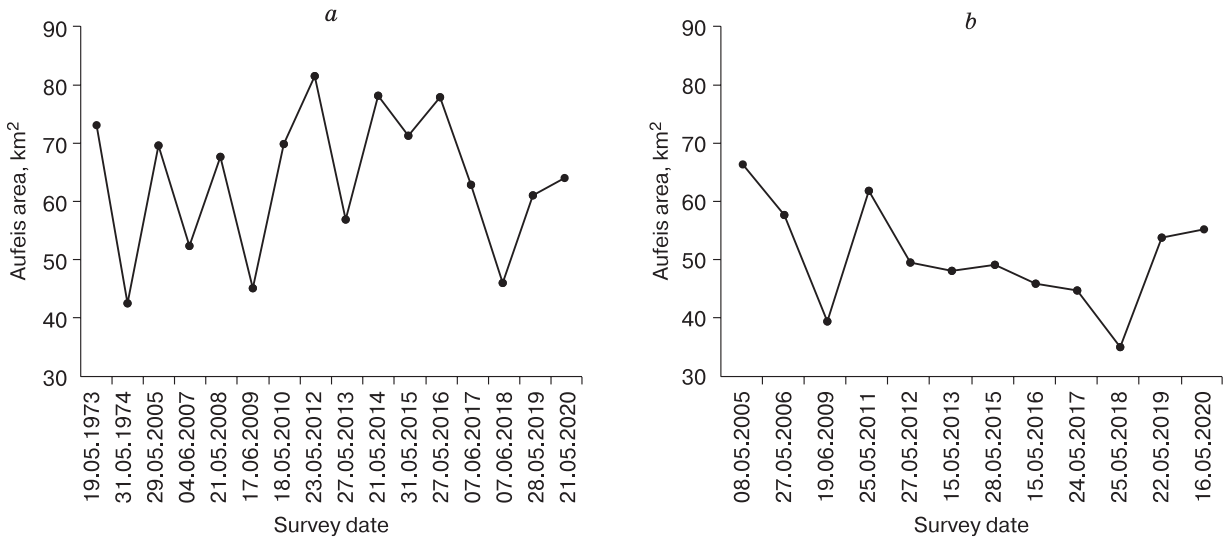

Fig. 6. Interannual variability of the area of the (*a*) largest aufeis in Syuryuktyakh River basin and (*b*) Bolshaya Moma aufeis at the end of spring (2005–2020) according to Landsat-7, 8 and Sentinel-2 images.

The Atlas considers single giant aufeis or their groups. For each giant aufeis in the Atlas, the long-term and interannual variability was analyzed on the basis of Landsat-1–8 and Sentinel-2 images, and series of maps and schemes were plotted. According to the dictionary [*Baranov et al., 1999*], these maps can be referred to as image-based maps.

The general view of an aufeis glade delineation of the aufeis proper during the periods of its maximum development (in the absence of snow cover) and maximum melting was based on the Sentinel-2 images in natural colors with a spatial resolution of 10 m. The maximum and minimum aufeis areas were determined using data for one specific year, not for the entire observation period.

The image-based maps of dynamics of the aufeis area in the initial period of ablation are based on multi-temporal Landsat images for the period from 1974 to 2020 (Fig. 5). They characterize the change in the maximum area of aufeis determined after the loss of the stable snow cover. Based on a series of the Landsat images for the period of 2000–2020, it was established that the average area of the largest aufeis in the Syuryuktyakh River basin during the period of its maximum development (64.9 km^2) is significantly larger than the area of the Big Moma aufeis (50.5 km^2), which was previously considered as the largest aufeis in Russia (Fig. 6).

The image-based maps of the aufeis area dynamics during the ablation were prepared using Sentinel-2 images for 2019. For this purpose, the images were selected from the moment of the snow loss in May–early June to the maximum ice melting in August–September. The aufeis were identified according to the method [*Makarieva et al., 2019e*] adopted for the Sentinel-2 images.

CONCLUSIONS

Aufeis-taryn are important element of mountainous landscapes in northeastern Asia and a powerful factor in the transformation of the environment. The development of the cartographic database and the Atlas of aufeis-taryns opens a new stage in the study of this phenomenon. The maps presented in the Atlas, demonstrate the location and size of ice fields 50–70 years after their first identification on aerial photos in the late 1940s.

The obtained characteristics of aufeis, including data on intra-annual and interannual variability of some of them, are the most important sources of information for analysis of current changes in the climatic and geocryological and hydrogeological conditions of the region. Estimates of the maximum aufeis percentage for river basins and the volume of aufeis resources can become the basis for determining the contribution of aufeis to the river discharge in the NER.

The comparison of aufeis characteristics according to data of the Cadaster of 1958 and modern satellite images (despite ambiguity of comparing these data sources) confirms that, over the last 50–70 years, the spatial distribution and the aufeis area has changed in the NER. However, it is difficult to accurately estimate these changes due to the differences in the methods of estimating the aufeis area. The reasons for these changes have not yet been analyzed, and their identification requires a comprehensive interdisciplinary study [*Makarieva et al., 2021e*].

Funding. *This study was supported by the Russian Geographic Society (project No. 07/2021-I "Atlas of Giant Aufeis in the Northeast of Russia (Continua-*

tion)"), Russian Foundation for Basic Research (project No. 20-05-00666), and St. Petersburg State University (project No. 75295776).

References

Alexeev V.R., 1987. Aufeis. Novosibirsk, Nauka, 159 p. (in Russian).

Alexeev V.R., 2016. Long-term variability of the spring taryn-aufeise. *Led i Sneg* **56** (1), 73–93 (in Russian).

Alexeev V.R., Boyarintsev E.L., Dovbysh V.N., 2012. Long-term dynamics of the size of the Anmangynda aufeis under climate change. Modern problems of stochastic hydrology and flow regulation. In: *Proc. All-Russia Sci. Conf. Dedicated to the Memory of A.V. Rozhdestvensky (Moscow, April 10–12, 2013)*. Moscow, p. 298–305 (in Russian).

Alexeev V.R., Gorin V.V., Kotov S.V., 2011. Aufeis-taryns of northern Chukotka. *Led i Sneg* **116** (4), 85–93 (in Russian).

Alexeev V.R., Makarieva O.M., Shikhov A.N., Nesterova N.V., Ostashov A.A., Zemlyanskova A.A., 2021. Atlas of Giant Aufeis-Taryns in Northeast of Russia. Novosibirsk, SB RAS, 302 p. (in Russian).

Atlas of Snow and Ice Resources of the World, 1997. Institute of Geography RAS. Moscow, Nauchnyi Mir, 371 p. (in Russian).

Baranov Yu.B., Berlyant A.M., Kapralov E.G., Koshkarev A.V., Serapinas B.B., Filippov Yu.A., 1999. Geoinformatics. Explanatory Dictionary of Basic Terms. Moscow, GIS-Association, 204 p. (in Russian).

Cadaster to the Map of Aufeis in Northeast of the USSR. Scale 1:2 M, 1958. Magadan, Central Thematic Expedition of the Northeastern Geological Department, 398 p. (in Russian).

Chekotillo A.M., 1941. The region of great icing (icing of Eastern Yakutia). *Byull. Akad. Nauk SSSR, Ser. Geol.*, No. 1, 94–113 (in Russian).

Danielson J.J., Gesch D.B., 2011. Global Multiresolution Terrain Elevation Data 2010 (GMTED2010). U.S. Geological Survey Open-File Rep. 2011–1073, 26 p.

Geocryological Map of the USSR on a Scale of 1:2.5 M. E.D. Ershov (Ed.), 1996. Vinnitsa (Ukraine), State Cartographic Factory, 16 sheets.

Geocryology of the USSR. Eastern Siberia and the Far East. E.D. Ershov (Ed.), 1989. Moscow, Nedra, 516 p. (in Russian).

GLIMS and NSIDC: Global Land Ice Measurements from Space Glacier Database. NSIDC, Boulder CO, USA. – https://doi.org/10.7265/ N5V98602, 2005 (updated 2017).

Hall D.K., Riggs G.A., Salomonson V.V., 1995. Development of methods for mapping global snow cover using moderate resolution imaging spectroradiometer (MODIS) data. *Remote Sens. Environ.* **54**, 127–140.

Ivanova L.D., Pavlova N.A., 2018. Formation and dynamics of aufeis in the Indigirka River basin in the last sixty years. In: *Proc. All-Russia Workshop Groundwater in the East of Russia* (XXII Meeting on Groundwater in Siberia and the Far East with International Participation, Novosibirsk, June 18–22, 2018). Novosibirsk, Izd. Novosib. Gos. Univ., 218–222 (in Russian).

Lvov A.V., 1916. Search and Testing of Water Supply Sources in the Western Part of the Amur Railway under Conditions of Permafrost. Irkutsk, Tip. P.I. Makushina & V.M. Posokhina, 881 p. (in Russian).

Makarieva O.M., Shikhov A.N., Ostashov A.A., Nesterova N.V., 2019. Historical and recent aufeis in the Indigirka River basin (Russia). *Earth Syst. Sci. Data* **11** (1), 409–420.

Makarieva O.M., Shikhov A.N., Ostashov A.A., Nesterova N.V., Zemlyanskova A.A., Semakina A.V., Alexeev V.R., 2021a. *Certificate of State Registration of Database No. 2021620267. Aufeis of the Northeast of Russia: GIS Catalog for the Chukchi Peninsula, Russian Federation*. Publ. February 12, 2021. – https://www1.fips.ru/registers-doc-view/fips_servlet?DB=DB&DocNumber=2021620267&TypeFile=html (in Russian).

Makarieva O.M., Shikhov A.N., Ostashov A.A., Nesterova N.V., Zemlyanskova A.A., Alexeev V.R., 2021b. *Certificate of State Registration of Database No. 2021620317. Aufeis of the Northeast of Russia: GIS Catalog for the Indigirka River Basin, Russian Federation*. Publ. February 24, 2021. – https://www1.fips.ru/registers-doc-view/fips_servlet?DB=DB&DocNumber=2021620317&TypeFile=html (in Russian).

Makarieva O.M., Shikhov A.N., Ostashov A.A., Nesterova N.V., Zemlyanskova A.A., Alexeev V.R., 2021c. *Certificate of State Registration of Database No. 2021620317. Aufeis of the Northeast of Russia: GIS Catalog for the Kolyma River Basin, Russian Federation*. Publ. February 26, 2021. – https:// www1.fips.ru/registers-doc-view/fips_servlet?DB=DB&DocNumber=2021620332&TypeFile=html (in Russian).

Makarieva O.M., Shikhov A.N., Ostashov A.A., Nesterova N.V., Zemlyanskova A.A., Alexeev V.R., 2021d. *Certificate of State Registration of Database No. 2021620317. Aufeis of the Northeast of Russia: GIS Catalog for the Kolyma River Basin, Russian Federation*. Publ. February 26, 2021. – https://www1.fips.ru/registers-doc-view/fips_servlet?DB=DB&DocNumber=2021620333&TypeFile=html (in Russian).

Makarieva O.M., Nesterova N.V., Ostashov A.A., Zemlyanskova A.A., Tumskoy V.E., Gagarin L.A., Ekaykin A.A., Shikhov A.N., Olenchenko V.V., Khristoforov I.I., 2021e. Perspectives of the development of complex interdisciplinary hydrological and geocryological research in the northeast of Russia. *Vestn. St. Petersburg Univ., Earth Sciences* **66** (1), 74–90.

Morse P.D., Wolfe S.A., 2015. Geological and meteorological controls on icing (aufeis) dynamics (1985 to 2014) in subarctic Canada. *J. Geophys. Res.: Earth Surface* **120** (9), 1670–1686.

National Atlas of Russia. Vol. 2. Nature and Ecology. A.A. Klochko, M.A. Romanovskaya (Eds.), 2004. Moscow, GOSGISTSENTR, 495 p. (in Russian).

Pavelsky T.M., Zarnetske J.P., 2017. Rapid decline in river icings detected in Arctic Alaska: Implications for a changing hydrologic cycle and river ecosystems. *Geophys. Res. Lett.* **44** (7), 3228–3235.

Petrov V.G., 1930. Aufeis on the Amur–Yakutsk Highway. Leningrad, Izd. Akad. Nauk SSSR & Avtodor. Inst. NKPS SSSR, 177 p. (in Russian).

Petrov V.G., 1934. Experience in determining the force of groundwater pressure in ice. In: *Proc. Commission for the Study of Permafrost*. Moscow, Izd. Akad. Nauk SSSR, vol. 2, 59–72 (in Russian).

Podyakonov S.A., 1903. Aufeis in Eastern Siberia and the causes of their occurrence. *Izvest. Ross. Geogr. Obshchestva* **39**, 305–337 (in Russian).

Prasolova A.I., Pizhankova E.I., Yakovenko E.D., 2013. Development of satellite image interpretation technique for updating the layer of aufeis on the digital geocryological map of Russia. In: *Conf. Geocryological Mapping: Problems and Prospects*, Moscow, RUDN, p. 121–124 (in Russian).

Reedyk S., Woo M.K., Prowse T.D., 1995. Contribution of icing ablation to streamflow in a discontinuous permafrost area. *Canad. J. Earth Sci.* **32**, 13–20.

Shvetsov P.F., 1951. Groundwater of the Verkhoyansk–Kolyma Mountainous Fold Area and Features of Its Manifestation Associated with Low-Temperature Permafrost. Moscow, Izd. Akad. Nauk SSSR, 279 p. (in Russian).

Shvetsov P.F., Sedov V.P., 1941. Giant Aufeis and Ground Water of the Tas-Khayata Ridge. Moscow; Leningrad, Izd. Akad. Nauk SSSR, 81 p. (in Russian).

Simakov A.S., 1949. Some data on the aufeis in the Kolyma–Indigirka region. In: *Materials on Geology and Mineral Resources of the Northeast of the USSR*. Magadan, vol. 6, p. 66–80 (in Russian).

Simakov A.S., Shilnikovskaya Z.G., 1958. The Map of Aufeis in the Northeast of the USSR. A Brief Explanatory Note. Magadan, Northeastern Geol. Survey, Dept. Geol. Subsoil Protection, 40 p. (in Russian).

Sokolov B.L., 1975. Aufeis and Streamflow. Leningrad, Gidrometeoizdat, 190 p. (in Russian).

Strahler A.N., 1952. Hypsometric (area-altitude) analysis of erosional topology. *Geol. Soc. Am. Bull.* **63**, 1117–1141.

Sumgin M.I., 1927. Permafrost of Soil within the USSR. Vladivostok, Dal'nevost. Geofizich. Observatoriya, 372 p. (in Russian).

Tolstikhin N.I., 1931. Groundwater in permafrost Regions. In: *Reports at the 1st All-Union Hydrological Congress*. Leningrad, Geolgiz, 5 p. (in Russian).

Tolstikhin O.N., 1974. Aufeis and Groundwater in the Northeast of the USSR. Novosibirsk, Nauka, 164 p. (in Russian).

Tolstikhin O.N., 1975. Aufeis and groundwater in the northeast of the USSR. In: *Study and Protection of Water Resources*. Moscow, Nauka, 18 p. (in Russian).

Topchiev A.G., 1979. Space methods in studying the valleys and aufeis of the Chulman region. In: *Problems of Geography*. Vol. 3. Geomorphology and Construction. Moscow, Mysl, p. 46–54 (in Russian).

URL: http://earthexplorer.usgs.gov (last visited: July 22, 2021).

URL: http://vsegei.com/ru/info/topo/ (last visited: July 22, 2021).

Yoshikawa K., Hinzman L.D., Kane D.L., 2007. Spring and aufeis (icing) hydrology in Brooks Range, Alaska. *J. Geophys. Res. Biogeosci.* **112**, 1–14.

Zonov B.V., 1944. Aufeis and aufeis fields on the rivers of the Yana–Kolyma mountainous country. In: *Proc. V.A. Obruchev Permafrost Institute, USSR Acad. Sci.* Moscow, Izd. Akad. Nauk SSSR, vol. **IV**, p. 33–92 (in Russian).

Received July 25, 2021
Revised December 22, 2021
Accepted May 19, 2022

Translated by V.A. Krutikova

EARTH'S CRYOSPHERE
SCIENTIFIC JOURNAL

Earth's Cryosphere, 2022, vol. XXVI, No. 4, pp. 51–58

PERMAFROST ENGINEERING

USE OF THE ANALYTICAL SOLUTION OF FUNCTIONING OF THE HORIZONTAL EVAPORATOR TUBULAR (HET) THERMOSIPHON SYSTEM FOR QUICK EVALUATION OF THE EFFICIENCY OF ITS WORK

G.V. Anikin[1,*], A.A. Ishkov[2,3,]**

[1] *Earth Cryosphere Institute, Tyumen Scientific Center, Siberian Branch of the Russian Academy of Sciences, ul. Malygina 86, Tyumen, 625000 Russia*
[2] *Tyumen Industrial University, ul. Volodarskogo 38, Tyumen, 625000 Russia*
[3] *LLC "PetroTrace", ul. Letnikovskaya 10, build. 4, Moscow, 115114 Russia*

**Corresponding author; e-mail: anikin@ikz.ru*
***e-mail: a.a.ishkov@yandex.ru*

This paper presents the analytical model of the functioning of the system of temperature stabilization of soils of the horizontal evaporator tubular (HET) type based on the integral method. The solutions of numerical and analytical models for temperature stabilization systems of soils of the HET type with different lengths of the evaporating part, as well as for the Arctic cities with different climates–Salekhard, Varandey, and Igarka. A comparison of the results obtained within the framework of numerical and analytical solutions indicates that the developed analytical model can be used for a quick assessment of the functioning of the HET system of temperature stabilization of soils for various design solutions and climatic characteristics.

Keywords: *permafrost, soil, seasonal cooling device, HET system, condenser, pipeline, evaporator.*

Recommended citation: Anikin G.V., Ishkov A.A., 2022. Use of the analytical solution of functioning of the horizontal evaporator tubular (HET) thermosiphon system for quick evaluation of the efficiency of its work. *Earth's Cryosphere*, XXVI (4), 51–58.

INTRODUCTION

Preservation of soils in a frozen state is an acute problem of construction works in permafrost regions. For objects with a relatively low heat release, heat-insulating coatings are sufficiently efficient , whereas for objects with intense heat release, it is necessary to use methods of active thermal stabilization of soils.

Among the currently available seasonal cooling devices, including both single devices and large collector systems with an increased depth of the evaporative part, a special place is occupied by the soil temperature stabilization system with a horizontal evaporator manufactured by NPO Fundamentstroiarkos LLC – the HET system (horizontal evaporator tubular system).

The works [*Anikin, 2009; Dolgikh et al., 2014*] are devoted to the development of a mathematical model of the functioning of this system and the numerical solution of the equations obtained. Thermal loads limiting the functioning of the system have been studied and analyzed [*Melnikov et al., 2017*], and optimal configurations of the system for various operating conditions have been determined [*Ishkov et al., 2019; Ishkov, Anikin, 2020*].

However, in order to determine all the parameters and assess the operating conditions of the HET system, it is necessary to use a complex numerical model and special software [*Anikin et al., 2017*], whereas for an ordinary engineer, the question of the efficiency of the system in the format "will the system cope with the thermal pressure from the structure under construction or not" is more interesting.

Therefore, the purpose of this article is to develop an analytical model that can be used for quick evaluation of the functioning of soil temperature stabilization system with a horizontal evaporator for various design solutions and climatic characteristics.

ANALYTICAL MODEL OF THE HET SYSTEM FUNCTIONING

Let us consider the general view of the HET system and the way it is installed. The scheme of the system is shown in Fig. 1.

The HET system is a steel structure with three functional units: an evaporator, a condenser, and a circulation accelerator. The evaporator is made in the form of a curved structure with 90°–180° rotations. The condenser has a developed fin surface with an area of about 100 m^2. The circulation accelerator is a pipe of a larger diameter than that of the evaporator, in which refrigerant vapors are separated from suspended droplets due to gravity. HET systems are

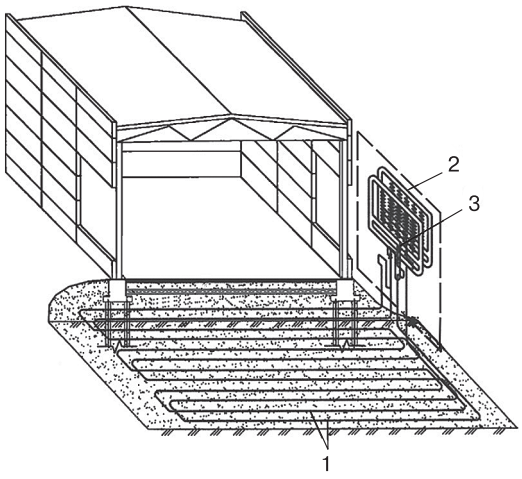

Fig. 1. Horizontal naturally acting evaporator tubular system (HET):

1 – evaporator; 2 – condenser; 3 – circulation accelerator (separator).

widely applied in the construction of structures on a pile foundation, with floors on the ground, as well as tanks with a base on a filling, etc.

The main advantage of this system is the ability to freeze large areas (and volumes) of soil under structures built on permafrost. In particular, for regions with virtually no winds (for example, Yakutia [*Pavlov, 2003*]), it is possible to install industrial refrigerators on a condenser fin grid. This increases the heat exchange between the condenser and the atmosphere, which, in turn, increases the efficiency of the HET systems.

To simplify the modeling of the soil freezing process, the HET system can be represented as straight pipe sections, the configuration of which is specified by their diameter and the distance between them (system laying step). Closing of soil freezing halos between the pipes of the HET system means the creation of a frozen soil stratum (volume) of high bearing capacity.

Let there be frozen soil around a pipe with radius b and length L, which is a cylinder with radius R_0 (Fig. 2).

If the boundary of the frozen soil moves much slower than the temperature inside the cylinder is set, a stationary solution can be considered for the temperature distribution:

$$\frac{1}{r}\frac{d\left(r\,dt(r)/dr\right)}{dr}=0, \tag{1}$$

where r is the radial coordinate, m; $t(r)$ is the temperature, °C. The solution of Eq. (1) is written as

$$t(r)=C\ln(r)+C_1, \tag{2}$$

where C, C_1 are constants to be determined.

The boundary conditions for the problem under consideration are written as

$$\begin{aligned} t(b)&=t_{ev},\\ t(R_0)&=t_{bf}, \end{aligned} \tag{3}$$

where t_{ev} is the temperature of the evaporator pipe, °C; t_{bf} is the temperature of the phase transition, °C.

From Eqs. (2) and (3), we get

$$t_{bf}-t_{ev}=C\ln\left(\frac{R_0}{b}\right)\;\rightarrow\;C=\frac{t_{bf}-t_{ev}}{\ln(R_0/b)}.$$

The heat flux dU, which is supplied to the element of the evaporation pipe of length dL, is equal in absolute value

$$dU=\lambda\frac{\partial t}{\partial r}2\pi r dL=2\pi\lambda\frac{t_{bf}-t_{ev}}{\ln(R_0/b)}dL, \tag{4}$$

where λ is the coefficient of thermal conductivity of frozen soil, W/(m·°C).

The total thermal power of the cooling system (U_{tot}) is limited by the efficiency of the condenser part ($\alpha S\eta$):

$$U_{tot}=\alpha S\eta\left(t_{con}-t_a\right). \tag{5}$$

Here U_{tot} is the total thermal power of the cooling system, W; α is the heat transfer coefficient of the condenser fins, W/(m^2·°C); S is the total surface area of the condenser fins, m^2; η is the heat transfer efficiency coefficient of the condenser fins (calculated to be 0.90); t_{con} is the temperature of the condenser fins, °C; t_a is the air temperature, °C.

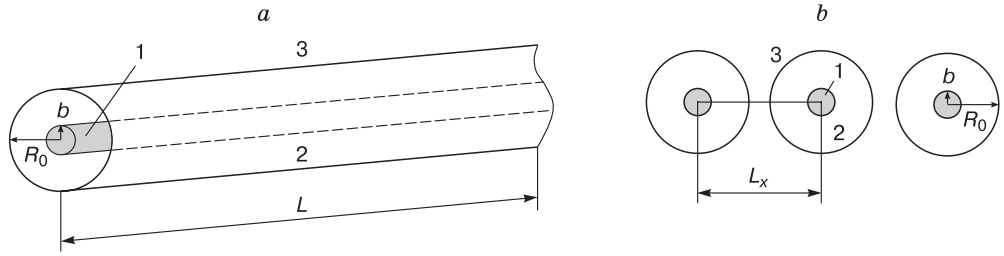

Fig. 2. View of the evaporator pipe from the side (*a*) and from the end (*b*).

1 – evaporator; 2 – frozen soil; 3 – unfrozen soil. L is the pipe length, m; L_x is the distance between the axes of the pipes of the evaporative system, m; b is the pipe radius, m; R_0 is the radius of the frozen soil cylinder, m.

As follows from the work [*Ishkov et al., 2019*], the temperatures of the condenser and the evaporator are related by the ratio

$$t_e = t_c + \frac{\rho_L g H}{dP/dt}, \quad (6)$$

where ρ_L is the density of the liquid refrigerant, kg/m^3; g is the acceleration of gravity, m/s^2; dP/dt is the dependence of the saturated vapor pressure on temperature, Pa; H is the height difference between the liquid level in the condenser and the considered point of the evaporator, m.

In turn, H is equal to

$$H = H_0 + L \sin \varphi, \quad (7)$$

where φ is the angle between the evaporator pipe and the ground surface.

Taking into account Eqs. (5)–(7), we have

$$t_{ev} = t_a + \frac{U_{tot}}{\alpha S \eta} + \frac{\rho_L g (H_0 + L \sin \varphi)}{dP/dt}. \quad (8)$$

Substituting (8) into (4), we get

$$dU = 2\pi\lambda \frac{\left(t_{bf} - t_a - \frac{U_{tot}}{\alpha S \eta} - \frac{\rho_L g (H_0 + L \sin \varphi)}{dP/dt} \right)}{\ln(R_0/b)} dL.$$

By performing integration over L, we obtain

$$U \frac{\ln(R_0/b)}{2\pi\lambda} = \left(t_{bf} - t_a - \frac{U_{tot}}{\alpha S \eta} - \frac{\rho_L g H_0}{dP/dt} \right) L_0 + \frac{\rho_L g \left(L_0^2 \sin \varphi \right)}{2 dP/dt},$$

or, what is the same thing:

$$U \frac{\ln(R_0/b)}{2\pi\lambda} = \left(t_{bf} - t_a - \frac{U_{tot}}{\alpha S \eta} - \frac{\rho_L g \bar{H}}{dP/dt} \right) L_0, \quad (9)$$

where H is the average excess of the liquid level in the condenser, given by the ratio:

$$\bar{H} = H_0 + L_0 \sin \varphi.$$

Let N be the number of pipes of the evaporation system connected to the condenser. Multiplying both parts of Eq. (9) by N, we get

$$U_{tot} \frac{\ln(R_0/b)}{2\pi\lambda} = \left(t_{bf} - t_a - \frac{U_{tot}}{\alpha S \eta} - \frac{\rho_L g \bar{H}}{dP/dt} \right) L_{tot}. \quad (10)$$

It is taken into account here that the following relations are fulfilled:

$$U_{tot} = UN,$$
$$L_{tot} = LN,$$

where L_{tot} is the total length of the evaporator pipes, m.

From Eq. (10), we find the value of the total thermal power

$$U_{tot} = \left(t_{bf} - t_a - \frac{\rho_L g \bar{H}}{dP/dt} \right) \left[\frac{1}{\alpha S \eta} + \frac{\ln(R_0/b)}{2\pi\lambda L_{tot}} \right]^{-1}. \quad (11)$$

Now we will consider the integral solution. The amount of total heat from the phase transition released by the soil during freezing of the cylinder with radius R_0 and length L_{tot} is written as

$$Q_{bf} = \sigma \pi R_0^2 L_{tot}, \quad \sigma = \sigma_0 \gamma (w - w_0),$$

where Q_{bf} is the heat of the phase transition, J; σ_0 is the specific heat of ice melting, J/kg; γ is the density of the rock matrix, kg/m^3; w is the total moisture content of the rock, unit fraction (u.f.); w_0 is the rock moisture due to unfrozen water, u.f.

The amount of heat Q_t that leaves the system due to temperature change:

$$Q_t = \int_b^{R_0} \left(c_1 (t_0 - t_{bf}) + c_2 (t_{bf} - t(r)) \right) L_{tot} 2\pi r dr, \quad (12)$$

where $t(r)$ is the temperature at a point with radius r, °C; c_1 is the volumetric heat capacity of thawed soil, J/(m^3·°C); c_2 is the volumetric heat capacity of frozen soil, J/(m^3·°C); t_0 is the initial temperature of the soil, °C.

The solution of Eq. (1) can be written as

$$t(r) = \frac{t_{bf} - t_{ev}}{\ln(R_0/b)} \ln\left(\frac{r}{b}\right) + t_{ev}. \quad (13)$$

Substituting (13) into (12), we get

$$Q_t = \left(c_1 (t_0 - t_{bf}) + c_2 (t_{bf} - t_{ev}) \right) L_{tot} \pi R_0^2 - $$
$$- c_2 L_{tot} \frac{t_{bf} - t_{ev}}{\ln(R_0/b)} \int_b^{R_0} \ln\left(\frac{r}{b}\right) 2\pi r dr.$$

Thus, the energy balance equation takes the form

$$\int_0^{\tau} U_{tot}(\tau') d\tau' = Q_t + Q_f, \quad (14)$$

where τ is the time, days.

Differentiating both parts of Eq. (14) by τ, we obtain

$$U_{tot} = \frac{dR_0}{d\tau} \left(\frac{\partial (Q_t + Q_{bf})}{\partial R_0} \right). \quad (15)$$

Note that the solution of the integral given below can be written as

$$\int_b^{R_0} \ln\left(\frac{r}{b}\right) 2\pi r dr = 2\pi b^2 \int_1^{\frac{R_0}{b}} x \ln(x) dx = $$
$$= 2\pi b^2 \left(F\left(\frac{R_0}{b}\right) - F(1) \right), \quad (16)$$

where $F(x)$ is a function that is given by the expression

$$F(x) = \frac{x^2}{2} \ln(x) - \frac{x^2}{4}. \quad (17)$$

Thus, the right side of Eq. (15), taking into account expressions (16) and (17), will be written as

$$\frac{\partial\left(Q_t+Q_{bf}\right)}{\partial R_0}=2\pi R_0 L_{tot}\left(\sigma+c_1\left(t_0-t_{bf}\right)\right)+$$

$$+c_2 L_{tot}\frac{t_{bf}-t_{ev}}{\left(\ln\left(R_0/b\right)\right)^2}\frac{2\pi b^2\left(F\left(R_0/b\right)-F(1)\right)}{R_0}. \quad (18)$$

Note that the following substitution can be made in expression (18):

$$2\pi b^2\left(F\left(\frac{R_0}{b}\right)-F(1)\right)=\pi R_0^2\ln\left(\frac{R_0}{b}\right)-\pi\frac{R_0^2}{2}+\frac{\pi b^2}{2}.$$

Thus, we get

$$\frac{\partial\left(Q_t+Q_{bf}\right)}{\partial R_0}=2\pi R_0 L_{tot}\times$$

$$\times\left[\sigma+c_1\left(t_0-t_{bf}\right)+c_2\left(t_{bf}-t_{ev}\right)\times\right.$$

$$\left.\times\frac{\left(\ln\left(R_0/b\right)-0.5+0.5b^2/R_0^2\right)}{2\left(\ln\left(R_0/b\right)\right)^2}\right]. \quad (19)$$

To assess the correctness of the obtained solution, we check the convergence of the right side of Eq. (19) under the condition $R_0 \to b$, i.e., under the condition that there is no frozen soil near the evaporation pipes.

Assuming $R_0 = b + x$, we get

$$\lim_{x\to 0}\frac{\ln\left(R_0/b\right)-0.5+0.5b^2/R_0^2}{2\left(\ln\left(R_0/b\right)\right)^2}=$$

$$=\lim_{x\to 0}\frac{x-0.5x^2-0.5+0.5\left(1-2x+6x^2\right)}{2x^2}=\frac{2.5}{2}.$$

Thus, Eq. (19) converges to a finite positive value, which indicates the correctness of the solution.

To simplify the expressions obtained, we introduce the function

$$\varphi(x)=\frac{\ln(x)-0.5+0.5/x^2}{\left(\ln(x)\right)^2}. \quad (20)$$

Then, we obtain the following differential equation from (11), (15), (19), and (20):

$$\left(t_{bf}-t_a-\frac{\rho_L g\bar{H}}{dP/dt}\right)\left[\frac{1}{\alpha S\eta}+\frac{\ln\left(R_0/b\right)}{2\pi\lambda L_{tot}}\right]^{-1}=\frac{dR_0}{d\tau}2\pi R_0 L_{tot}\times$$

$$\times\left(\sigma+c_1\left(t_0-t_{bf}\right)+c_2\left(t_{bf}-t_{ev}\right)\varphi\left(\frac{R_0}{b}\right)\right),$$

or, which is the same:

$$d\tau\left(t_{bf}-t_a-\frac{\rho_L g\bar{H}}{dP/dt}\right)=dR_0\frac{2\pi R_0}{\lambda}\left(\frac{\lambda L_{tot}}{\alpha S\eta}+\frac{\ln\left(R_0/b\right)}{2\pi}\right)\times$$

$$\times\left(\sigma'+c_2\left(t_{bf}-t_{ev}\right)\varphi\left(\frac{R_0}{b}\right)\right), \quad (21)$$

where the value σ' is given by the ratio

$$\sigma'=\sigma+c_1\left(t_0-t_{bf}\right).$$

Let us consider the case, when the following condition is met:

$$c_2\left(t_{bf}-t_{ev}\right)\varphi\left(\frac{R_0}{b}\right)\ll\sigma',\quad \alpha=\text{const}.$$

Then, Eq. (21) can be interpreted explicitly:

$$\tau\left(t_{bf}-\overline{t_a}(\tau)-\frac{\rho_L g\bar{H}}{dP/dt}\right)=\frac{\pi\left(R_0^2-b^2\right)}{\lambda}A\sigma'+$$

$$+\frac{b^2}{\lambda}\left(\left(\frac{R_0^2}{2b^2}\ln\left(\frac{R_0}{b}\right)-\frac{R_0^2}{4b^2}\right)+0.25\right)\sigma'. \quad (22)$$

Here, the values of $\overline{t_a}$ and A are given by the following relations:

$$\overline{t_a}(\tau)=\frac{1}{\tau}\int_0^\tau t_a(\tau')d\tau',$$

$$A=\frac{\lambda L_{tot}}{\alpha S\eta}.$$

Thus, an analytical solution has been obtained that can be applied to evaluate the efficiency of the functioning of the "HET" type soil temperature stabilization system. It is also worth noting that the proposed analytical solution is based on the integral formulation of the problem given in [*Naterer, 2003*].

ASSESSMENT OF CORRESPONDENCE BETWEEN ANALYTICAL AND NUMERICAL SOILUTIONS

Comparison of the numerical solution with experimental data [*Ishkov et al., 2018*] showed a high degree of agreement between theory and practice, which confirms the viability of the developed model.

To assess the degree of agreement between the data obtained via solving the numerical and analytical models, let us consider the freezing of soils by the "HET" system for various climatic zones. For this, meteorological parameters were taken from archival data for the Arctic cities of Varandey, Salekhard, and Igarka. The mean monthly temperatures and wind speeds for these cities are given in Table 1.

It should be noted that the efficiency of the HET system was evaluated for a number of variable parameters that can be combined into two large groups: climatic (air temperature, wind speed) and technical

Table 1. **Mean monthly air temperature (t_a) and wind speed (v) in settlements**

Month	Varandey		Salekhard		Igarka	
	t_a, °C	v, m/s	t_a, °C	v, m/s	t_a, °C	v, m/s
January	–14.7	6.9	–22.9	2.2	–26.1	3.1
February	–18.9	6.3	–19.2	2.2	–18.2	2.6
March	–13.0	6.2	–12.7	2.8	–14.6	2.9
April	–7.1	5.7	–5.5	3.2	–1.9	3.2
May	–1.5	5.6	1.1	3.4	3.9	3.4
June	6.1	5.6	11.6	3.5	11.4	3.1
July	10.8	5.8	16.0	2.9	15.8	2.8
August	9.2	6.1	11.5	2.9	11.2	2.8
September	6.5	5.7	6.3	2.9	7.1	3.1
October	1.5	6.9	–2.5	2.7	–4.2	3.3
November	–7.8	5.7	–13.4	2.5	–19.2	2.8
December	–21.3	2.8	–17.6	2.1	–24.4	3.2

(total length of evaporator pipes). All other parameters of the HET system and environmental conditions for each of the solutions have constant values.

There can be much more parameters, but those that have the greatest impact on the efficiency of the system were chosen. Thus, we get:

– Total length of evaporator pipes L_{tot} = = 300–3000 m;

– Air temperature depending on the region t_a = –34.1...+16.0°C;

– Wind speed depending on the region v = = 2.1–6.9 m/s.

The dynamics of the last two parameters (t_a, v) are different for each region for which the calculations of the system functioning are carried out. The calculation of the operating time of the HET system for each region, except for Varandey, has been carried out from the beginning of October (the first month with a subzero temperature). For Varandey, the calculation starts from November.

The radius of the frozen soil around the evaporator pipe acts as an output parameter by which the numerical and analytical solutions are compared and a conclusion is made about the efficiency or inefficiency of the HET system.

It should be noted that the discreteness of the obtained values of the soil freezing radius is 1 day for the numerical solution and 1 month for the analytical solution.

In all calculations, it is assumed that the soil has the following thermal characteristics: $\gamma = 1600$ kg/m^3, $w_0 = 0$, $w = 0.2$, $\lambda = 2.0$ W/(m·°C), $c_1 = 1.60 \cdot 10^6$ J/(kg·°C), $c_2 = 1.47 \cdot 10^6$ J/(kg·°C).

The heat transfer coefficient between the condenser and the atmosphere is given by the following expression [*Royzen, Dulkin, 1977*]:

$$\alpha(t) = 0.105 \frac{\lambda_a(t)}{s} \left(\frac{d}{s}\right)^{-0.54} \left(\frac{h}{s}\right)^{-0.14} \left(\frac{vs}{\nu_a(t)}\right)^{0.72},$$

where s is the distance between the capacitor fins, m; d is the diameter of condenser pipes, m; h is the length of the rib condenser, m; $\lambda_a(t)$ is the thermal conductivity of air, W/(m·°C); $\nu_a(t)$ is the kinematic viscosity of air, Pa·s; and v is the wind speed, m/s.

For the installation presented in this study, the characteristics of the condenser have the following values: $d = 32$ mm, $s = 7$ mm, $h = 34$ mm, $S = 100$ m^2, $H_{con} = 5$ m. The viscosity and thermal conductivity of air depend on the temperature of the atmosphere and are set according to the reference data [*Babichev et al., 1991*].

Thus, solving Eq. (22) for the meteorological parameters of Salekhard, we obtain the dependence of the radius of the soil freezing on time within the framework of the analytical and numerical solutions (Table 2).

Their graphic representations are given in Fig. 3.

The solutions for the meteorological parameters of Varandey are presented in Table 3 and Fig. 4; analogous solutions for Igarka, in Table 4 and Fig. 5.

After analyzing the results obtained from the numerical and analytical models, we can conclude that, on average, for all lengths of the evaporator, the degree of correspondence between the values of the soil freezing radius obtained by the two methods is 97.3% (Table 5).

It should be noted that for the evaporator length of 300 m, the difference in soil freezing radii between the numerical and analytical solutions is 10.5%, while for all other lengths it does not exceed 8%. Of course, there is a certain error, but it is worth recalling that the use of an analytical model is much simpler than the use of a numerical one, so the resulting accuracy is acceptable. Thus, the use of an analytical model to evaluate the efficiency of the HET-type soil temperature stabilization system for various design solutions and climatic conditions is quite justified and is suitable for quick assessment.

Table 2. **Dependence of soil freezing radius R_0 on time τ for Salekhard**

τ, days	R_0, m (analytical solution)				R_0, m (numerical solution)			
	Evaporator length							
	300 m	600 m	1000 m	3000 m	300 m	600 m	1000 m	3000 m
1	0.016	0.016	0.016	0.016	0.059	0.048	0.040	0.027
20	0.200	0.179	0.158	0.109	0.205	0.174	0.148	0.095
40	0.361	0.328	0.295	0.209	0.378	0.327	0.282	0.185
60	0.526	0.481	0.436	0.314	0.544	0.474	0.412	0.274
80	0.673	0.619	0.563	0.409	0.690	0.603	0.524	0.350
100	0.803	0.741	0.676	0.495	0.820	0.719	0.627	0.420
120	0.928	0.858	0.784	0.577	0.945	0.831	0.726	0.488
140	1.021	0.945	0.865	0.639	1.039	0.914	0.800	0.540
160	1.090	1.010	0.926	0.685	1.110	0.978	0.858	0.580
180	1.141	1.058	0.970	0.719	1.165	1.029	0.903	0.613
200	1.165	1.081	0.991	0.735	1.190	1.052	0.924	0.628

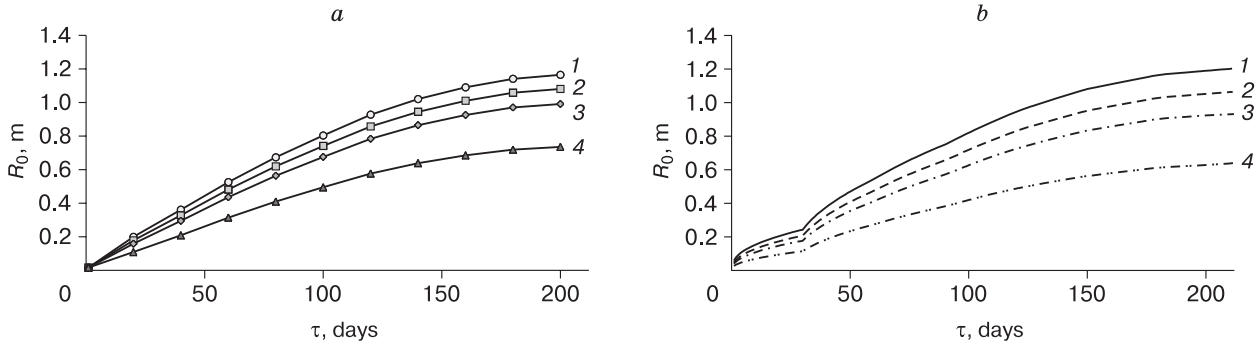

Fig. 3. Dependence of the freezing radius R_0 on time τ for Salekhard.

a – analytical solution; *b* – numerical solution. Evaporator length: *1* – 300 m; *2* – 600 m; *3* – 1000 m; *4* – 3000 m.

Table 3. **Dependence of soil freezing radius R_0 on time τ for Varandey**

τ, days	R_0, m (analytical solution)				R_0, m (numerical solution)			
	Evaporator length							
	300 m	600 m	1000 m	3000 m	300 m	600 m	1000 m	3000 m
1	0.016	0.016	0.016	0.016	0.057	0.048	0.041	0.028
20	0.172	0.160	0.148	0.110	0.183	0.163	0.144	0.099
40	0.304	0.286	0.267	0.206	0.328	0.296	0.265	0.185
60	0.437	0.414	0.388	0.305	0.465	0.423	0.380	0.270
80	0.564	0.536	0.505	0.400	0.603	0.554	0.503	0.365
100	0.676	0.644	0.607	0.485	0.723	0.667	0.609	0.447
120	0.784	0.748	0.706	0.567	0.837	0.774	0.709	0.524
140	0.896	0.856	0.810	0.653	0.955	0.886	0.812	0.603
160	0.983	0.940	0.890	0.720	1.045	0.970	0.890	0.662
180	1.047	1.002	0.949	0.769	1.112	1.033	0.948	0.706
200	1.084	1.037	0.983	0.798	1.151	1.068	0.981	0.731

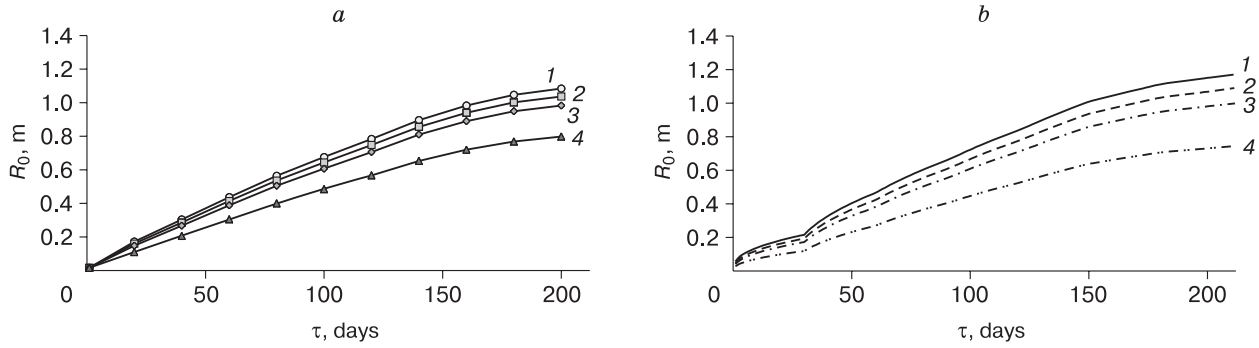

Fig. 4. Dependence of the freezing radius R_0 on time τ for the city of Varandey.

a – analytical solution; *b* – numerical solution. Evaporator length: *1* – 300 m; *2* – 600 m; *3* – 1000 m; *4* – 3000 m.

Table 4. **Dependence of soil freezing radius R_0 on time τ for Igarka**

τ, days	R_0, m (analytical solution)				R_0, m (numerical solution)			
	Evaporator length							
	300 m	600 m	1000 m	3000 m	300 m	600 m	1000 m	3000 m
1	0.016	0.016	0.016	0.016	0.078	0.062	0.052	0.034
20	0.253	0.230	0.207	0.146	0.264	0.228	0.197	0.130
40	0.440	0.405	0.369	0.268	0.463	0.406	0.355	0.238
60	0.632	0.585	0.536	0.396	0.654	0.578	0.508	0.344
80	0.800	0.744	0.684	0.510	0.829	0.739	0.654	0.449
100	0.939	0.875	0.806	0.604	0.972	0.870	0.773	0.535
120	1.061	0.990	0.913	0.688	1.098	0.985	0.877	0.610
140	1.141	1.066	0.985	0.744	1.178	1.057	0.941	0.655
160	1.205	1.126	1.041	0.788	1.243	1.116	0.993	0.691
180	1.258	1.176	1.088	0.824	1.298	1.166	1.038	0.723
200	1.269	1.187	1.098	0.832	1.308	1.175	1.046	0.729

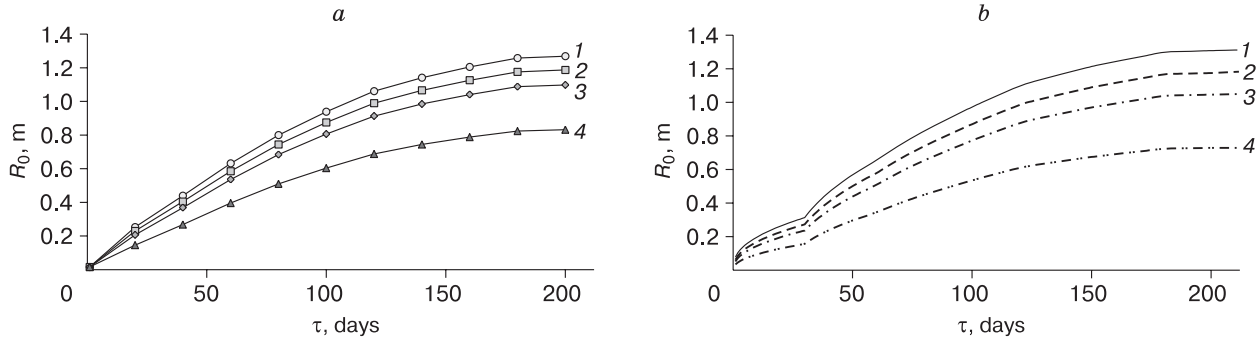

Fig. 5. Dependence of the freezing radius R_0 on time τ for the city of Igarka.

a – analytical solution; *b* – numerical solution. Evaporator length: *1* – 300 m; *2* – 600 m; *3* – 1000 m; *4* – 3000 m.

Table 5. **Degree of correspondence between analytical and numerical solutions for the radius of frozen soil (unit fraction)**

City	Evaporator length			
	300 m	600 m	1000 m	3000 m
Salekhard	0.912	0.963	1.010	1.114
Varandey	0.878	0.913	0.949	1.049
Igarka	0.896	0.939	0.979	1.075
Average	0.895	0.938	0.979	1.079

It follows from the presented data that if the distance between the pipes of the HET system is 1 m, then the entire soil will freeze in 100 days, i.e., in half of the winter season, since the freezing radius will usually be more than 0.5 m during this time However, for the Varandey case at L_{tot} = 3000 m, the radius of the frozen ground is 0.485 m, which is close to 0.5 m.

In addition, according to the calculated values of the soil freezing radius, it is possible to make a quick assessment of the volume of soil frozen under the object. To do this, we calculate the volume of the resulting soil cylinder with an evaporator laying step of 1 m. We get

$$V_{tot} = \pi R_0^2 LN = \pi R_0^2 \frac{L_{tot}}{N} N = \pi R_0^2 L_{tot},$$

where V_{tot} is the total volume of frozen soil, m^3; L is the length of one pipe of the evaporative system, m; N is the number of pipes in the evaporator system.

Thus, with a finning area of the condenser part of 100 m^2, in 100 days of operation of the HET-type soil temperature stabilization system with a total length of the evaporative part of 3000 m, it is almost always possible to freeze soil with a volume of 2356 m^3.

CONCLUSIONS

1. An analytical model of the functioning of the system for thermal stabilization of soils of the HET type was developed on the basis of the integral method.

2. A comparison of the results of numerical and analytical solutions for the soil freezing radii for different Arctic cities (Varandey, Salekhard, Igarka) demonstrated a high degree of correlation between the results obtained.

3. Based on the comparison of numerical and analytical solutions, it was concluded that the developed analytical model can be used for quick evaluation of the functioning of the HET-type soil temperature stabilization system for various design solutions and climatic characteristics.

4. A method for estimating the volume of frozen soil based on the data obtained within the framework of the analytical model solution is shown.

Funding. *This study was carried out within the framework of the state assignment No. 121041600047-2.*

References

Anikin G.V., 2009. Simulating the Operation of Cooling Systems with Horizontal Tubes. IKZ RAN. Moscow. Deposited at VINITI Oct. 30, 2009, No. 674-V2009 (in Russian).

Anikin G.V., Plotnilov S.N., Spasennikova K.A., Ishkov A.A., 2017. Method of stochastic prediction of soil temperatures with HET systems. *Soil Mech. Found. Eng.* **54** (1), 65–70.

Babichev A.P., Babushkina N.A., Bratkovsky A.M., 1991. Physical Quantities. Reference. I.S. Grigoriev, E.Z. Meilikhov (Eds.). Moscow, Energoatomizdat, 1232 p. (in Russian).

Dolgikh G.M., Okunev S.N., Anikin G.V. et al., 2014. Comparison of experimental and numerical modelling data of the work of HET cooling system on the example of fire depot of the Vankorsky field. *Kriosfera Zemli*, XVIII (1), 65–69 (in Russian).

Ishkov A.A., Anikin G.V., 2020. Determination of the optimal step of installation between the evaporator pipes and the number of condenser units of the system of temperature stabilization of soils HET. *Tyumen State Univ. Herald. Physical and Mathematical Modelling. Oil, Gas, Energy* **6** (1), 100–117.

Ishkov A.A., Anikin G.V., Dolgikh G.M., Okunev S.N., 2018. Horizontal evaporator tube (HET) thermosyphons: physical-mathematical modeling and experimental data, compared. *Earth's Cryosphere* XXII (5), 51–56.

Ishkov A.A., Gubarkov A.A., Anikin G.V., 2019. Determination of the efficiency of the functioning of temperature stabilization system of soils with a horizontal evaporator filled with different refrigerants. *Tyumen State University Herald. Physical and Mathematical Modeling. Oil, Gas, Energy* **5** (4), 37–57.

Melnikov V.P., Anikin G.V., Ishkov A.A. et al., 2017. Maximum and minimum critical thermal loads constraining the operation of thermosyphons with horizontal evaporator tubes (HET). *Earth's Cryosphere* XXI (3), 38–44.

Naterer G.F., 2003. Heat Transfer in Single and Multiphase Systems. Washington, CRC Press LLC, 570 p.

Pavlov A.V., 2003. Permafrost and climatic changes in the north of Russia: observations, forecast. *Izv. Ross. Akad. Nauk. Ser. Geogr.*, No. 6, 39–50 (in Russian).

Royzen L.I., Dulkin I.N., 1977. Thermal Calculation of Ribbed Surfaces. Moscow, Energiya, 244 p. (in Russian).

Received July 5, 2021
Revised January 11, 2022
Accepted July 11, 2022

Translated by A.V. Muravyev